

University of Bradford eThesis

This thesis is hosted in [Bradford Scholars](#) – The University of Bradford Open Access repository. Visit the repository for full metadata or to contact the repository team



© University of Bradford. This work is licenced for reuse under a [Creative Commons Licence](#).

**MODEL AND DESIGN OF SMALL COMPACT
DIELECTRIC RESONATOR AND PRINTED
ANTENNAS FOR WIRELESS COMMUNICATIONS
APPLICATIONS**

FAUZI O. M. ELMEGRI

PHD

2015

MODEL AND DESIGN OF SMALL COMPACT DIELECTRIC RESONATOR AND PRINTED ANTENNAS FOR WIRELESS COMMUNICATIONS APPLICATIONS

Model and Simulation of Dielectric Resonator (DR) and Printed Antennas for wireless applications; Investigations of dual Band and wideband responses including Antenna Radiation Performance and Antenna Design Optimization using Parametric Studies

FAUZI O. M. ELMEGRI

BSc, MSc

Submitted for the Degree of

Doctor of Philosophy

Faculty of Engineering and Informatics

University of Bradford

2015

Abstract

MODEL AND DESIGN OF SMALL COMPACT DIELECTRIC RESONATOR AND PRINTED ANTENNAS FOR WIRELESS COMMUNICATIONS APPLICATIONS

Model and Simulation of Dielectric Resonator (DR) and Printed Antennas for wireless applications; Investigations of dual Band and wideband responses including Antenna Radiation Performance and Antenna Design Optimization using Parametric Studies

Keywords

Planar Printed Antenna, Dielectric Resonator Antenna (DRA), Antenna Bandwidth, Antenna Radiation, Planar monopole antenna, Ultra Wideband (UWB); defected ground plane, Aperture slot antenna; UMTS, WLAN, X-band

Dielectric resonator antenna (DRA) technologies are applicable to a wide variety of mobile wireless communication systems. The principal energy loss mechanism for this type of antenna is the dielectric loss, and then using modern ceramic materials, this may be very low. These antennas are typically of small size, with a high radiation efficiency, often above 95%; they deliver wide bandwidths, and possess a high power handling capability.

The principal objectives of this thesis are to investigate and design DRA for low profile personal and nomadic communications applications for a wide variety of spectrum requirements: including DCS, PCS, UMTS, WLAN, UWB applications. X-band and part of K_u band applications are also considered. General and specific techniques for bandwidth expansion, diversity performance and balanced operation have been investigated through detailed simulation models, and physical prototyping.

The first major design to be realized is a new broadband DRA operating from 1.15GHz to 6GHz, which has the potential to cover most of the existing mobile service bands. This antenna design employs a printed crescent shaped monopole, and a defected cylindrical DRA. The broad impedance bandwidth of this antenna is achieved by loading the crescent shaped radiator of the monopole with a ceramic material with a permittivity of 81. The antenna volume is $57.0 \times 37.5 \times 5.8 \text{ mm}^3$, which in conjunction with the general performance parameters makes this antenna a potential candidate for mobile handset applications.

The next class of antenna to be discussed is a novel offset slot-fed broadband DRA assembly. The optimised structure consists of two asymmetrically located cylindrical DRA, with a rectangular slot feed mechanism. Initially, designed for the frequency range from 9GHz to 12GHz, it was found that further spectral improvements were possible, leading to coverage from 8.5GHz to 17GHz.

Finally, a new low cost dual-segmented S-slot coupled dielectric resonator antenna design is proposed for wideband applications in the X-band region, covering 7.66GHz to 11.2GHz bandwidth. The effective antenna volume is $30.0 \times 25.0 \times 0.8 \text{ mm}^3$. The DR segments may be located on the same side, or on opposite sides, of the substrate. The end of these configurations results in an improved diversity performance.

Acknowledgements

I would like to thank my lord Allah, who gave me the guidance and the ability to fulfil my study.

I wish to express my deepest gratitude to Prof Raed A. Abd-Alhameed, Dr Neil J. McEwen and Prof Iqbal M. Mujtaba the supervisor team of my PhD project. I would like to thank them for letting me do this project in such topic. Actually, They have never hesitated to help me during the difficult starting times and gave me useful advices.

I would also like to thank, Dr C.H. See and Mr M.B. Child, for their help and advice throughout this work. Moreover, I extend my thanks to all members of the antenna lab, workshop and computer officers, for their great support and help. I wish to express my deepest thanks to my friends for their endless support throughout my research.

The financial support and sponsorship by the General Secretariat of Education and Scientific Research Libya are highly acknowledged and appreciated. Finally, my parents and my wife who supported and encouraged me a lot during my study in UK; I thank them very much

Table of Contents

Acknowledgements	ii
Acronyms	vi
List of Tables	xvi
Chapter 1 Introduction	1
1.1 Overview	1
1.2 Background	2
1.3 Motivation and Design Problems of the DRA	6
1.4 Project Objectives	7
1.5 Organization of project	9
Chapter 2 Literature Review	13
2.1 History of Dielectric Resonator Antennas	13
2.1.1 Compact DRAs	15
2.1.2 Multi-band DRAs	17
2.1.3 Wideband DRAs	19
2.2 Characteristics and Major Features of DRAs	22
2.3 Geometries of DRA	24
2.4 Feeding structures method of DRA	27
2.5 Resonant Frequency	33
2.5.1 Cylindrical DRA	34
2.5.2 Rectangular DRA	36
2.6 Q-factor and Bandwidth	36
2.6.1 Cylindrical DRAs	38
2.6.2 Rectangular DRAs	40
2.7 Conclusions	41
Chapter 3 Broadband Dielectric Resonator Antenna (DRA) Design for Mobile Wireless Applications	43
3.1 Introduction	43
3.2 Antenna Design Concept and Structure	45
3.3 Parametric Design Study	46

3.4 Result and Discussion	48
3.5 Conclusions	53
Chapter 4 Dielectric Resonator Antenna Design for UWB Applications	54
4.1 Introduction	54
4.2 The Antenna Design Concept	55
4.3 Parameter Study	58
4.4 Results and Discussion	61
4.5 Conclusions	65
Chapter 5 Aperture-Coupled Asymmetric Dielectric Resonators Antenna for Wideband and Broadband Applications.....	66
5.1 Introduction.....	66
5.2 Antenna Design Concepts and Structure.....	67
5.3 Parametric Study	70
5.4 The Optimized Antenna Design and Measurement Results	74
5.5 Conclusions.....	81
Chapter 6 Offset Aperture-Coupled Two Cylindrical Dielectric Resonators Antenna for Extended-Wideband Applications	82
6.1 Introduction	82
6.2 Proposed Antenna Geometry	84
6.3 Results and Discussion	87
6.4 Conclusions.....	92
Chapter 7 Dual Segment S-Shaped Aperture-Coupled Cylindrical Dielectric Resonator Antenna For X-Band Applications	93
7.1 Introduction.....	93
7.2 Antenna Design Concepts and Structure.....	94
7.3 Parametric Design Studies and Optimized Design	96
7.4 Results and Discussion	99
7.4.1 Magnitudes of Electric and Magnetic Fields	104
7.4.2 Positioning of the Dielectric Resonators.....	107
7.5 Conclusions.....	111

Chapter 8 Balanced Dual-Segment Cylindrical Dielectric Resonator Antenna for Ultra-	
Wideband Applications.....	112
8.1 Introduction.....	112
8.2 Frist Design: Without a C-shape Strip.....	115
8.2.1 Antenna Geometry.....	115
8.2.2 Parametric Study.....	118
8.2.3 Experimental Results and Discussions	124
8.3 Second Design: Adding a C-shape Strip.....	132
8.3.1 Antenna Performance.....	133
8.4 Conclusions.....	139
Chapter 9 Conclusions and Recommendations for Future Work.....	140
9.1 Conclusions.....	140
9.2 Future Work.....	145
References.....	147
Appendix.....	174

Acronyms

CP	Circular Polarisation
CPW	Co-Planar Waveguide
dB	Decibel
DCS	Digital Cellular System
DGS	Defected ground structures
DR	Dielectric Resonator
DRA	Dielectric Resonator Antenna
DVB-H	Digital Video Broadcasting - Handheld
EM	Electro Magnetic
FDTD	finite Difference Time Domain
GPS	Global Positioning System
HE	Hybrid Electric
HEM	Hybrid Electromagnetic
HFSS	High Frequency Structure Simulator
IEEE	Institute of Electrical And Electronics Engineers
ISM	Industrial, Scientific And Medical
PC	Personal Computers
PCS	Personal Communication System
Q-Factor	Quality Factor
RF	Radio Frequency
RFID	Radio- Frequency Identification
SMA	Sub Miniature Version A Connector
TE	Transverse Electric
TM	Transverse Magnetic
UMTS	Universal Mobile Telecommunication System

UWB	Ultra -Wideband
WiMax	Worldwide Interoperability for Microwave Access
WLAN	Wireless Local Area Network

List of Figures

Figure 2.1: Various geometrical shapes of dielectric resonators (DRs)	24
Figure 2.2: Geometries of DRA, (a) rectangular (b) cylindrical (c) hemisphere	25
Figure 2.3 Three Dimension of Common DRA Feeding Schemes, (a) Micro-slot (b) Coaxial Probe (c) Microstrip	28
Figure 2.4: Equivalent circuits for some typical feeding techniques	28
Figure 2.5: Aperture feeding in various shapes.....	30
Figure 2.6: Probe feeding in various shapes	31
Figure 2.7: microstrip line feeding of various shapes	32
Figure 2.8: Coplanar feeding of various shapes.....	33
Figure 3.1: Geometry of the proposed antenna. (a) Top view, (b) Bottom view, and (c) Dielectric resonator on the printed antenna.	45
Figure 3.2: Simulated return loss corresponding to the variation parameters of: (a) permittivity of the DR and (b) height of the DR.....	48
Figure 3.3: Return loss of proposed antenna with and without DR.....	49
Figure 3.4: Prototype antenna.....	50
Figure 3.5: Measured and simulated reflection coefficient $ S_{11} $	50
Figure 3.6: Simulated and measured gains of the proposed antenna with and without DR	51

Figure 3.7: Simulated and measured normalised radiation patterns of the proposed antenna for three planes ((a): x-z plane, (b): y-z plane, (c): x-y plane) at (i) 2100 MHz (ii) 2800 MHz xxxx' simulated cross-polarization 'oooo' simulated co-polarization '----' measured cross-polarization '—' measured co-polarization.....	52
Figure 4.1: Basic antenna geometry model	57
Figure 4.2 Simulated $ S_{11} $ of the proposed antenna with and without dielectric resonator (DR).	58
Figure 4.3 Simulated $ S_{11} $ corresponding to the variation parameters of Length of DR (DR_L).	59
Figure 4.4: Simulated $ S_{11} $ corresponding to the variation parameters of Width of DR (DR_W).....	60
Figure 4.5 Simulated $ S_{11} $ corresponding to the variation parameters of Length of T-strip (T_L).	61
Figure 4.6: Verification of the predicted $ S_{11} $ by (a) using two software with without DR and by (b) using two software with measured.....	62
Figure 4.7: Simulation and measurement of radiation patterns of the proposed antenna for two planes: xz-plane (E-plane) and xy plane (H-plane).....	64
Figure 5.1: Aperture-coupled asymmetric dielectric resonator antenna (a) top view and (b) side view with design dimensions and parameters.....	68
Figure 5.2: Simulated reflection coefficient as a function of frequency for different slot lengths S_l with $S_w=1.1\text{ mm}$, $L_{\text{stub}}=4\text{ mm}$, $y_d=3.75\text{ mm}$, $y_{d1}=-2.1\text{ mm}$.	70

Figure 5.3: Simulated reflection coefficient as a function of frequency for different slot widths S_w with $S_l=6.6\text{mm}$, $L_{\text{stub}}=4\text{mm}$, $y_d=3.75\text{mm}$, $y_{d1}=-2.1\text{mm}$.	71
Figure 5.4: Simulated reflection coefficient as a function of frequency for various stub lengths l_{stub} with $s_l=6.6\text{mm}$, $s_w=1.2\text{mm}$, $y_d=3.75\text{mm}$, $y_{d1}=-2.1\text{mm}$.	72
Figure 5.5: Simulated reflection coefficient as a function of frequency for various stub lengths y_d with $s_l=6.6\text{mm}$, $s_w=1.2\text{mm}$, $l_{\text{stub}}=4\text{mm}$, $y_{d1}=-2.1\text{mm}$.	73
Figure 5.6: Simulated reflection coefficient as a function of frequency for varying position of lower DR y_{d1} with $s_l=6.6\text{mm}$, $s_w=1.2\text{mm}$, $l_{\text{stub}}=4\text{mm}$, $y_d=3.75\text{mm}$.	74
Figure 5.7: Photograph of the fabricated antenna (a) front view and (b) back view.	75
Figure 5.8: Simulated and measured reflection coefficients (S_{11}) of the proposed DRA.	76
Figure 5.9: Comparison of simulated and measured antenna gain of the proposed antenna.	77
Figure 5.10: Simulated and measured impedance of the proposed antenna.	77
Figure 5.11: Simulated and measured radiation pattern; (a) and (c) at xz plane, (b) and (d) at yz plane; simulated E_θ : dashed line, simulated E_ϕ : dotted line, measured E_θ : 'o-o-o', measured E_ϕ : solid line.	79
Figure 5.12: Magnitude of electric (top, xz plane) and magnetic (bottom, xy plane) fields distribution for (a) 10.8 GHz, (b) 12.3 GHz.	80

Figure 6.1: Aperture-coupled asymmetric DRA; (a) top view and (b) side view with design dimensions and parameters.	84
Figure 6.2: Aperture-coupled asymmetric DRA top view with steps of the designed antenna. (a) Antenna proposed in [4], (b) a second proposed antenna and (c) our proposed antenna.	86
Figure 6.3: Simulated return loss of the three different DRAs shown in Figure 6.2.	87
Figure 6.4: Simulated and measured return loss of the proposed DRA.....	88
Figure 6.5: Photograph of the fabricated antenna (a) front view, (b) back view and (c) with DRs.	88
Figure 6.6: Simulated and measured impedance of the proposed antenna.....	89
Figure 6.7: Simulated and measured antenna gain of the proposed antenna ..	90
Figure 6.8: Measured radiation patterns (a) in xz-plane, (b) in yz-plane.....	91
Figure 7.1: Geometry of the proposed antennas. (a) top view and (b) side view with design dimensions and parameters	95
Figure 7.2: Simulated reflection coefficient versus frequency for different vertical slot lengths s_1 ; $s_1=3.25\text{mm}$ (solid), $s_1=3.5\text{mm}$ (dashed), $s_1=3.75\text{mm}$ (dotted), $s_1=4\text{mm}$ (dash-dotted).	97
Figure 7.3: Simulated reflection coefficient versus frequency for various horizontal slot lengths of the two slot ends sl_1 ; $sl_1=3.8\text{mm}$ (solid), $sl_1=3.9\text{mm}$ (dashed), $sl_1=4.0\text{mm}$ (dotted) and $sl_1=4.1\text{mm}$ (dash-dotted).	97

Figure 7.4: Simulated reflection coefficient verses frequency for various slot widths S_w ; $S_w=1.1\text{mm}$ (solid), $S_w =1.2\text{mm}$ (dashed) and $S_w =1.3\text{mm}$ (dotted)..	98
Figure 7.5: Simulated reflection coefficient verses frequency with varying position of S-slot along feeding line x ; $x=0.6\text{mm}$ (solid), $x=0.8\text{mm}$ (dashed), $x=1.0\text{mm}$ (dotted), $x=1.2\text{mm}$ (dash-dotted) and $x=1.4\text{mm}$ (circles)	99
Figure 7.6: Fabricated antenna (a) front view (b) back view	101
Figure 7.7: Simulated and measured reflection coefficient versus frequency for the proposed antenna.....	101
Figure 7.8: (a) Comparison of simulated and measured antenna gain of the proposed antenna, (b) Impedance Vs. Frequency plot of the proposed antenna	103
Figure 7.9: Far-field radiation patterns at (a) xz-plane and (b) yz-plane; E_θ Meas.(solid-circles), E_ϕ Meas.(triangle), E_θ HFSS (solid) and E_ϕ HFSS (solid-*).	105
Figure 7.10 : Magnitude of (a) Electric and (b) Magnetic fields distribution of the proposed dual segment S-shaped aperture coupled CDRA antenna at 7.92GHz, 9GHz and 10.49GHz.	106
Figure 7.11: Investigated positions of DR's (a) Simulated with HFSS, (b) fabricated antenna with lower DR on the slot side and upper DR on feed side and (c) fabricated antenna with upper DR on the slot size and lower DR on feed side.	108

Figure 7.12: Simulated and measured (a) Reflection coefficient magnitude (S_{11}) and (b) Gain (dBi) vs. frequency plots with different DR's positions.	109
Figure 7.13: 2D E-field radiation patterns at 9.5GHz and 10.5GHz (a) Two DR's on the slot side, (b) lower DR on the slot side and upper DR on feed side, (c) upper DR on the slot size and lower DR on feed side.	110
Figure 8.1: Balanced dual-segment cylindrical dielectric resonator antenna; (a) top view and (b) side view with design dimensions and parameters.	116
Figure 8.2 S Simulated effects on reflection coefficient of the horizontal slot length s_l ; $s_l=3.0$ (solid), $s_l=3.5$ (dashed), $s_l=4.0$ (dotted), $s_l=4.5$ (dash-dotted), $s_l=5.0$ (circles).	119
Figure 8.3: Simulated reflection coefficient versus frequency for various vertical slot lengths y ; $y=2.5$ (solid), $y=2.875$ (dashed), $y=3.25$ (dotted), $y=3.625$ (dash-dotted) and $y=4.0$ (circles).	119
Figure 8.4: Simulated reflection coefficient versus frequency for various horizontal slot width s_w ; $s_w=0.2$ mm(solid), $s_w=0.275$ mm(dashed), $s_w=0.35$ mm(dotted), $s_w=0.425$ mm(dash-dotted) and $s_w=0.5$ mm(circles).	120
Figure 8.5: Simulated reflection coefficient versus frequency for different vertical slot width x ; $x=0.5$ mm (solid), $x=0.75$ mm (dashed), $x=1.0$ mm (dotted), $x=1.25$ mm (dash-dotted) and $x=1.5$ mm (circles).	121
Figure 8.6: Simulated reflection coefficient versus frequency for various vertical L-section lengths f_l ; $f_l=2.5$ mm(solid), $f_l=3$ mm(dashed), $f_l=3.5$ mm(dotted) and $f_l=4$ mm (dash-dotted).	121

Figure 8.7: Simulated reflection coefficient versus frequency for different vertical L-section width W_{f2} ; $W_{f2} = 0.5$ mm (solid), $W_{f2} = 0.75$ mm (dashed) and $W_{f2} = 1.0$ mm (dotted) $W_{f2} = 1.25$ mm (dash-dotted) and $W_{f2} = 1.5$ mm (circles).	122
Figure 8.8: Simulated reflection coefficient versus frequency for various horizontal L-section lengths L_{f2} ; $L_{f2} = 3$ mm (solid), $L_{f2} = 3.5$ mm (dashed), $L_{f2} = 4.0$ mm (dotted), $L_{f2} = 4.5$ mm (dash-dotted) and $L_{f2} = 5.0$ mm (circles).	123
Figure 8.9: Simulated reflection coefficient versus frequency for various horizontal L-section width W_{f1} ; $W_{f1} = 0.5$ mm (solid), $W_{f1} = 1.0$ mm (dashed) and $W_{f1} = 1.5$ mm (dotted).	124
Figure 8.10: Photo of the proposed antenna; (a) front view and (b) rear view.	125
Figure 8.11: Simulated and measured reflection coefficients versus frequency for the proposed antenna.	126
Figure 8.12: Measured and simulated peak gains of the proposed DRA.	127
Figure 8.13: Simulated and measured radiation patterns; (a) at xz plane, (b) at yz plane; simulated E_θ : dashed line, simulated E_ϕ : dotted line, measured E_θ : 'o-o', measured E_ϕ : solid line.	128
Figure 8.14: Magnitude of electric and magnetic field distributions of the proposed T-slot fed balanced dual segment CDRA at (a) 6.8 GHz, (b) 11 GHz.	129
Figure 8.15: current distribution on the ground plane.....	131
Figure 8.16: Geometry of the modified antenna with a C-shaped strip.....	133

Figure 8.17: Simulated realized gain verses frequency for various widths W_c of the C-shaped strip; $W_c = 0.5$ mm (solid), $W_c = 1.0$ mm (dashed) , $W_c = 1.5$ mm (dotted).....	134
Figure 8.18: Simulated realized gain verses frequency for various vertical separation between ground plane and center of C-shaped strip y_c ; $y_c = 13$ mm (solid), $y_c = 13.5$ mm (dashed), $y_c = 14.0$ mm (dotted).....	135
Figure 8.19: Simulated realized gain versus frequency for various horizontal separations between the center of the C-shaped strip and the edge of the substrate x_c ; $x_c = 10.5$ mm (solid), $x_c = 11.5$ mm (dashed), $x_c = 12.5$ mm (dotted), $x_c = 14.5$ mm (dash-dotted), $x_c = 16.5$ mm (solid-circle).....	136
Figure 8.20: Fabricated antenna (a) front view and (b) rear view	137
Figure 8.21: Simulated and measured (a) reflection coefficient and (b) gain versus frequency for the proposed antenna with strip and without strip.	138

List Of Tables

Table 5-1 Dimensions of the optimized antenna.....	75
Table 6-1: Dimensions of the optimized antenna.....	85
Table 7-1: Optimum dimensions (in mm) for the prototype antenna assembly.	100
Table 8-1: Detailed parameters of the proposed antenna (all dimensions are in millimetres)	118
Table 8-2: Optimum parameters of the proposed antenna. (All dimensions are in millimetres).	125

CHAPTER 1

INTRODUCTION

1.1 Overview

Wireless communication systems have progressed significantly over the last three decades, with ever great numbers of applications and wider approval; their requirements keep presenting more challenges to the antenna and microwave communities in terms of special requirements for antenna design, fabrication and integration. These antennas are used as the front-end devices, and it is becoming more problematic to of satisfy the demanding requirements, such as miniaturised size, bandwidth, performance and improved radiation patterns. Conventionally, printed circuit (microstrip) or metallic rods (monopole) have been commonly used. Recently, many new wireless system antennas have been derived from dielectric materials especially dielectric resonator antennas (DRAs), which offer potential for enhanced performance.

Dielectric resonators (DR) have primarily been used in microwave circuits for filters and oscillators. A while DRs were established to radiate many years ago, it is more recently that their use as an antenna radiator has developed. Such devices were identified as DRA and for several years, their particular

advantages for a number of applications have been identified, including low profile and negligible conductor loss. This category of element can be an efficient radiator as has been shown experimentally. With the use of a DR a small size and high radiation efficiency antenna can be obtained. Theoretical and experimental assessments of DRAs have been reported by many investigators. Several attempts have been made to reduce the size of DRAs, especially to enable their use in mobile handsets. These studies have covered wide frequency bands from high microwave frequencies to low GSM 900 and 1800 mobile bands. This chapter starts with a review of research work on the use of DRAs and an evaluation of their important performance characteristics it then presents the target objectives of the current research and finally outlines the details of the thesis contents.

1.2 Background

For the past decade, DRAs have been considered as an important antenna research area by most antenna designers and researchers as they may offer several advantages compared to many other antennas. Activity has been encouraged by the availability of ceramic materials with very high relative permittivity and very low loss. This section will review the work carried out by a number of people in this area of antenna design.

In 1939, R. D. Richtmyer [1] showed that non - metalized dielectric objects can function as electrical resonators which he called dielectric resonators. In 1965, a technical report by H.Y. Yee [2][2] discuss of and presented both theoretical and experimental work on dielectric resonators, including resonant frequencies and modes of the natural resonant frequency of a DR . Further experimental data on circuit implementations of DR was discussed by Karp[3]. The work carried out by Yee represents the basic foundation of the work established by other researchers in more recent times.

Significant theoretical work on the modal and resonant behaviour of a low-loss, very high permittivity resonator was performed by Van Bladel [4, 5]. Further work on analytic models, based on variations of the dielectric waveguide mode1 developed through the work of Okaya, Barash and Marcatili [6], yielded more accurate determinations of DR circuit properties [7-9]. With computers, the applications of numerical methods to electromagnetic problems in the 1980's led to the solution of the resonant frequency and Q-factor for many shapes of dielectric resonators, summarized in[10].

For the last 3 decades, DR|As have been one of the classes of novel antennas that have been investigated and extensively reported on .Since the1970s , DRs have been used to achieve the reduction of passive and active microwave components, such as oscillators and filters[10, 11]. The idea of using a DR as

an antenna had not been widely accepted until the original paper on the cylindrical DRA [12] was published in 1983. Long and McAllister extended the dielectric resonator antenna investigation to rectangular [13] and hemispherical [14] DRAs. Other shapes were also studied, including the triangular [15], spherical-cap [16], and cylindrical-ring [17, 18] DRA.

DRAs have a limited bandwidth of operation due to their resonant nature, but this can be improved by reducing the inherent Q-factor of the resonant antenna or by introducing additional resonances. Emphasis has been on compact designs for portable wireless applications, and on new DRA shapes or hybrid antennas for enhanced bandwidth performance to meet the requirements for emerging broadband or ultra-wideband systems. DRAs can achieve larger impedance bandwidths by adopting various enhancement techniques. During 1990s, emphasis was placed on applying analytical or numerical techniques to determine the input impedance, the fields inside the resonator and the Q-factor [19]. DRs made of low permittivity materials ($8 \leq \epsilon_r \leq 20$) and placed in open environments show small radiation Q-factors if excited in their lower-order modes as demonstrated in [12]. The effects of an air gap in a lower effective dielectric constant were reported in [20, 21], which entails both a decrease in shift of the resonance frequencies and the Q-factor results, was reported. A design for a millimetre-wave high Q-factor parallel feeding scheme for DRA arrays was modelled demonstrated in [22].

In 1989 Kishk *et. al.* [23] were the first to investigate stack in two different DRAs on top of one another. Since the two coupled DRAs exhibit two different resonant frequencies, even if they have the same resonant frequency in isolation, the configuration has a dual-resonance operation, thus broadening the antenna bandwidth. There are many models of developed bandwidths using multiple DRAs in multiple stacked, coplanar embedded used of an air gap, used of collinear parasitic elements, and used of a DR coating with impedance bandwidths ranging from 25% to nearly 80% [23-33]. Similar bandwidth results can be achieved by modifying the shape of the DRA or by adopting new feeding structures [30, 34-43].

[44] Discusses measuring radiation efficiency of a DRA. The efficiency was measured by directly placing the DR on a metal plane; the results report that the conductor loss was small compared to the radiated power. This measurement illustrates that dielectric resonators, fabricated with low loss dielectric materials, have high radiation efficiency. The measured efficiency was found to be 98% for a hybrid operating mode of the DR.

1.3 Motivation and Design Problems of the DRA

Dielectric resonator antennas DRAs have been widely adopted. They can be integrated into wireless applications and offer several advantages compared with microstrip patch antennas. Such antennas with low conductor loss, small size, high radiation efficiency and low profile are of considerable interest for use in wireless applications. The DRA is also the one potential candidate that will fulfil the entire set of antenna design requirements; this has been mentioned by most of the relevant researchers in their publications such as [3], [19, 45-47]. The integration of the DRA into a wireless communication system; the operating bandwidth, volume and the size of the DRA need to be considered carefully.

The resonant frequency of the DRA is closely related to the dielectric constant (ϵ_r) of the resonator materials. This will be related to the DRA dimensions because they have to be of the order of the wavelength in the material. Thus, the dimensions of a DRA can be significantly reduced by choosing a high value of ϵ_r , example: $\epsilon_r \approx (10 - 100)$. In general, the DRA presents a high Q-factor coefficient since it has a high dielectric constant. In spite of the dimension requirements, the DRA size can be reduced by using high-dielectric-constant materials, but this will result in a well-known drawback: the Q-factor will increase and consequently will reduce the operating bandwidth. A simple technique to reduce the volume of DRA is to place it on a large ground plane in

which it will act as though an image is present. This halves the linear dimension that is normal to the ground plane. Thus, the volume of the DRA can be reduced by a factor of two. This technique can only be applied when the ground plane does not violate the boundary conditions of certain resonant modes of the DR.

1.4 Project Objectives

The objective of this thesis is to develop design and characterization methodologies for the proposed compact DR antennas. Hence, it involves much design and simulation of DR antennas with specifications on bandwidth, radiation pattern and gain. Therefore, DRAs are designed and investigated, based on this concept. The following summarized the objectives of the technical procedures applied through this present work and demonstrate the design concepts of several new DR antennas:

- The DRA geometry was optimised, subject to the DRA size, the height and the permittivity parameters and as a result, the resonant frequency and impedance bandwidth were significantly improved. Simulated radiation patterns for these antennas are observed to be smooth and symmetrical, suitable for usage in various wireless applications.

- A new low-profile compact-size multi-frequency band DRA antenna was developed on defected ground. The DR was excited by a stripline and implemented from a thin polymer cavity filled by ionized water. It indicates that the antenna can operate for most of the existing wireless standards, including DCS (1710-1880MHz), PCS (1850-1990MHz), UMTS (1920-2170MHz), and the Industrial, Scientific and Medical (ISM) band (2400-2485MHz), IEEE 802.11 a/b/g.
- This DRA was designed to operate for most of the existing wireless standards, and provided sufficient frequency spectrum bandwidth/s, more than adequate for a wireless system examples 3G, WLAN, WiMAX, and X-band. Besides, some of the DRA bandwidth enhancement techniques have been applied to the proposed DRA in order to get good impedance matching.
- A compact dielectric resonator antenna (DRA) with band-notched characteristics for ultra-wideband applications was designed, developed and tested at x-band spectrum bandwidth. The notch has been easily integrated into the feeding transmission lines.
- A new low-cost dual-segmented dielectric resonator (DR) antenna design has been proposed for wideband applications in the X-band region. The

locations of the two DR segments including a new proposed feeding network through S-slot were investigated in supporting various DRs locations on the substrate.

- Balanced dual segment cylindrical dielectric antennas (CDRA) with ultra wide-band operation are optimised, developed and tested. The feeding network was achieved through balanced striplines resulted from the excitation of slot with microstrip line. The antenna gain was improved by introducing passive element on the same antenna substrate.

1.5 Organization of project

This thesis is presented in a number of chapters. This chapter has summarized a short review of the importance of the DR antennas that particularly related to the wireless communications development; in addition the problem statement, project objective and the scope of the project have also been highlighted. The following are briefly described the contents of the upcoming chapters:

Chapter 2 reviews the history of DRAs and their characteristics and geometries. This also includes the feeding methods and resonant modes of the antennas and their state of the art into the design procedure. It also contains a brief

overview of the Q-factor and bandwidth, on Dielectric Resonator Antennas contains a review of.

Chapter 3 covers the low-profile multi-frequency band DRA antennas. I also provides an explanation on the design procedure and antenna design of a UWB printed monopole antenna. The return loss and radiation pattern are compared between the simulation and measurement results. This chapter presents a new proposed DRA of higher relative permittivity.

Chapter 4 presents results and discussions of small dielectric resonator antenna design technique for UWB uses; by adopting a modified T-shaped feeding structure to excite the DR. The proposed antenna design, geometry structure and parameters specifications are presented. The simulation, fabrication process, and measurement stage are explained. The overall dimensions of this antenna, including the ground plane (i.e. equivalent terminal size) are found around $30.0 \times 21.0 \times 0.8 \text{ mm}^3$ which is small enough to be adopted in many mobile/wireless enclosures.

Chapter 5, a compact dielectric resonator antenna design for wideband applications was demonstrated. The feed microstrip line is placed symmetrically with respect to the coupling aperture. The asymmetric location of the DR pair, the dimensions and the shape of the aperture together constitute another

parameter for the designer to optimize the design. In this study, an impedance bandwidth of about 29%, covering the frequency range from 9.62 GHz to 12.9 GHz, and a realized gain of 8 dBi are achieved.

In Chapter 6, a new shape of aperture coupling to DRA was investigated for use in broadband spectrum application. The shape of the aperture in terms of zigzag geometry results in multi resonances when coupled to the DRAs that enhance wider bandwidth compared to the designed DRA presented in chapter 5. The simulation and measurement results were confirmed of such significant improvement of the DRA operation. Parametric study of the antenna geometry was considered to aid the subsequent design process in terms the return loss, gain and radiation pattern.

Chapter 7 presents the investigation of a new design of dual segment S-Shaped Aperture-Coupled Cylindrical Dielectric Resonator Antenna for X-Band Applications was investigated in Chapter 7. The antenna is excited using an L-shaped feed line, and internal antenna coupling is achieved using an S-shaped slot. The effective antenna volume is $30.0 \times 25.0 \times 0.8 \text{ mm}^3$. The measured prototype performance shows an average gain of 6.0 dBi over the frequency range 7.66 GHz to 11.2 GHz, with stable radiation patterns. The DR posts may be arranged in two distinct configurations: (i) occupying space on one side of the substrate, and (ii) on opposing sides. The first configuration results in a

higher gain performance, whilst the second results in improved radiation uniformity.

In chapter 8, a balanced dual segment CDR antenna fed with balanced striplines was considered. The feed lines are excited by T- Shaped slot as coupling mechanism for feeding power to dual segment DRAs through L-shaped feeding line. Parametric studies have been carried out to optimize the antenna design. The resultant antenna offered good impedance bandwidth from 6.4GHz to 11.734 GHz (58.7% for $S_{11} \leq -10$ dB). It also provides a maximum gain of 2.66dBi at 7GHz. The gain of this antenna was enhanced by adding a C-shaped strip that resulted in an increase of maximum gain of 2.24 dBi while maintaining nearly the same impedance bandwidth. The measurements of the proposed antenna showed good agreement between simulated and measured results.

Finally chapter 9 indicates the summarized conclusions of the research work and some proposals for future work. In fact, a summary of conclusions points are addressed for each chapter and then recommendations for further work and related topics, subject to the great demands of using DRAs for future applications.

CHAPTER 2

LITERATURE REVIEW

2.1 History of Dielectric Resonator Antennas

For many years, dielectric resonators (DRs) were widely used in microwave subsystems, such as filters and oscillators, for their low loss material characteristics ($\tan \delta \approx 10^{-4}$, or less) and high relative permittivity (dielectric constants of $\epsilon_r \approx 20-100$). The unloaded DR Q-factor is usually between 50 and 500; but it can be as high as 10,000 [46]. Because of these traditional applications, the DR was operated as an energy storage device rather than as a radiator. However, the Q-factor of a DR in the lowest order mode can be reduced significantly, to 10-100, when the DR is placed in an open environment. In this condition, power is lost in the radiated fields. This suggests the idea of using a DR as an antenna element.

DR is a ceramic puck characterised by a definite volume, shape, high dielectric constant and low loss. The concept of a DR first appeared in 1939, when Richtmeyer realized that it was possible to let open DRs radiate into free-space [1]. Gastine reported the Q-factor, including radiation, of a spherical dielectric

resonator, in 1967 [48]. Subsequently, Sager and Tisi started to consider the possibility of designing a very small antenna by using a dielectric resonator [49]. However, to create new devices more research was required that could classify more of their circuit properties like: resonant frequency, modes, coupling to other microwave circuits and Q-factors. Some significant papers were published by Yee [5].

In 1975, Van Bladel [4] reported on detailed theory to evaluate the modes of a dielectric resonator (DR). In this study, he derived the general theory of the internal fields and radiation fields for the dielectric resonator of arbitrary shape in high dielectric constant materials (including resonant frequencies and radiation fields) [4, 5]. DRs of different shapes have various modes of oscillation. With the proper excitation of certain modes and with no shielding, these resonators can actually become efficient radiators instead of energy storage devices. This idea led to investigation of DRs as antennas.

In 1983, the first original theoretical and experimental analysis paper on a possible antenna application was published by Long, McAllister and Shen [12], concerning the cylindrical dielectric resonator antenna (DRA). An increasing amount of literature has been produced on dielectric resonator antennas, which examined the characteristics of dielectric resonator antennas (DRAs) of hemispherical, cylindrical, and rectangular, shapes [12-14]. Other shapes were

also studied, including the triangular [15], spherical-cap [16], and cylindrical-ring [17, 18]. DRAs could be considered to be attractive alternatives to traditional low-gain antenna elements, such as microstrip patches, monopoles, and dipoles.

In the early 1990s, several piece of research applied analytical and numerical techniques to dielectric resonator antennas, and analyzed the various modes of excitation of dielectric resonator antennas with simple shapes, also examining a variety of feed mechanisms [50, 51].

Nevertheless, more literature on the DRA appeared in recent decades [19, 45, 46, 52]. This literature showed many investigators were active, and the number of publications has significantly increased. These works have continued in the areas of compact designs, multi-band and wideband designs, miniaturization techniques, and low-profile designs.

2.1.1 Compact DRAs

Compact DRAs has always been a challenging issue among antenna design researchers. By using a small volume of DR, a high dielectric constant material can resonate at a lower resonant frequency. But the Q-factor and hence a lower

bandwidth with the resonant frequency becoming highly temperature dependent will increase [53].

The existence of specific DR shapes which isolated one or more planes of symmetry has been noted. This plane of symmetry serves as an electric wall for certain modes; it works as a magnetic wall for the other modes. Half-split cylindrical DR was placed over a metallic ground plane, which was at the plane of symmetry ($\phi = 0^\circ$) were the motivation for the work in [8]. The particular antenna configuration was excited in $TE_{01\delta}$ mode with a low Q_r by this means facilitating more than 8% bandwidth. Numerical analysis of a half split cylindrical DRA on a ground plane excited in the low Q, modes $TE_{01\delta}$ and $HEM_{12\delta}$ using a method of moment approach for the coupling between a body of revolution (BOR) geometry and a non-BOR geometry is reported [54].

Half-volume design for the broadside modes of a cylindrical ($HEM_{11\delta}$) and rectangular ($TE_{11\delta}$) DRAs based on the aforesaid approach is presented in [55]. However, they used an additional metallic plate attached to the plane of symmetry of the DR which was oriented in the orthogonal plane to that in [8]. In the same paper, the authors put forward the concept for further size reduction of the DRA of using a metallic post in its place of the metallic plate. The above design was analysed by FDTD and additionally representative a higher directivity for the half-volume DRA was carried out by [56].

revolutionizing low-volume design by using circular and annular sector DRAs was reported where a 75 % reduction in volume is established [57]. The design used different inner to outer radius ratios, sector angles and boundary conditions (metallic, open or mixed) for the sector DRA. The structure modification in [55] was used to create circular polarisation [58]. The bandwidth enhancement of split-cylinder DRAs numerically and experimentally exhaustively studied in [59]. Rectangular DRA has been use of partial vertical and horizontal metallization on proposed to reduce the overall dimensions of the DRA to be used at WLAN applications [60]A compact , stacked, rectangular dielectric resonator antenna was designed for UWB applications. Shorting plate is attached to one narrow wall of the DRA to reduce its size volume up to 67%, has been achieved [61]. A thorough rectangular DRA analysis of a reduced volume based on the above principle using FDTD and measurements has been presented in [31].

2.1.2 Multi-band DRAs

A dual-band antenna can replace two single band antennas of suitable operating bands. The work in [23] on stacked wideband DRA shows the design of dual-band DRAs by choosing two DRAs of different dimensions, excited by a single feed. A wideband antenna unless it is operating over a useful application band, is useless. This paper [62] recommends the design of independent

application bands where the antenna radiates only over those bands introduced a slot excited double element rectangular DRA for dual or wideband application. Stacking of two cylindrical DRAs excited by an annular ring excited by a probe has shown three-band behaviour [63]. Dual frequency operation was achieved by incorporating additional DRA in a parent DRA, both cylindrical in shape, so that the volume of the structure remains unchanged is presented in [64]. A cylindrical ring DRA is fed with two orthogonal microstrip feeds for dual resonance is reported [65]. This also has the effect of producing orthogonally polarised bands but with similar broadside radiation patterns. Special eye-shaped DRA is also shown to be effective in producing dual radiating modes [66]. Compact multiband antenna system using a dielectric resonator antenna (DRA) was presented in [67]. The antenna designed to cover three frequency bands operating for different wireless applications (DVB-H, WiFi and WiMAX).

Dual-frequency operation can be achieved by adding an additional radiator to the DRA. This principle is implemented in [68] where a cylindrical DRA and a ring-slot are fed together by a circular slot thereby allowing radiation from the two at respective resonances. It will be advantageous in this context, if the feed to the DRA is also radiating at a particular frequency. The rectangular slot-feed to the DRA is made radiating by adjusting its dimensions where this technique is explained in [69]. Furthermore design introduced another by using a T-shaped microstrip feed that radiates in addition to exciting the DRA [70]. A

ceramic loaded annular ring monopole antenna is found to resonate in the dual W/LAN bands [71].

2.1.3 Wideband DRAs

In the early 90s, studies on stacked DRA designs were carried out both experimentally and numerically [72-74]. Two rectangular DRAs separated by a metallic plate yielded a much broader bandwidth of 76.8% [29]. Keeping the separate DR elements as a single entity in the above cases was tiresome and was avoided by fabricating single stacked DRA structures in the form of flipped staired pyramid [40], T and L shaped equilateral triangular [75, 76] which offered a maximum bandwidth in excess of 60%. Furthermore, an air gap between a cylindrical DRA and the ground plane, a kind of fabrication imperfection can cause increase of the resonant curve of the DRA [21, 77]. This was the effect of reduced unloaded or radiation Q-factor of the DRA due to an increased effective radiating area. Later, an aperture fed rectangular DRA was proposed, with its centre portion removed. This DRA and its image formed a rectangular ring DRA to obtain a 28 % bandwidth [30]. This was motivated by the work of [78] which reported that the Q_r of certain modes of a cylindrical ring DR is lower than those of the corresponding cylindrical DR.

Special DRA shapes similar to conical [79] and split-cylinder [59] were also reported to have wide bandwidths. Such geometries however suffered from an increased antenna dimension, specifically the DRA height, compared to an individual element. Embedding one DRA within another, in the form of an annular ring solved the above problem where the antenna dimensions are the same as that of the parent DRA [25, 80]. A detailed comparative study of the stacked and embedded wideband DRAs with the homogeneous DRA was also carried out [37] [81]. Later, a stacked-embedded DRA design improved the bandwidth to 68 % [82]. Designs using a simple DRA is also presented for bandwidth enhancement [83, 84], where an aspect ratio greater than unity led to acceptable excitation and merging of dual modes of similar radiation properties. Feeding techniques like T shaped [85] and L shaped [86] microstrip also improved the impedance bandwidth. To be suitable with low- Q_r , DRA shapes like cylindrical cup, novel feeds like L, hook and J shaped probes [87, 88] were also found suitable in addition to the probe or slot feed. Modification of the feed geometry proved to be a successful method for improving the impedance matching and bandwidth used a vertical metallic stub extended from a coaxial probe [89] or a microstrip line [90] enhanced the bandwidth to 43% and 19% respectively for cylindrical and rectangular DRAs. In addition, this was also shown to improve the impedance matching. A fork-like tuning stub [91] coupling energy from a microstrip through a circular aperture to the DRA also improved the bandwidth. An aperture feed which excites the DRA in addition to radiating

itself [92, 93] was capable of producing two merged resonances causing wide bandwidth operation. A hybrid dielectric resonator antenna for ultra wideband was presented in [94]. The dielectric structure enhanced the impedance bandwidth of the antenna to 148.4% with frequency range (6.2 - 42 GHz). As square ring di-electric resonator (SRDR) was presented with 'U' shaped microstrip feed[95]. The proposed DRA achieves an impedance bandwidth of 46.7% for 3.9 to 6.20 GHz. A simple dielectric resonator antenna with a notch band for ultra wideband was reported in[96]. The design gives band width from 3.71 GHz to 13.01 GHz. a notch was created at 5.725 GHz which reduces the interference due to local Wi-MAX communication system.

Nevertheless, more literature on the DRA has appeared in recent decades. This literature showed many investigators were active, and the number of publications has significantly increased. These works have continued in the areas of compact designs, multi-band and wideband designs, miniaturization techniques, and low-profile designs; in 1994, Mongia *et al.* demonstrated the radiation properties of a low-profile rectangular DRA with a very high permittivity ($\epsilon_r = 100$) [97], and Esselle studied a low profile DRA of low-permittivity ($\epsilon_r = 10.8$) [98]. For a long time, DRAs have concentrated on linear polarisation (LP), but systems using circular polarisation (CP) are sometimes preferred because they are insensitive to the transmitter and receiver orientations. In 1985,

Haneishi & Takazawa presented the first CP DRA [99]. Consequently, more effort has been devoted to the CP DRA in recent years.

A large part of this research includes the revision of new dielectric resonator antenna shapes, including hexagonal, conical, elliptical, tetrahedral, and stair-stepped shapes. Alternatives are hybrid antenna designs, using dielectric resonator antennas in combination with microstrip patches, slots, or monopoles. Many of the recent publications were concerned with designing dielectric resonator antennas for specific applications, including integration into mobile handsets for PCS, IMT-2000, and WLAN applications; use in UWB applications; radar applications; breast-cancer imaging; cellular base-station antennas; RFID; spatial power combining; direction finding; and all-dielectric wireless receivers. The literature has also investigated linear and planar array techniques for dielectric resonator antennas, and ways of improving their manufacture and integration in systems.

2.2 Characteristics and Major Features of DRAs

The DRA has some motivating characteristics, like the small size, ease of fabrication; high radiation efficiency, increased bandwidth and low production

cost, and DRA are very promising for application in wireless communications.

The advantages of the DRA are briefly stated as:

- A DRA can be designed in any 3D shape as shown in Figure 2.1; having more geometric parameters adds more degrees of freedom to the design.
- A DRA is made up of high dielectric constant material with no conducting parts and has very small dissipation loss. Therefore, it can handle high power. The limitation might be caused by the excitation mechanisms.
- Its physical size is small since the DRA is made of high dielectric constant material. Therefore, the DRA size decreases as the dielectric constant increases, in proportion to the wavelength in the dielectric which is $(\lambda_0 / \sqrt{\epsilon_r})$ where λ_0 is the free space wavelength and ϵ_r is the dielectric constant of the resonator material.
- DRA is not limited to linear polarization. The DRA can be designed for single, dual, or circular polarization.
- DRAs allow several feeding mechanisms (probe, slot, microstrip line feeding, dielectric image guides, and coplanar waveguide lines) to efficiently excite DRAs, making them amenable to integration with various existing technologies. DRAs can support different far-field radiation patterns.
- The DRAs impedance and bandwidth varies over a wide range with the resonator parameters like the geometries and resonant modes.

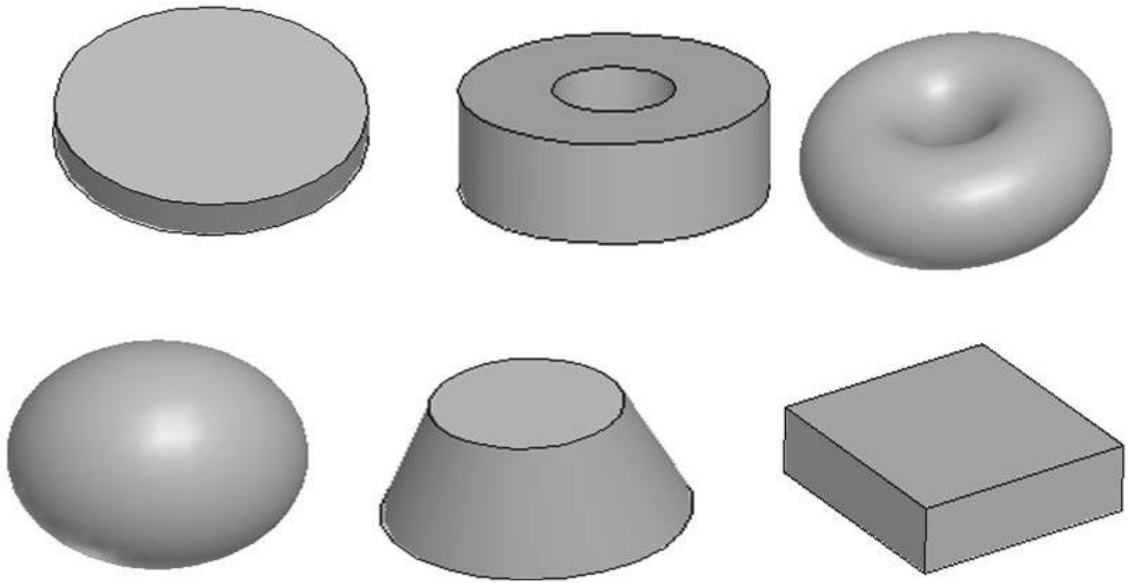


Figure 2.1: Various geometrical shapes of dielectric resonators (DRs).

2.3 Geometries of DRA

DRA's are simple to design in many shapes and sizes. The popular shapes are circular cylinder [12], rectangular cuboid [13], hemisphere [100], cylindrical ring [101] and triangular [15, 102] as shows in Figure 2.2. These categories of DR are popular for common designs since the mathematical formulations are very simple when used to predict the performance of the antenna.

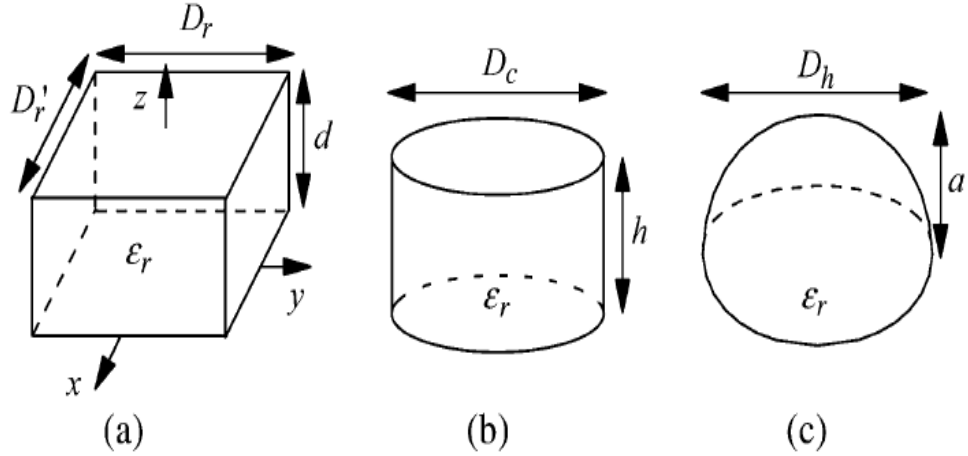


Figure 2.2: Geometries of DRA, (a) rectangular (b) cylindrical (c) hemisphere

Most important for the design of the DRA is the degree of dimensional freedom. The geometries of circular cylinder, rectangular cubic and spherical shapes, and their dimensions can be tuneable. In addition to these three forms of DRA, cylindrical and rectangular shapes have more degrees of freedom compared with the spherical dimensions. Therefore cylindrical and rectangular forms are often used.

The cylindrical DRA is defined by radius, a , and height, h . An analysis of the simple cylindrical DRA using the magnetic wall model was carried out in [12]. It offers greater design flexibility, where the ratio of radius/ height controls the resonant frequency and Q- factor, so that for a given dielectric constant and resonant frequency there is usually some scope for varying the aspect ratio, the

ratio of radius over height (a/h). The DRA will resonate at a specific frequency with a number of radius/height ratios. For different values of radius/height ratio, it may give different values of bandwidth, directivity and physical volume. The cylindrical DRA can be easily excited in different modes, which results in different radiation patterns. The three spatial coordinate for the cylindrical DRA are the radius, ρ , the azimuthal angle, ϕ , and the axial length, z . The coordinate system is shown in Figure 2.2(b).

The rectangular cuboid DRA offers greatest design flexibility of the three basic shapes, having two degrees of freedom (length/width and depth/width). The earliest rectangular DRA was investigated experimentally by McAllister et al. [13]. The parameters can be controlled by the three dimensions of the resonator to optimize for particular requirements. For fixed dielectric constant, several aspect ratios can be chosen to all resonate at a given frequency, while offering different radiation Q-factor. This allows the designer more options in tailoring the DRA for particular applications. The coordinate system is shown in Figure 2.2(a).

The hemispherical DRA of limited practical value, however, due to the difficulty involved in fabrication and lack any degrees of freedom in choosing the design parameters. For a material of a given dielectric constant, the radius of the sphere will determine both the resonant frequency and the radiation Q-factor,

leaving the designer no control over the antenna size or its impedance bandwidth. The coordinate system is shown Figure 2.2: Geometries of DRA, (a) rectangular (b) cylindrical (c) hemisphere(c).

The hemispherical DRA has the simplest structure for the analytical analysis, it having only one tunable dimension. theoretical and experimentally analysis for the hemispherical DRA reported by Leung *et al.* [103]. Although this shape of DRA is easy to optimize during the design process, in certain materials the resonant frequency of hemisphere DRAs is determined by the radius and the other parameters like bandwidth are fixed. This will make hemisphere DRAs difficult to optimize for particular requirements. Therefore the hemisphere-shape DR is less frequently used as a DRA. The hemisphere offers an advantage over the rectangular and cylindrical shapes in that the interface between the dielectric and air is simpler; and thus, a closed form expression can be obtained for the Green's function.

2.4 Feeding structures method of DRA

The feeding mechanisms considerably affect the resonant frequency and radiation Q-factor of a DRA. Many feeding techniques have been developed. One significant parameter in designing a feed to excite the DRA is the input impedance. The feed and location selection both show a significant part in

determining which feeding mode. This in turn will determine the input impedance and radiation characteristics of the DRA. Some of these methods are shown in Figure 2.3 and the equivalent circuits of some of the feeding techniques used for

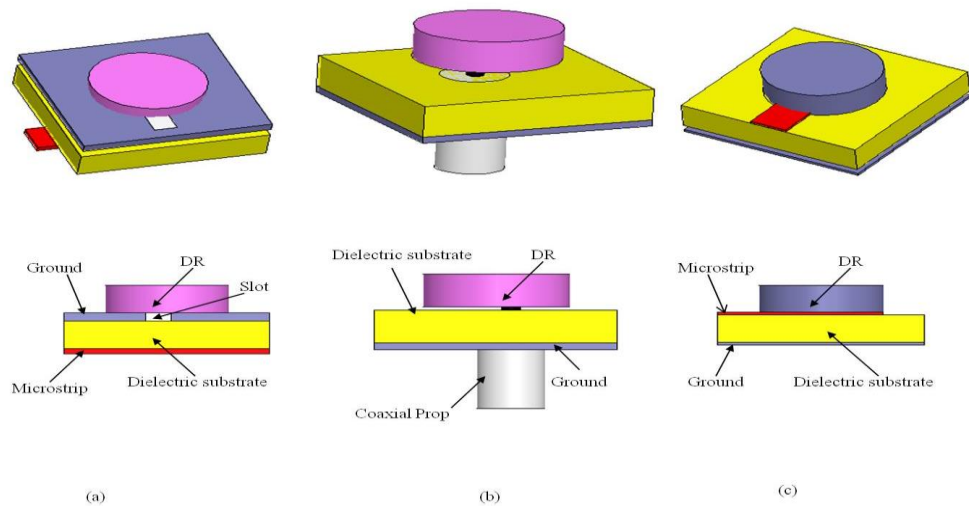


Figure 2.3 Three Dimension of Common DRA Feeding Schemes, (a) Microslot (b) Coaxial Probe (c) Microstrip

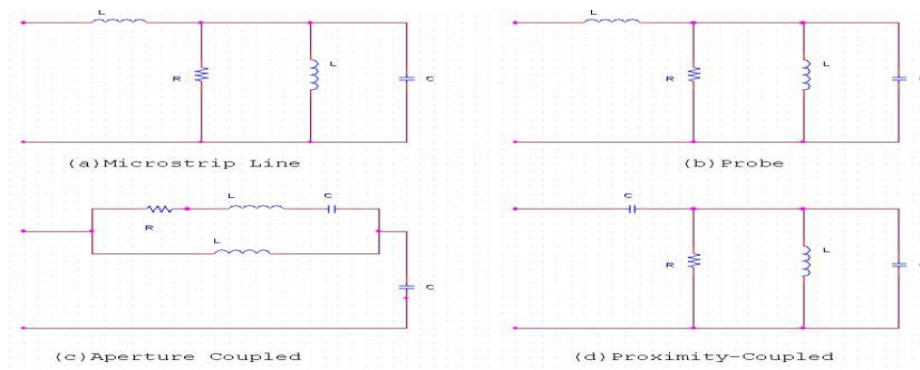


Figure 2.4: Equivalent circuits for some typical feeding techniques

DRAAs shown in Figure 2.4. These include, for example, aperture coupling with a microstrip feedline [15, 16, 104], coaxial probe [12-14, 105, 106], aperture coupling with a coaxial feedline [107, 108], waveguide coupled aperture [109, 110], direct microstrip feedline [111, 112], coplanar feed [113], soldered through probe [18], slot line[102], conformal strip[114] and direct image guide [115]. The following the reviews more common examples presented of feeding mechanism to highlight the practical design considerations.

Aperture feeding methods are one common technique of feeding a DRA, where power passes through an aperture in the ground plane upon which the DRA is placed. The aperture can be of any shape, such as narrow slot, loop, cross, or C shape cut in the ground plane, and can be fed by a microstrip line or coaxial feedline beneath the ground plane; some of the shapes are shown in Figure 2.5. The advantage of this technique is that it has the feed located below the ground plane, isolating the radiating aperture from any unwanted coupling or spurious radiation from the feed.

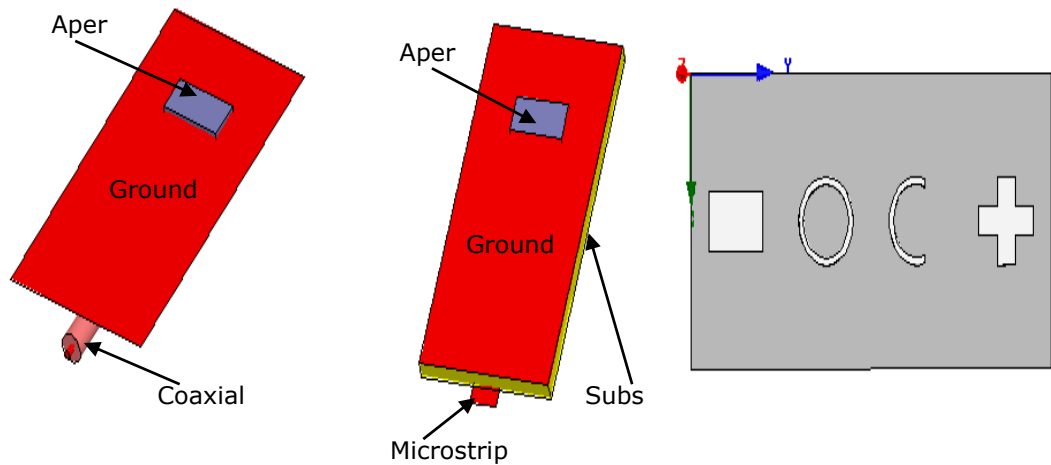


Figure 2.5: Aperture feeding in various shapes

Probe feeding methods are another common method of feeding a DRA. The probe can either be located adjacent to the DRA or can be embedded within the body. Figure 2.6 shows some of the probe shapes that have been used for feeding. The amount of coupling can be optimized by adjusting the probe height and the DRA location. In this technique, depending on the location of the probe, various modes can be excited. The advantage of this method is that the antenna system can be directly connected to a 50Ω circuit without the need for a matching network. Probes are useful at lower frequencies where aperture-feeding may not be practical due to the large size of the slot required.

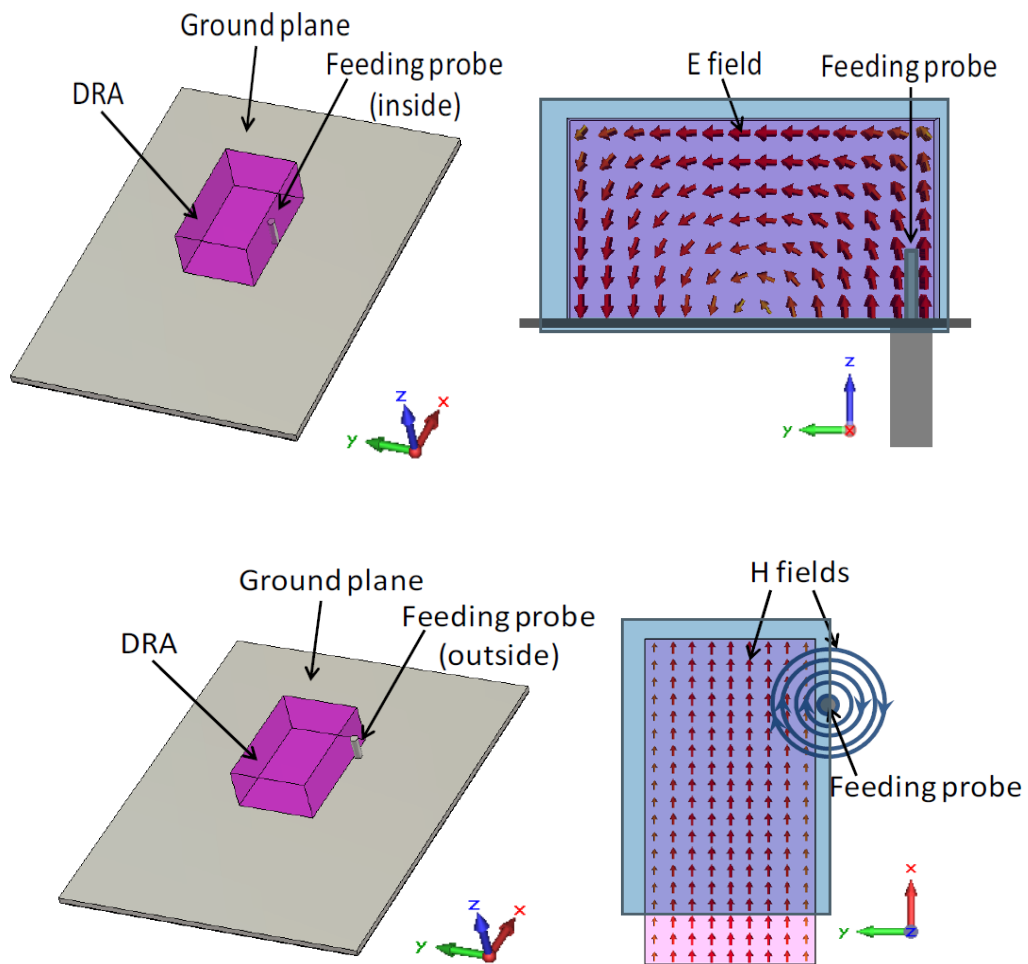


Figure 2.6: Probe feeding in various shapes

The microstrip line feeding method is also another common method of feeding a DRA, and it is the simplest method to energize DRAs. Figure 2.7 shows some of the probe shapes that have been used for feeding. In this method, a microstrip line printed on the same substrate feeds a DR that could be placed

directly over the microstrip line or nearby over the dielectric substrate. The level of coupling can be adjusted by the side position of the DR with respect to the microstrip line and by using substrate with different permittivity.

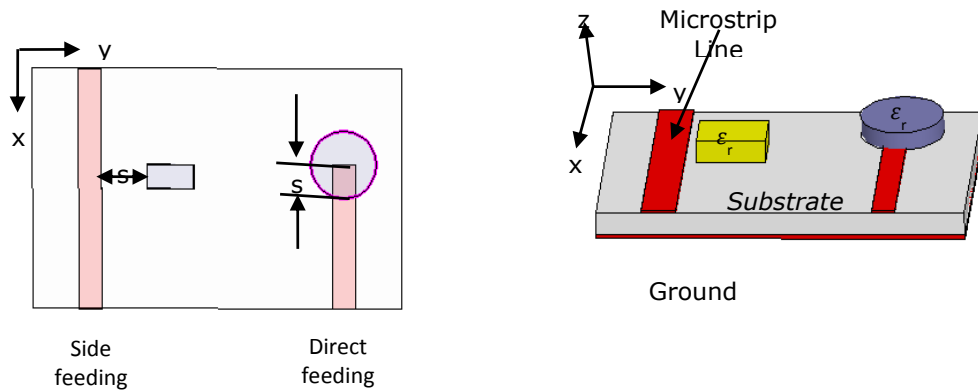


Figure 2.7: microstrip line feeding of various shapes

Another common method for feeding to DRAs is with a coplanar conductor. Figure 2.8 shows some of the coplanar shapes that have been used for feeding. The feed lines of the DRs using the coplanar waveguide seem very promising because it enables easy feeding. In this case, the coupling level can be adjusted by positioning the DRA over the coplanar structure. Impedance tuning can be done by adding stubs, slots, or loops at the end of the coplanar line. Despite the fact that coaxial probes and coplanar loops work similarly, the latter has the advantage of unobtrusive and planar structure to benefit integration. By

moving the position of the DR over the loop, the operating mode can be selected.

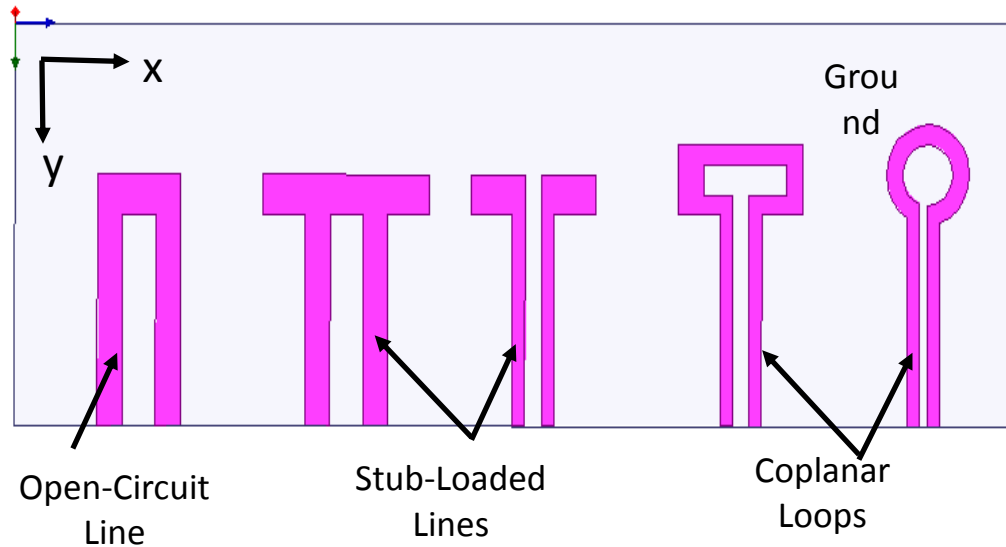


Figure 2.8: Coplanar feeding of various shapes

2.5 Resonant Frequency

For a DRA design of any geometry, different specifications must be satisfied such as the resonant frequency, the field distribution inside the resonator and the radiated fields. Based on that, it is possible to classify resonant modes into three types that can be excited in dielectric resonators: Transverse Electric (TE), Transverse Magnetic (TM) or hybrid electromagnetic (HEM) modes. The fields for *TE* and *TM* modes are axisymmetric, whereas hybrid modes are azimuthally dependent.

The TE , TM , and hybrid modes are classified as $TE_{mnp+\delta}$, $TM_{mnp+\delta}$ and $HE_{mnp+\delta}$ respectively. The first index denotes the number of full-period field variations in an azimuthal direction, the index n ($n = 1, 2, 3\dots$) denotes the order of variation of the field along the radial direction and the index $p + \delta$ ($p = 0, 1, 2\dots$) denotes the order of variation of the fields along the Z -direction. Here, the third index denotes the fact that the dielectric resonator is shorter than integer multiples of half the dielectric wavelength. The actual value of δ depends on the relative dielectric constant of the resonator and the substrate and on the proximity to the top and bottom conductor planes. An interesting feature of a DR is the variation in field distribution of different modes, because the modes behave like electric and magnetic multiples.

2.5.1 Cylindrical DRA

The resonant frequency equations for the $TE_{01\delta}$, $TM_{01\delta}$ and $HE_{11\delta}$ modes of a cylindrical DRA with radius a , dielectric constant ϵ_r , and height h kept above an infinite ground plane and fed by an electromagnetic signal of free space velocity areas shown.

The resonant frequency for the mode governed by npm is given by

$$f_{npm} = \frac{1}{2\pi a \sqrt{\mu\epsilon}} \sqrt{\left(\frac{X_{np}^2}{X_{np}^{\prime 2}}\right) + \left[\frac{\pi a}{2d}(2m+1)\right]^2} \quad (2.1)$$

Resonant frequency of isolated cylindrical DRAs:

TE_{01δ} Mode

$$k_0 a = \frac{2.327}{\sqrt{\epsilon_r + 1}} \left(1 + 0.2123 \frac{a}{h} - 0.00898 \left(\frac{a}{h} \right)^2 \right) \quad (2.2)$$

where the above formula is valid in the range $0.33 \leq a/H \leq 5$.

TM_{01δ} Mode

$$k_0 a = \frac{\sqrt{3.83^2 + \left(\frac{\pi a}{2h}\right)^2}}{\sqrt{\epsilon_r + 2}} \quad (2.3)$$

where the above formula is valid in the range $0.33 \leq a/H \leq 5$.

HE_{11δ} Mode

$$k_0 a = \frac{6.324}{\sqrt{\epsilon_r + 2}} \left\{ 0.27 + 0.36 \frac{a}{2h} - 0.02 \left(\frac{a}{2h} \right)^2 \right\} \quad (2.4)$$

where c is the velocity of light in free-space. Range of validity for the above equation is $0.4 \leq a/H \leq 6$.

2.5.2 Rectangular DRA

Fundamental electromagnetic fields theory suggests that the modes of a dielectric waveguide can be of the TE type, of the TM type or hybrid. Therefore, for the ongoing analysis of the RDRA modes, only the TE_{mnl} modes will be discussed, with the indices m , n and l denoting the order of variation along the x, y and z directions of the Cartesian coordinate system, respectively. The normalized frequency is defined as:

$$F = \frac{2\pi\omega f_0 \sqrt{\epsilon_r}}{c} \quad (2.5)$$

2.6 Q-factor and Bandwidth

The choice of the mode to utilize for antenna applications depends on the Q factor and also on the radiation pattern. The Q factor or quality factor is a measure of the bandwidth of operation. It is used as a figure of merit for assessing the performance or quality of a resonator. The Q factor is defined by:

$$Q = \frac{\omega_0 U}{P} \quad (2.6)$$

where ω_0 is the resonant frequency, U is the stored energy, and P is the power dissipation. There are many different Q's that are defined. First there is the

unloaded Q *which* is the Q when the resonator is freely oscillating without being driven externally by an external source. When an external source is connected to the resonator and is continuously provided with energy, the appropriate Q would be the loaded Q . For antennas, the important Q -factor is Q_{rad} , where the power dissipated term P in equ 2.6 is the radiated power. A number of assumptions are made to compute the Q -factor of a cylindrical DR. For a particular mode, the value of the radiation Q -factor depends on the aspect ratio and dielectric constant of the resonator. Van Bladel [4] has stated that the Q_{rad} is proportional to r , for dielectric resonators and this relationship for high ϵ_r is given as:

$$Q_{rad} \propto \epsilon_r^P \quad (2.6)$$

where

$P=1.5$ for modes that radiate like a magnetic dipole

$P=2.5$ for modes that radiate like an electric dipole

$P=2.5$ for modes that radiate like a magnetic quadrupole

The bandwidth is defined as the frequency bandwidth in which the input Voltage standing wave ratio (VSWR) of the antenna is less than a specified value S . The larger bandwidth the more coverage over frequency space that the antenna can be utilized. Using the expressions for the internal field structure of the DRA

an analytic expression for the bandwidth of the antenna is be developed, as presented by Mongia [46] .This relationship is given as:

$$BW = \frac{S - 1}{Q_u \sqrt{S}} \quad (2.7)$$

where Q_u is the unloaded Q. Dielectric resonator antennas have negligible dielectric and conductor loss compared to their radiated power. Therefore the radiated Q,

$$Q_u \cong Q_{rad} \quad (2.8)$$

The values of P are only valid for very high ϵ_r (> 100). For low ϵ_r , numerical results from published sources [46] have found that the relationship given by equation 2.6 is still valid, although the values of P have to be adjusted. Another important result is that the values of P are nearly independent of the aspect ratio of the resonator. The lower order modes typically have a lower Q_{rad} making them more suitable for practical applications. The Q_{rad} -factor is important because a low Q_{rad} would indicate a large bandwidth but a high Q_{rad} would indicate a small bandwidth of operation.

2.6.1 Cylindrical DRAs

The equations for the resonant frequency and Q-factor of the lower order modes as published in[46, 116]. The formulas are valid between $0.5 < a/H < 5$.

TE_{01δ} Mode:

$$Q = 0.078192\varepsilon_r^{1.27} \left(1 + 17.31 \left(\frac{h}{a} \right) + 21.57 \left(\frac{h}{a} \right)^2 - 10.86 \left(\frac{h}{a} \right)^3 - 1.98 \left(\frac{h}{a} \right)^4 \right) \quad (2.9)$$

TM_{01δ} Mode:

$$Q = 0.00872\varepsilon_r^{0.888413} e^{0.0397475\varepsilon_r} \left(1 - \left(0.3 - 0.2 \frac{a}{h} \right) \left(\frac{38 - \varepsilon_r}{28} \right) 10.86 \left(\frac{h}{a} \right)^3 \right) X \left(9.498186 \frac{a}{h} + 2058.33 \left(\frac{a}{h} \right)^{4.322261} e^{-3.50099 \left(\frac{a}{h} \right)} \right) \quad (2.10)$$

HE_{11δ} Mode:

$$Q = 0.01007\varepsilon_r^{1.3} \frac{a}{h} \left(1 + 100e^{-2.05 \left(\frac{a}{2h} - \frac{1}{80} \left(\frac{a}{h} \right)^2 \right)} \right) \quad (2.11)$$

The equations for the resonant frequency and Q-factor of the TE_{01δ}, TM_{01δ}, and HE_{11δ} modes offer a good starting point for the design of cylindrical DRAs.

2.6.2 Rectangular DRAs.

The DRA is determined the radiation Q-factor for rectangular using, its total stored energy W and radiated power P_{rad} must be determined. The final expressions for the total stored energy W and the radiated power P_{rad} are [50]:

$$Q = \frac{2\omega W_e}{P_{rad}} \quad (2.12)$$

where P_{rad} and W_e are radiated power and the stored energy, respectively.

These quantities are given by:

$$W_e = \frac{\epsilon_0 \epsilon_r \omega b d A^2}{32} \left(1 + \frac{\sin(k_z d)}{k_z d} \right) (k_x + k_y) \quad (2.13)$$

$$P_{rad} = 10k_0^4 |P_m|^2 \quad (2.14)$$

where P_m is the magnetic dipole moment of the DRA:

$$P_m = \frac{-j\omega 8\epsilon_0(\epsilon_r - 1)A}{k_x k_y k_z} \sin(k_x d/2) \hat{x} \quad (2.15)$$

The normalised Q-factor (Q_e) defined as:

$$Q_e = \frac{Q}{\epsilon_r^{3/2}} \quad (2.16)$$

2.7 Conclusions

Several DRAs have been presented in terms of their design configurations, resonance modes, and operational spectrum bandwidth and radiation efficiencies. It was concluded that the characteristics of the DRAs were well-motivated to many mobile and wireless communications applications that covering a wide range of bandwidth/s with acceptable antenna performances. It was observed that certain designs of DRAs could be found as single element or array configuration including that they could provide suitable wave polarization, frequency and pattern reconfigurations with the edition of simple excitations and feeding network techniques. It was noticed that the printed excitation methods were interested compared to attached (i.e., probe feed) or embedded inside the DR. On top of that the simplicity of applying the resonance modes or well-defined DRs Structures to adjust the required excitation. This is clearly explained on how one can apply such rules in estimating the hybrid modes for example to a wide DRA design principles.

On the basis of the above it was confirmed the uniplanar printed feeding networks for one or multi DRs Structures were interested for so many applications; in addition to its integration simplicity to various DRs and many applications. It was also shown that quite possible to excite and control hybrid

modes for wide operational bandwidth. The following chapters were applied such principles design procedures with new added values in terms the size, DR structures, feeding network, and notch frequency bands. The new design antennas provide the state of the art of the main contribution of the present work in this thesis.

CHAPTER 3

BROADBAND DIELECTRIC RESONATOR ANTENNA (DRA) DESIGN FOR MOBILE WIRELESS APPLICATIONS

3.1 Introduction

In the last decade, the rapid evolution of wireless communication systems has stimulated the development of the mobile handset in terms of hardware and software, which has led to a diversification of its applications. Hence, today, the mobile handset is not only a handheld transceiver, it is also a portable mini-computer offering all the required applications.

To keep abreast with this progression, the mobile manufacturers are seeking new antenna technologies to cater for this demand. In general, the next generation antennas are expected to provide effective broadband matching, an acceptable gain and consistent radiation patterns throughout the designated frequency bands and operate within a small enclosure. Therefore, bandwidth

enhancement and size miniaturisation are the challenging tasks for the modern antenna designer.

Dielectric resonator antennas (DRAs) have gained immense attentions from the antenna designer due to the advantages of zero conductor loss, low profile, compactness, high radiation efficiency and not suffering from surface-wave losses [12, 117, 118]. However, conventional DRAs have inherently narrow bandwidth [19]. In order to enhance the impedance bandwidth of the antenna, several methods have been proposed in the published literature [23, 30, 87, 119, 120], including implementing multilayers of different dielectric materials[23], and modifying the shapes of DR and introducing new feeding mechanisms [30, 87, 119-121]. These published results have demonstrated that the impedance bandwidth can be further enhanced to the range from 25% to 70% for a return loss better than 10 dB.

In this chapter, a crescent-shaped printed monopole antenna incorporating a high permittivity defected cylindrical dielectric resonator to form a DRA antenna, has been designed, analysed and characterised. By adopting the crescent-shaped feeding structure to excite the DR, this antenna achieves a broadband impedance bandwidth covering the current frequency band allocations from 1.15 GHz to 6 GHz. The overall dimensions of this antenna, including the ground size (i.e. equivalent terminal size) are $57 \times 37.5 \times 5.8 \text{ mm}^3$.

3.2 Antenna Design Concept and Structure

The antenna geometry is given in Figure 3.1. As can be seen, this antenna is formed by a printed monopole antenna and a defected cylindrical dielectric resonator. The top and bottom views of the printed monopole antenna are shown in Figure 3.1 (a) and (b). The monopole antenna is very similar to the previous work as in [122]. It consists of a crescent shaped radiator which is fed by a $18 \times 1 \text{ mm}^2$ 50Ω microstrip line and a defected L-shaped ground plane.

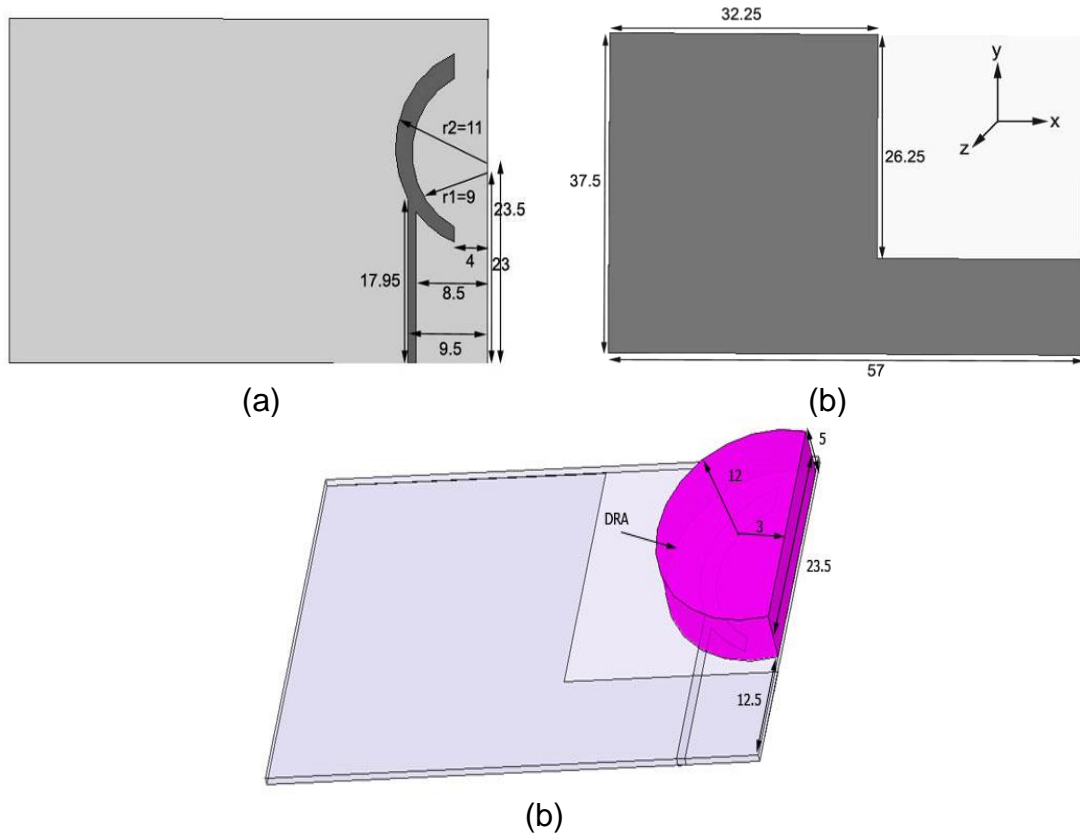


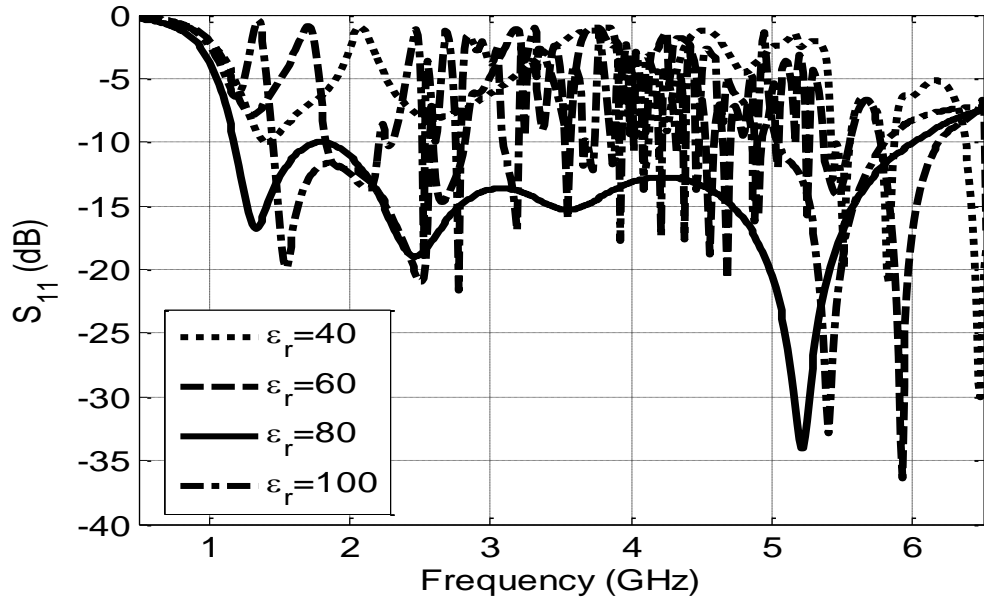
Figure 3.1: Geometry of the proposed antenna. (a) Top view, (b) Bottom view, and (c) Dielectric resonator on the printed antenna.

The total size of this monopole antenna is about $57 \times 37.5 \text{ mm}^2$. FR4 epoxy is used as the substrate throughout this printed structure, with thickness of 0.8mm, and the dielectric constant (ϵ_r) is assumed to be uniformly 4.4, with a loss tangent of 0.017 over the target range. Shows the proposed high permittivity ($\epsilon_r = 81$) cylindrical DR, which has radius $a = 12\text{mm}$ a height $h = 5\text{mm}$ and a circular segment has been removed at $w = 23.5\text{mm}$, $l = 3\text{mm}$. This DR is placed on the top of the crescent shaped radiator of the monopole printed structure. By exciting the resonant modes of the DR, the wider impedance bandwidth can be attained.

3.3 Parametric Design Study

This parametric study is useful because it provides a comprehensive picture of the antenna's characteristics and allows understanding of the influence of the DR geometry parameters on the return loss of the antenna. Two geometric parameters including the height and the permittivity of the DR were analysed in this study. The Finite element based simulator (Ansoft HFSS [123]) is used to carry out this analysis. In Figure 3.2, showing the simulated return loss for different antenna heights, a -10dB return loss bandwidth of the antenna is achieved from around 1.17 GHz to 6 GHz.

By gradually increasing the permittivity of the DR from 40 to 100 by increments of 20, it can be seen that when the permittivity of 80 is adopted, the best broadband impedance response can be achieved. However, when other values are used, the impedance bandwidth response deteriorates. It can be seen in Fig. 2(b) that the height of the DR is varied from 3mm to 9 mm with 2mm increments; these values were chosen arbitrarily to fit within the required envelope size; the optimal values for h_1 and h_2 were found to be 3 mm and 5mm, respectively. Through this parametric study process, a set of optimal geometry parameters for the DR can be easily identified.



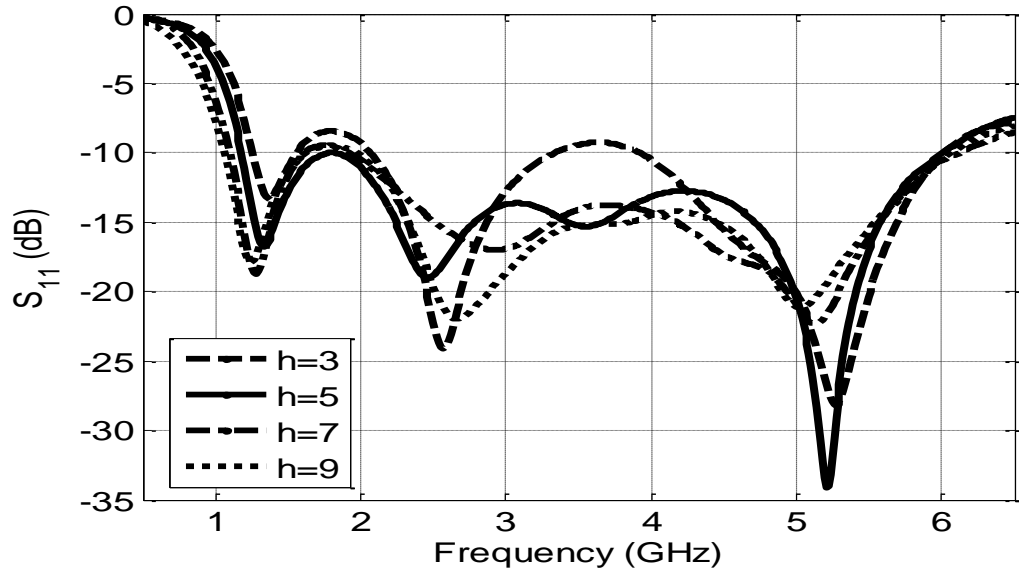


Figure 3.2: Simulated return loss corresponding to the variation parameters of: (a) permittivity of the DR and (b) height of the DR.

3.4 Result and Discussion

The simulated and measured return loss of the proposed antenna with and without the presence of the DR on the antenna structure is shown in Figure 3.3. As can be noticed, when the DR is not adopted in the antenna model, the impedance bandwidth only encompasses the 1.7 GHz to 3.1 GHz frequency spectrum, which corresponds to 58.3 % bandwidth at a centre frequency of 2.4 GHz, for return loss better than 10 dB. However, when the DR is introduced to the antenna model, the impedance can be further extended from 1.15GHz to 6GHz which is equivalent to an impedance bandwidth of 135.7 % at a centre frequency of 3.58 GHz.

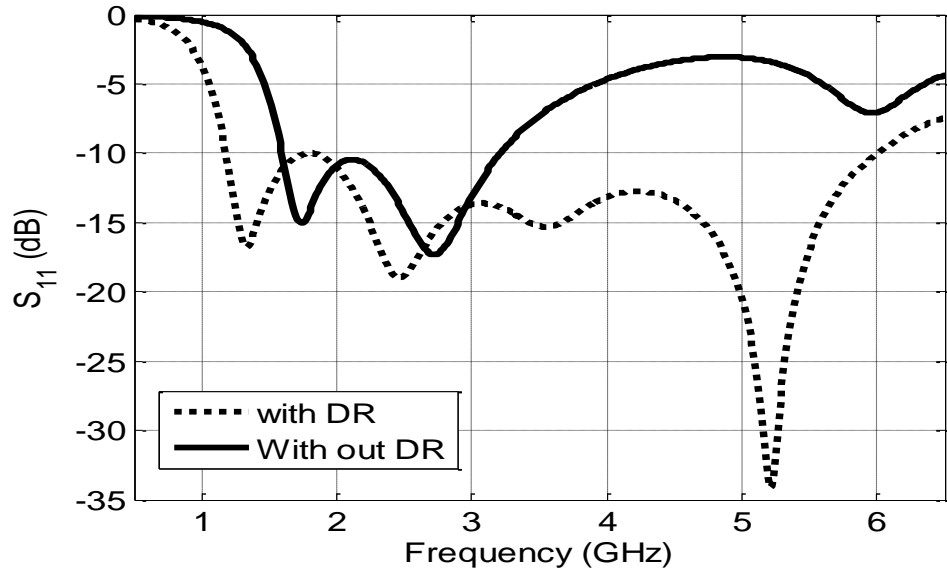


Figure 3.3: Return loss of proposed antenna with and without DR.

The prototype sample of dielectric resonator antenna (DRA) is shown in Figure 3.4 and Figure 3.5 shows the typical measured and computed antenna performance in terms of the impedance bandwidth. It may be clearly seen that the two adjacent resonant frequencies in the range of 1.15GHz and 6.0GHz at $|S_{11}| \leq -10$ dB. It is worth noting that this prototype's impedance bandwidth is 4.85GHz, or equivalently 135.7 % with respect to the centre frequency of 3.58 GHz.

This indicates that the antenna can operate for most of the existing wireless standards, including DCS (1710-1880MHz), PCS (1850-1990MHz), UMTS (1920-2170MHz), and the Industrial, Scientific and Medical (ISM) band (2400-2485MHz), IEEE 802.11 a/b/g.

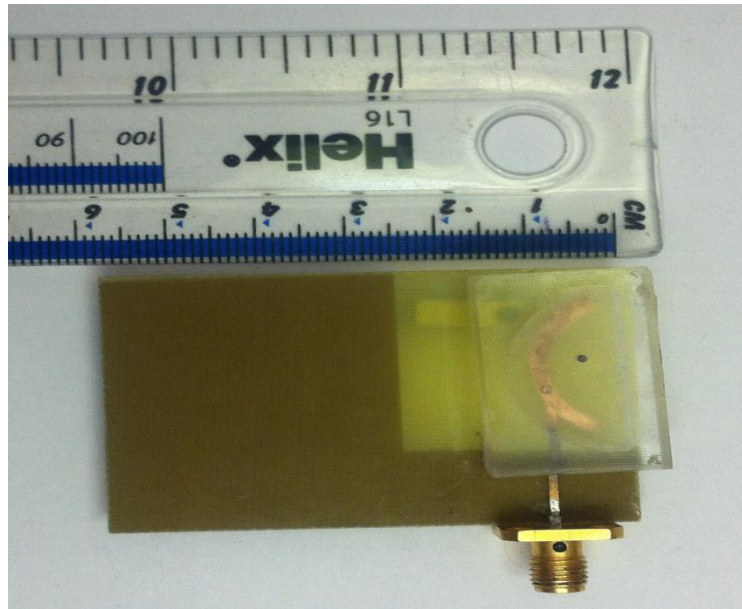


Figure 3.4: Prototype antenna

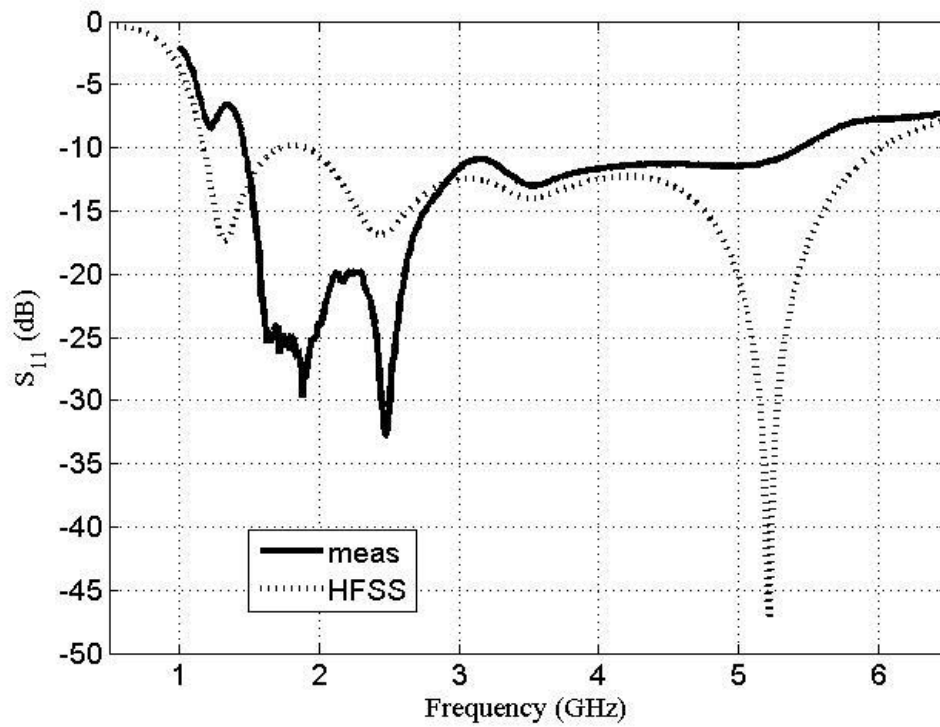


Figure 3.5: Measured and simulated reflection coefficient $|S_{11}|$

Both simulated and measured gains with and without the DR are depicted in Figure 3.6. The maximum simulated gains of proposed antenna without the DR were found to be between 0.7 and 3.1 dBi within the operating spectrum band, while the maximum simulated gains of the proposed antenna with DR were varied between 1.1 and 4.4 dBi within the broadband operating spectrum band.

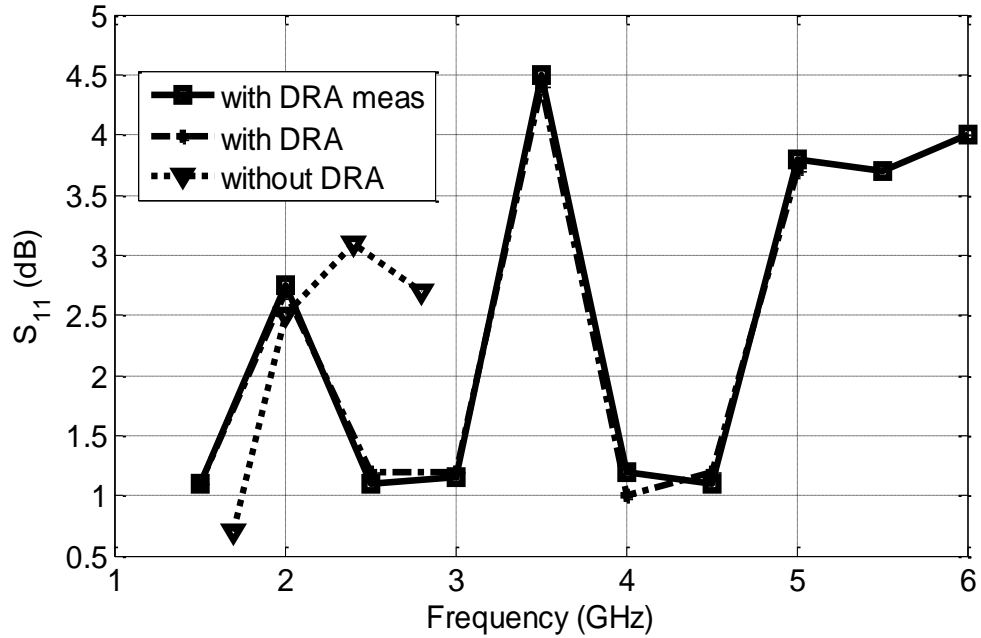


Figure 3.6: Simulated and measured gains of the proposed antenna with and without DR

The simulated and measured far field radiation patterns of the proposed antenna are presented in Figure 3.7. Two pattern cuts (the xz and xy planes) were taken at three selected operating frequencies which cover the aggregate bandwidth. The radiation patterns were found to stable and consistent at all the

designated frequencies. Significantly, it also indicates that the maximum co-polarized component appears at the direction of boresight (+z) for both the E and H planes.

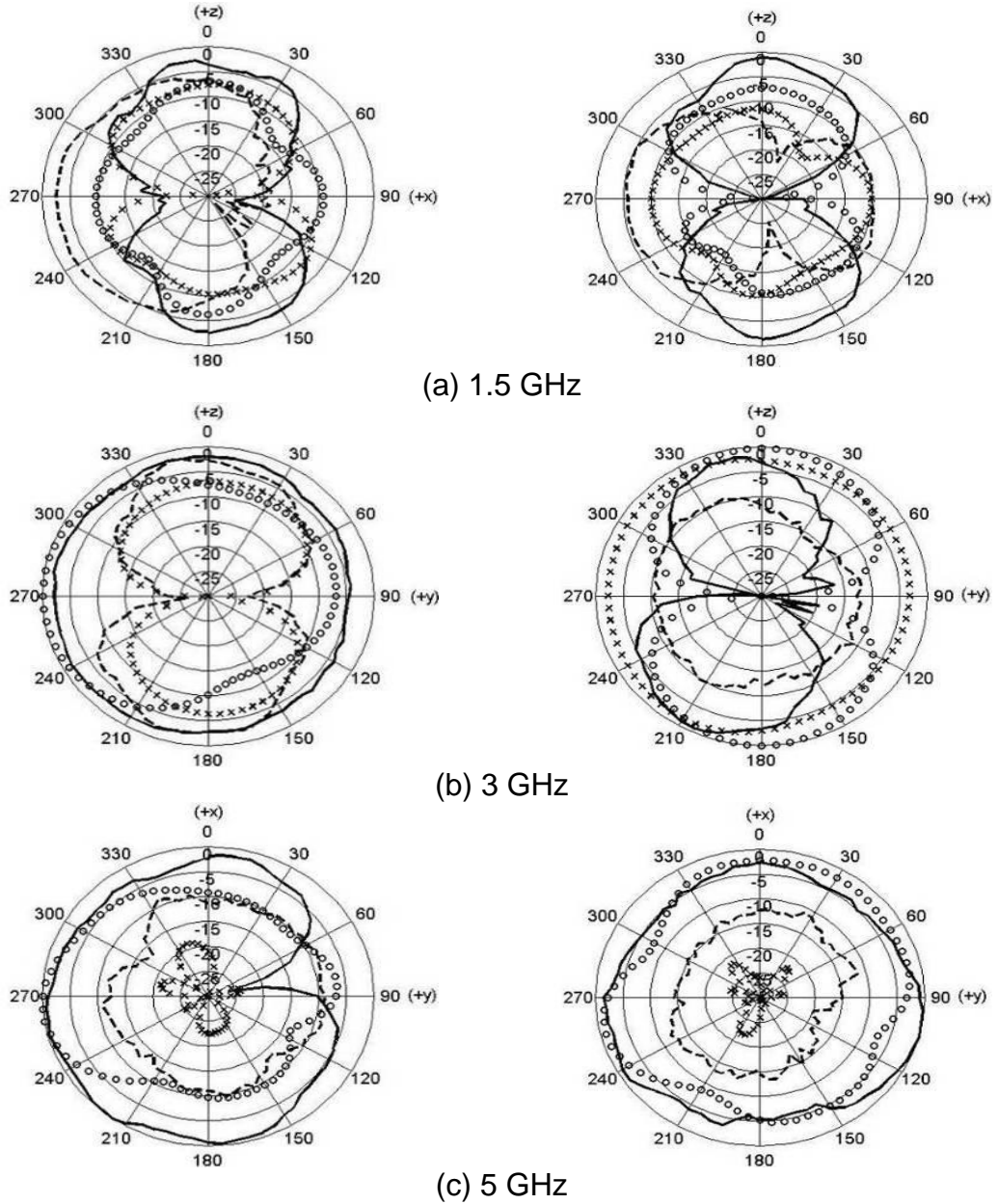


Figure 3.7: Simulated and measured normalised radiation patterns of the proposed antenna for three planes ((a): x-z plane, (b): y-z plane, (c): x-y plane) at (i) 2100 MHz (ii) 2800 MHz xxx' simulated cross-polarization 'oooo'

simulated co-polarization '----' measured cross-polarization '—' measured
co-polarization

3.5 Conclusions

In this chapter, a low-profile multi-frequency band DRA antenna has been presented. The prototype antenna structure has shown a relative bandwidth of 135.7% and an average gain of 2.2 dBi over the frequency interval from 1.15 GHz to 6.0 GHz at return loss better than 10 dB. The radiation pattern is of a broad-beam type, of approximately dumbbell shape, that is appropriate for a mobile terminal application. The antenna size was optimized at $57 \text{ mm} \times 37.5 \text{ mm} \times 5.8 \text{ mm}^3$, which is suitable for integration with a variety of mobile terminals operating over DCS, PCS, UMTS, Bluetooth and IEEE 802.11a/b/g wireless standards.

It follows from such DRA design the feeding networks could play the main role of the resonance modes of the DR, thus new design procedure was implemented to achieve wide spectrum bandwidth by reconfigure the feeding striplines to the DR.

CHAPTER 4

DIELECTRIC RESONATOR ANTENNA DESIGN FOR UWB APPLICATIONS

4.1 Introduction

Dielectric resonator antennas (DRA) have been investigated over a significant period of time for a variety of wireless communications systems [117, 118, 124]. Typically DRAs are fabricated from low-loss dielectric material, for which the resonant frequency is predominantly a function of size, shape and permittivity. DRAs may offer the advantages of small size, low profile lightweight constructions, and high radiation efficiency, making them attractive candidates for a number of wireless applications [19, 23]. A recent trend for DRA design has been in meeting UWB specifications in high data rate wireless LANs, as well as the remarkable established applications in radar and imaging systems [30, 87, 119-123]. Various bandwidth enhancement techniques have been applied within the DRAs using different excitation mechanisms to excite several modes covering wide bandwidth.

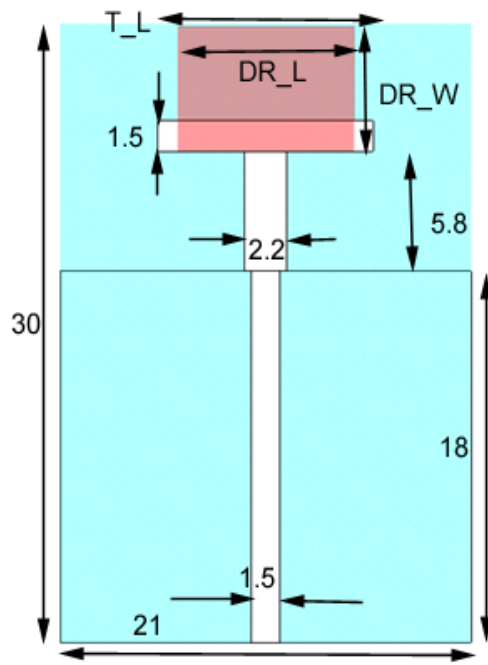
In this chapter, a small dielectric resonator antenna has been designed and characterized for UWB uses. By adopting a modified T-shaped feeding structure

to excite the DR, a wide broadband impedance bandwidth from 3100 MHz to 5500 MHz can be obtained, covering the body area network (BAN) frequencies as well as the IEEE 802.11a WLAN frequencies. The overall dimensions of this antenna, including the ground plane (i.e. equivalent terminal size) are $30.0 \times 21.0 \times 0.8$ mm³ which is small enough to be adopted in many mobile/wireless enclosures.

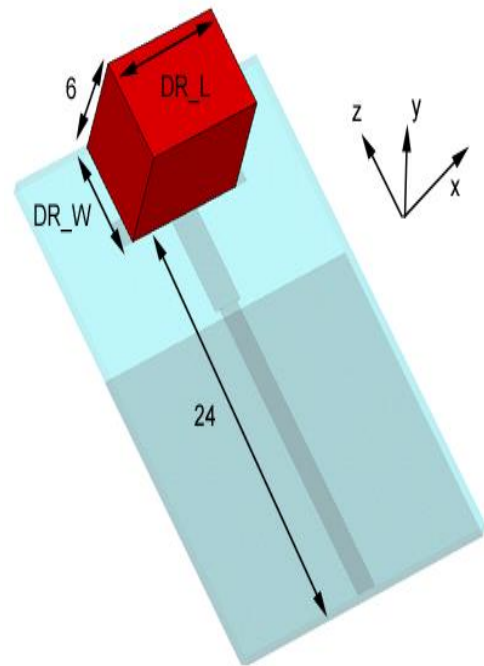
4.2 The Antenna Design Concept

For this design, the target frequency band is the lower UWB band which is from 3.1 to 4.9 GHz. In order to achieve this target, the dimensions of the ceramic block must cut for the dominant mode to be commensurate with this requirement. A dielectric constant of 9.4 was selected based on the available material in the research laboratory. The dimensions for the ceramic block were optimized and analyzed from simulation package. This will ensure the desired mode of the DR is excited. Three design goals including the impedance bandwidth, realized gain and radiation patterns were considered in the optimization process. However, by weighting these three objectives in the cost function of the optimization process, a tradeoff between the wide bandwidth and radiation performance has been compromised.

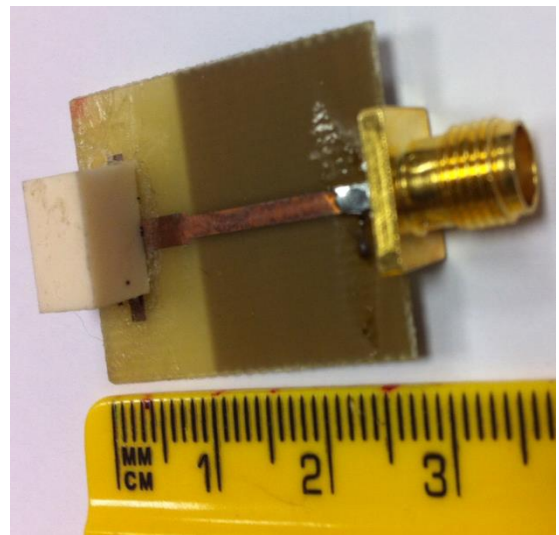
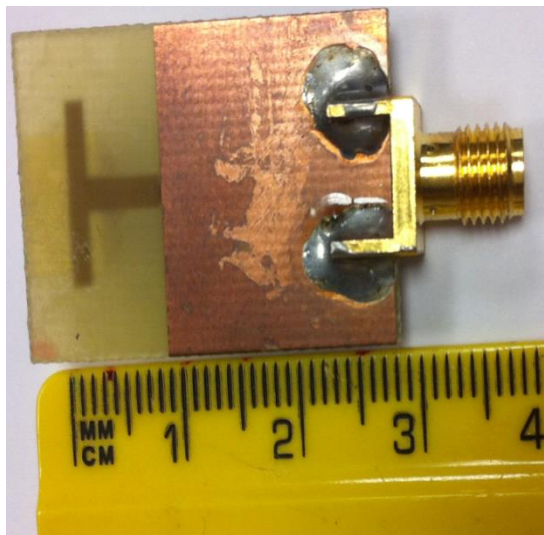
The proposed antenna geometry is shown in Figure 4.1. The radiator is a rectangular ceramic block with dimensions 6.00 mm × 9.00 mm × 6.00 mm. A 0.8 mm thick FR4 substrate with relative permittivity of 4.5 is used in the construction. The total PCB size has being 30.0 mm × 21.0 mm. The antenna ground plane is partially printed on the FR4, and has optimized dimensions of 18 mm × 21.0 mm, and a feed line of 18 mm × 1.5 mm track is printed on the substrate to realize a 50 Ω microstrip line. At the end of the 50 Ω , a T-shaped element is used to excite the DR. This element plays significant role in controlling the impedance matching and width bandwidth response. To understand the contribution of the DR, Figure 4.2 shows the $|S_{11}|$ of the proposed antenna with and without the DR; as can be clearly seen, without the DR the antenna only operating from 3.7 GHz to 5.8 GHz. When the DR is introduced to the antenna structure, this operating band is shifted to 3.1 to 5.5 GHz. This enables the antenna to operate at the lowest UWB operating frequency (3.1 GHz) and providing a further 300 MHz bandwidth enhancement.



(a) Top view



(b) Auxiliary view



(c) Antenna prototype

Figure 4.1: Basic antenna geometry model

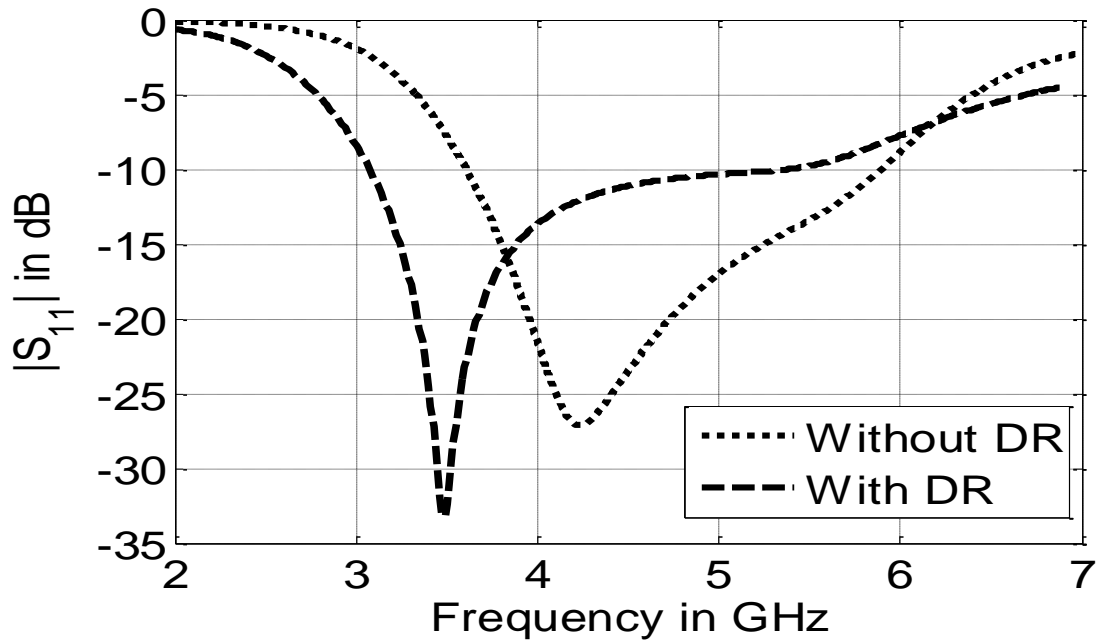


Figure 4.2 Simulated $|S_{11}|$ of the proposed antenna with and without dielectric resonator (DR).

4.3 Parameter Study

A parameter study is needed to understand the antenna return loss as a function of the DRA geometry. Three sensitive parameters, i.e. DR_W, DR_L and T_L, were taken into account in this study, as shown in Figure 4.1. Initially, each simulation run was set up with one variable structure parameter and the default value of DR_W, DR_L and T_L are 6 mm, 9 mm and 11 mm respectively. In this analysis, the target operating frequency band and idea performance is 3.1 GHz to 4.9 GHz at a reflection coefficient $|S_{11}|$ better than -10 dB.

Figure 4.3 illustrates the three analyzed geometry parameters. As can be observed, by changing of the length of the dielectric resonator (DR_L) from 4 mm to 8 mm with increment of 2 mm, the operating frequency band gradually moves to the lower band and meeting the design goal. Further increasing DR_L to 10 mm will impair the impedance matching at the higher operating frequency band.

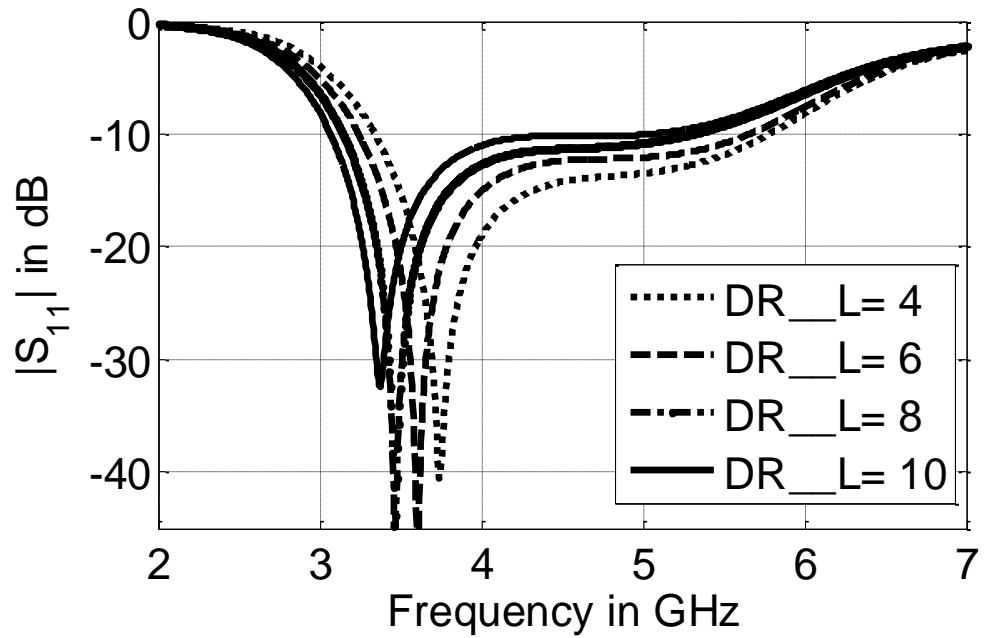


Figure 4.3 Simulated $|S_{11}|$ corresponding to the variation parameters of Length of DR (DR_L).

Interestingly, the variations of the $|S_{11}|$ show the similar changes, as gradually increasing DR_W from 2 to 8 mm, as depicted in Figure 4.4. For the best performance of the antenna, it is suggested that DR_L should be chosen between 8 to 10 mm, whereas DR_W should be selected between 6 to 8 mm.

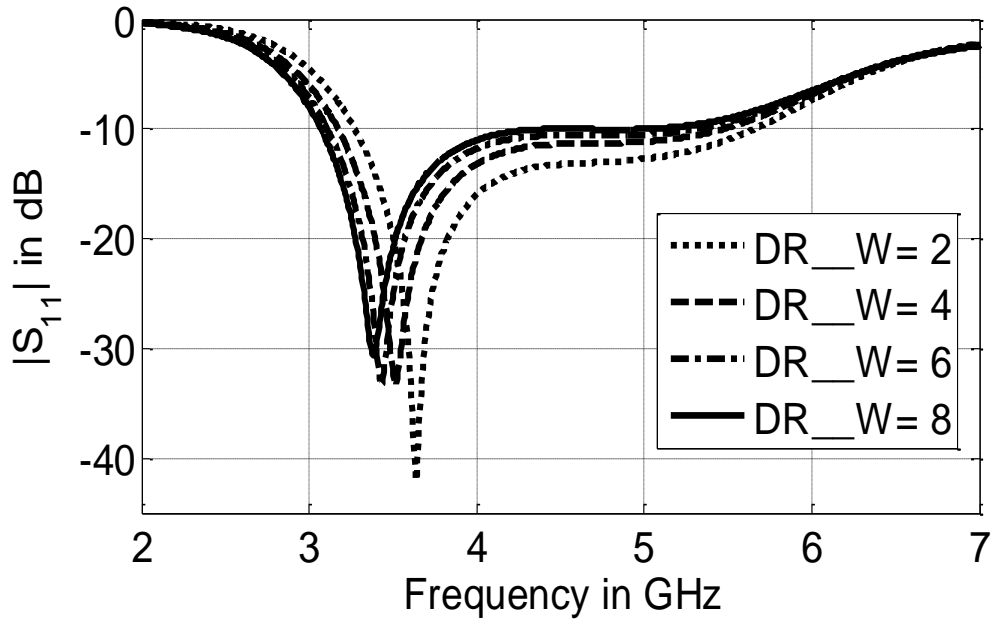


Figure 4.4: Simulated $|S_{11}|$ corresponding to the variation parameters of Width of DR (DR_W).

Figure 4.5 plots the influences of the T_L parameter on the $|S_{11}|$ of the proposed antenna. As can be noticed, T_L needs to be adjusted to an optimum value in order to achieve the desired operating performance. It is clear that extending the T_L value from 6 to 10 mm, the initial lower and upper cut off frequencies of the band are shifted to the lower band while maintaining a good impedance matching bandwidth. As further increasing this parameter to 12 mm, the impedance matching at the higher frequency band deteriorates

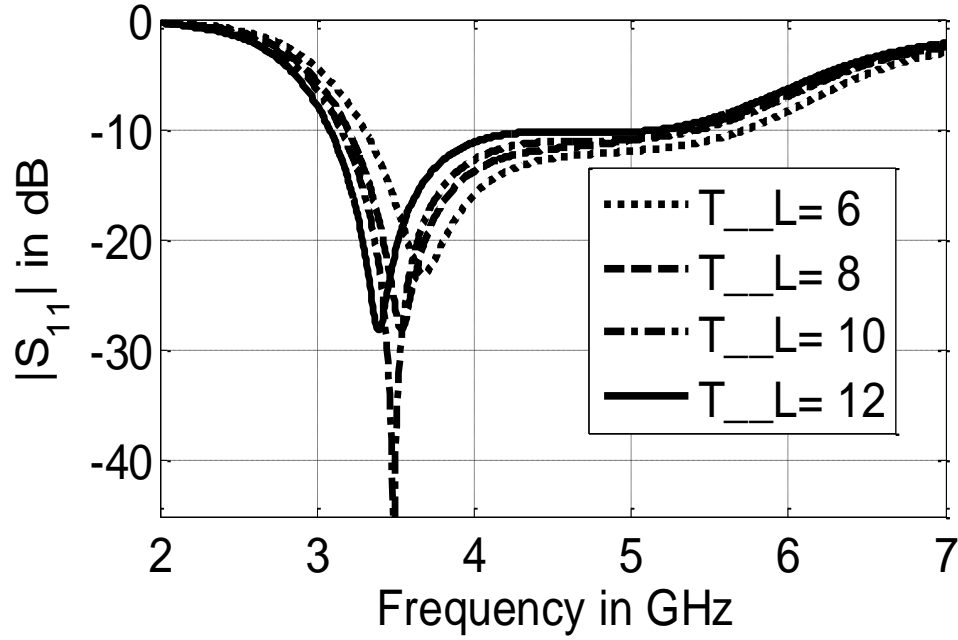
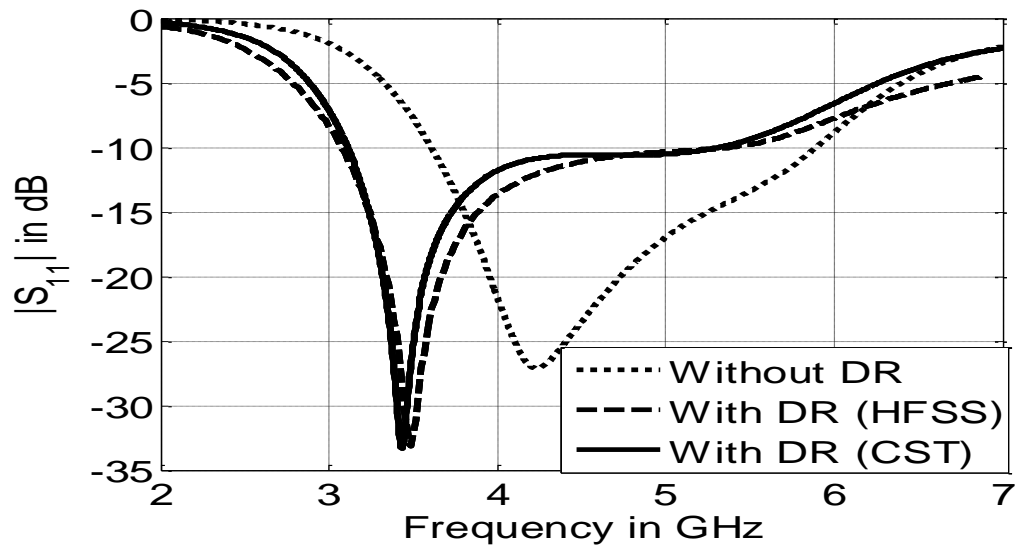


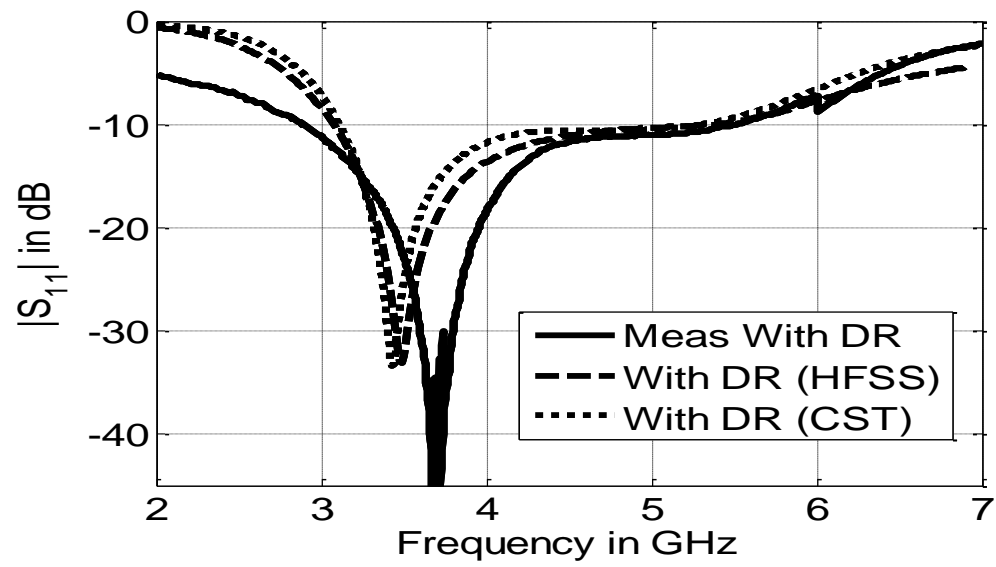
Figure 4.5 Simulated $|S_{11}|$ corresponding to the variation parameters of Length of T-strip (T_L).

4.4 Results and Discussion

In order to validate the measured and simulated results, two software packages, i.e. ansoft HFSS and CST, were used for comparison. The obtained reflection coefficient $|S_{11}|$ of the proposed antenna from these packages are shown in Fig.4. It should be noted that 9 mm, 6 mm, 11 mm for DR_L , DR_W and T_L , were selected in the design model. As can be seen, the antenna is operating from 3.1 to 5.5 GHz at the reflection coefficient $|S_{11}|$ better than -10 dB. This is equivalent to 55.8 % relative impedance bandwidth and corresponding to 2.4 GHz.



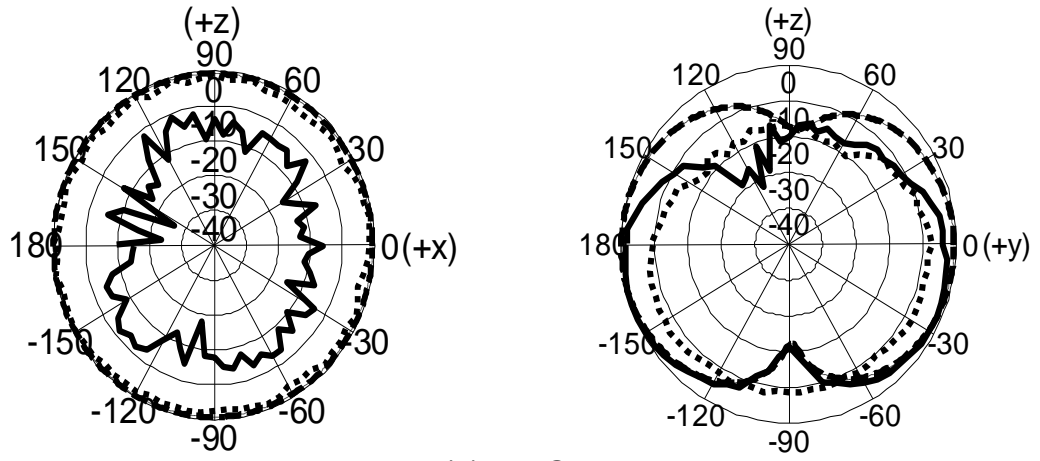
(a)



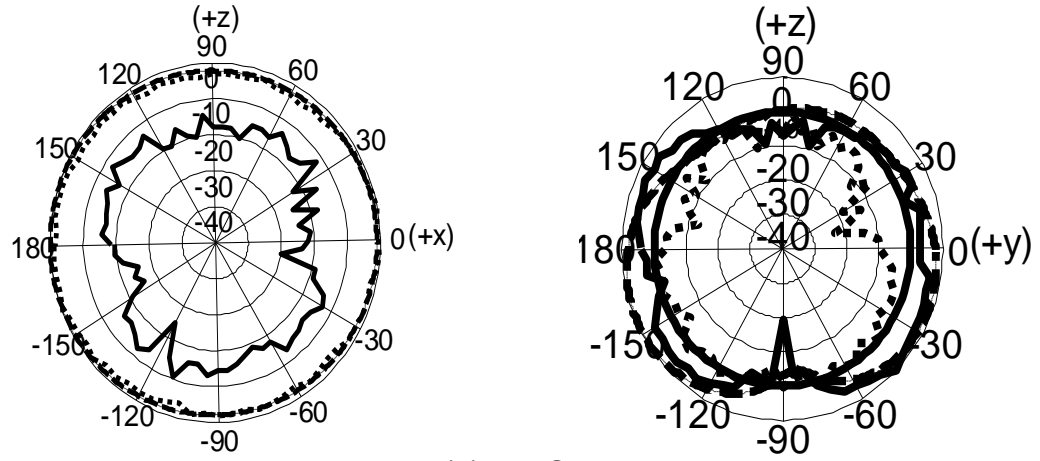
(b)

Figure 4.6: Verification of the predicted $|S_{11}|$ by (a) using two software with without DR and by (b) using two software with measured.

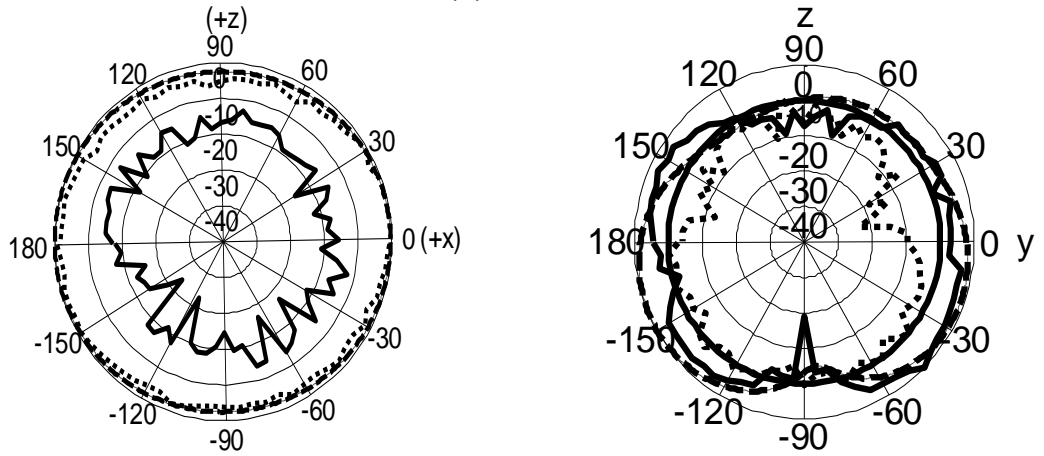
The far-field radiation patterns measurements of the prototype antenna were carried out in an anechoic chamber using an elevation-over-azimuth positioner, with the elevation axis coincident with the polar axis ($\theta = 0^\circ$) of the antenna's coordinate system. The fixed transmitting antenna was a broadband horn (EMCO type 3115) positioned 4 m from the antenna being tested. The azimuth drive thus generates cuts at constant ϕ . The azimuth positioner was rotated from $\theta = -180$ to 180 at increments of 5 for the selected measurement. Two patterns cuts, $\phi = 0^\circ$ and 90 , were taken at two selected operating frequencies for which the matching was optimal. Figure 4.7 shows the simulated and measured normalized radiation patterns is also plotted at two planes, i.e. E-plane (XZ- plane) and H-plane (XY-plane). Three operating frequencies, i.e. 3.1 GHz, 4.5 GHz and 5.5 GHz, were chosen to cover the entire operating band. As can be clearly seen, the antenna exhibits consistent onmi-directional patterns across of the operating band. It should be highlighted that the simulated gains and radiation efficiencies are (2.3 dBi, 2.9 dBi, 4.2 dBi) and (80%, 90%, 78 %) at these three given frequencies.



(a) 3.1 GHz



(b) 4.5 GHz



(c) 5.5 GHz

Figure 4.7: Simulation and measurement of radiation patterns of the proposed antenna for two planes: xz-plane (E-plane) and xy plane (H-plane).

4.5 Conclusions

A small quasi-omni-directional dielectric resonator antenna has been proposed for the lower UWB band, which is suitable for a variety of body area network and IEEE802.11a/WiMAX applications. The antenna is constructed from a low permittivity ceramic as a rectangular block, with microstrip feed and broadband matching lines on FR4. The radiation patterns were quite stable with an average gain of around 3dBi covering the lower UWB spectrum bandwidth. The radiation efficiency was reasonable over the total bandwidth and do confirm the advantage of using such antenna structures.

The idea learned for this chapter, that it could be possible to apply aperture feeding with different structure configuration to improve the bandwidth through exciting various modes of one or two DRs.

CHAPTER 5

APERTURE-COUPLED ASYMMETRIC DIELECTRIC RESONATORS ANTENNA FOR WIDEBAND AND BROADBAND APPLICATIONS

5.1 Introduction

Since the first proposal in 1983 [124], dielectric resonator antennas (DRAs) have received increasing interest due to their many attractive features, such as high radiation efficiency, smaller size, the freedom to design their shape (rectangular, cylindrical, spherical, etc.) and their ability to use different feeding structures, for example probe, microstrip line, slot or coplanar line. However, one major drawback of the DRA is the limited bandwidth. For a single-mode excitation, the bandwidth is often below 10%, which is not sufficient for many wideband applications. To overcome this limitation, various bandwidth enhancement techniques have been developed, over the last few decades. One approach is to utilize different features of the dielectric resonators (DRs), such as structures of high aspect ratio [125], stacked multiple DR with different

materials to merge multi resonance operation [40, 81], and inserting an air gap in the DR to lower the Q-factor [76, 121]. In [126] a single cylindrical DR is excited by two crossed slots. The centres of the two slots are set at different positions and taking into consideration the partial independence of the slot modes from the DRA mode, wider band was attained.

In this chapter, a novel wideband slot-fed asymmetric dielectric resonator antenna is presented. A pair of cylindrical DR's is placed adjacently and asymmetrically with respect to the feeding rectangular aperture. A single slot here feeds the two DR's in such a way where more design freedom can be obtained, as the two DRA's can resonate at slightly different frequency resulting in wider band. By optimizing the design parameters have been optimised in which an impedance bandwidth of about 29%, covering the frequency range from 9.62GHz to 12.9 GHz, and a gain of 8dBi are obtains. Design details of the proposed antenna and the results of both simulation and experiment are presented and discussed.

5.2 Antenna Design Concepts and Structure

The geometry of the proposed asymmetric wide band antenna is illustrated in Figure 5.1. The prototype antenna is fabricated on 30mm × 25mm FR4 substrate with relative permittivity of $\epsilon_{rs}= 4.5$, a loss tangent of 0.017, and

thickness $t = 0.8$ mm. The feed microstrip line is placed symmetrically with respect to the coupling aperture.

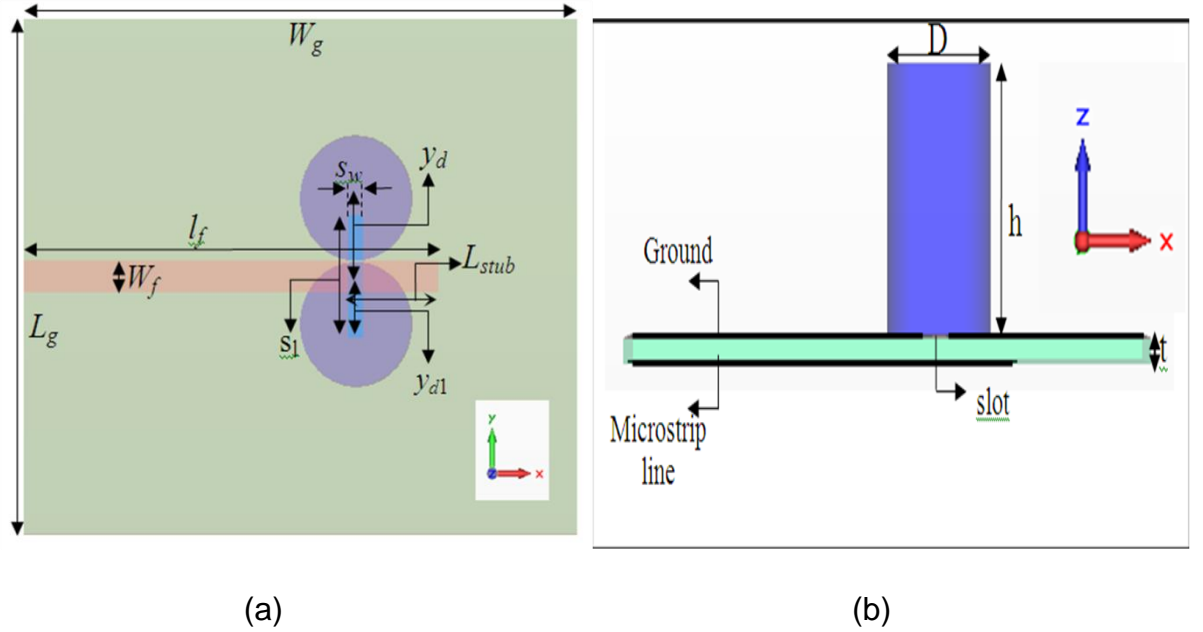


Figure 5.1: Aperture-coupled asymmetric dielectric resonator antenna (a) top view and (b) side view with design dimensions and parameters.

The microstrip line dimensions were calculated using empirical formulas given in [126] resulting in length $L_f = 22.5$ mm and width $W_f = 1.5$ mm. A rectangular aperture (slot) of length S_l and width of S_w is etched on the ground plane. The dimensions of the aperture influence the resonant frequency of the structure and the amount of the undesired radiation in the back direction of the antenna. They also determine the coupling between the radiating DR's and the microstrip line. At the end of feed line, there is a 'stub' of length L_{stub} as shown in Figure 5.1. If the slot is modelled as shunt impedance connected to the feed line, then

the stub can be visualized as a reactance canceller. Practical experience [127] has shown that the stub length should be close to $\lambda_g/4$, and optimization started from this point. An alumina material of alumina-96pct, with $\epsilon_{rd} = 9.4$, diameter $D = 6\text{mm}$ and a height $h = 9\text{ mm}$ is used for the DR structure. The two DRs are offset-placed from the centre of the slot ($y_d \neq y_{d1}$) as shown in Figure 5.1 (a).

The resonant frequency of a single segment CDRA excited in $HE_{M11\delta}$ mode can be as [51],

$$f_{r2} = \frac{c}{2\pi a \sqrt{\epsilon_{rdr}}} \left[1.71 + 2 \left(\frac{a}{2h} \right) + 0.1578 \left(\frac{a}{2h} \right)^2 \right] \quad (5.1)$$

where $a = D/2$, D is the diameter of CDRA, c is the velocity of light, h is the height of the CDRA above ground plane, and ϵ_r is the relative permittivity of CDR material. For the dimensions of the CDR described above of $D = 6\text{mm}$, $h = 9\text{mm}$, $\epsilon_r = 9.4$, the calculated resonance frequency according to Eq. 5.1 was found to be 10.63GHz . The slot length and the permittivity's of the substrate including the DRA determine the frequency of the slot resonance. The DRA modes depend on the DR dimensions, permittivity, as well as the feeding mechanism. Since the two DRA's are asymmetrically located with respect to the slot, then two nearby resonance frequencies are excited leading to wide band operation.

5.3 Parametric Study

The parametric study using Ansys HFSS allows the influences of various parameters on the response of DRA antenna to be investigated[123].

Figure 5.2, shows the simulated reflection (S_{11}) a coefficient as function of frequency for various slot lengths S_l . As the aperture length is reduced, the input resistance of the antenna decreases.

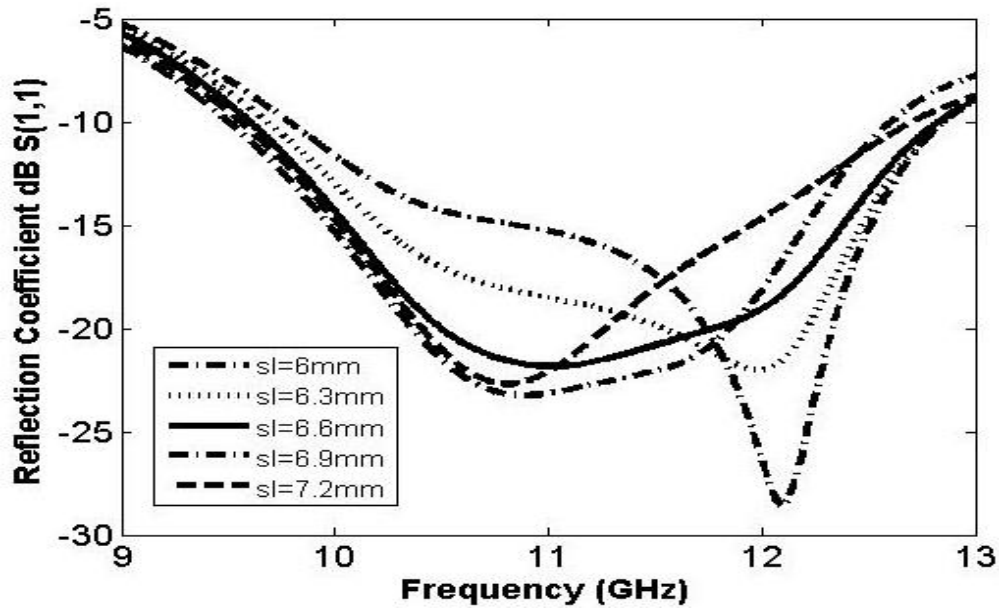


Figure 5.2: Simulated reflection coefficient as a function of frequency for different slot lengths S_l with $S_w=1.1\text{mm}$, $L_{\text{stub}}=4\text{mm}$, $y_d=3.75\text{mm}$, $y_{d1}=-2.1\text{mm}$.

This might be thought of as decreasing the coupling factor between the feed line and the antenna. The slot length also affects the coupling to the DR, and this can be seen from the fact that best matching is obtained for slot length of S_l

= 6.6mm. This analysis shows that slot length mostly affects both the reflection coefficient and the resonant frequency, but it slightly affects the impedance bandwidth of antenna as well.

Figure 5.3 shows the simulated reflection coefficient of the DRA with slot width S_w varied from 0.6mm to 1.4mm. It is clear that the optimum impedance bandwidth is achieved at slot width of $S_w=1.2$ mm.

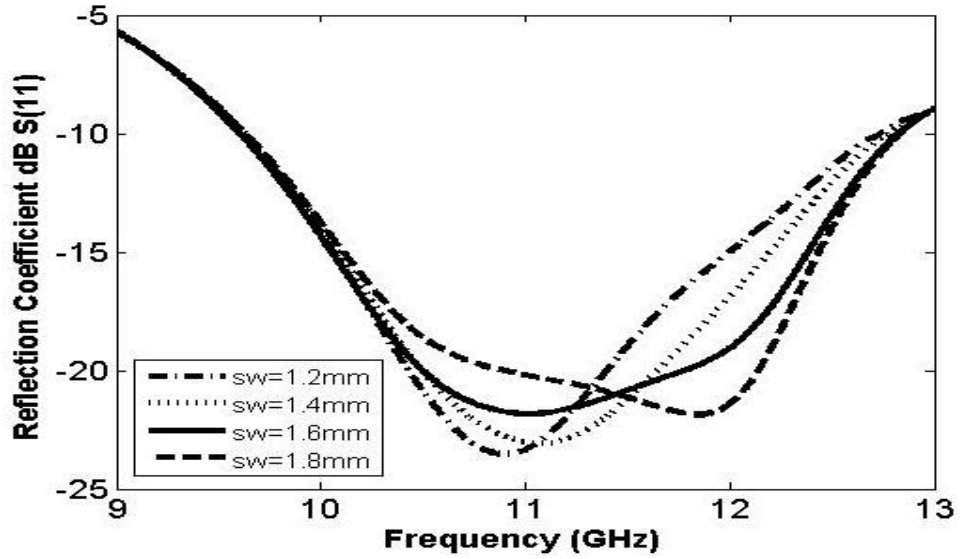


Figure 5.3: Simulated reflection coefficient as a function of frequency for different slot widths S_w with $S_l=6.6$ mm, $L_{stub}=4$ mm, $y_d=3.75$ mm, $y_{d1}=-2.1$ mm.

Figure 5.4 shows the effect of the stub length L_{stub} , where it is clear that tuning the stub length can affect the bandwidth and matching of the resonant modes. The design is optimized at $L_{stub} = 4$ mm, a value close to the estimated one of $\lambda_g/4 = 4.08$ mm.

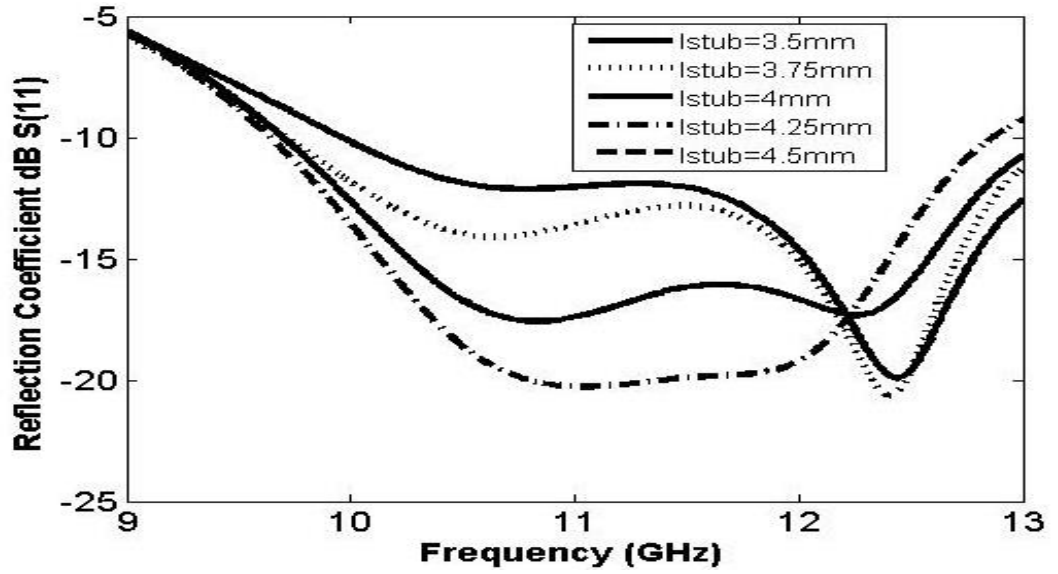


Figure 5.4: Simulated reflection coefficient as a function of frequency for various stub lengths l_{stub} with $s_l=6.6\text{mm}$, $s_w=1.2\text{mm}$, $y_d=3.75\text{mm}$, $y_{d1}=-2.1\text{mm}$.

The effects of asymmetric location of the two DR's were investigated by moving one of the DR's along the length of the slot. The results obtained by moving the upper DR are shown in Figure 5.5, where it can be seen that the position of the DR affects the bandwidth and matching. A good compromise has been obtained for the position $y_d = 3.75\text{ mm}$.

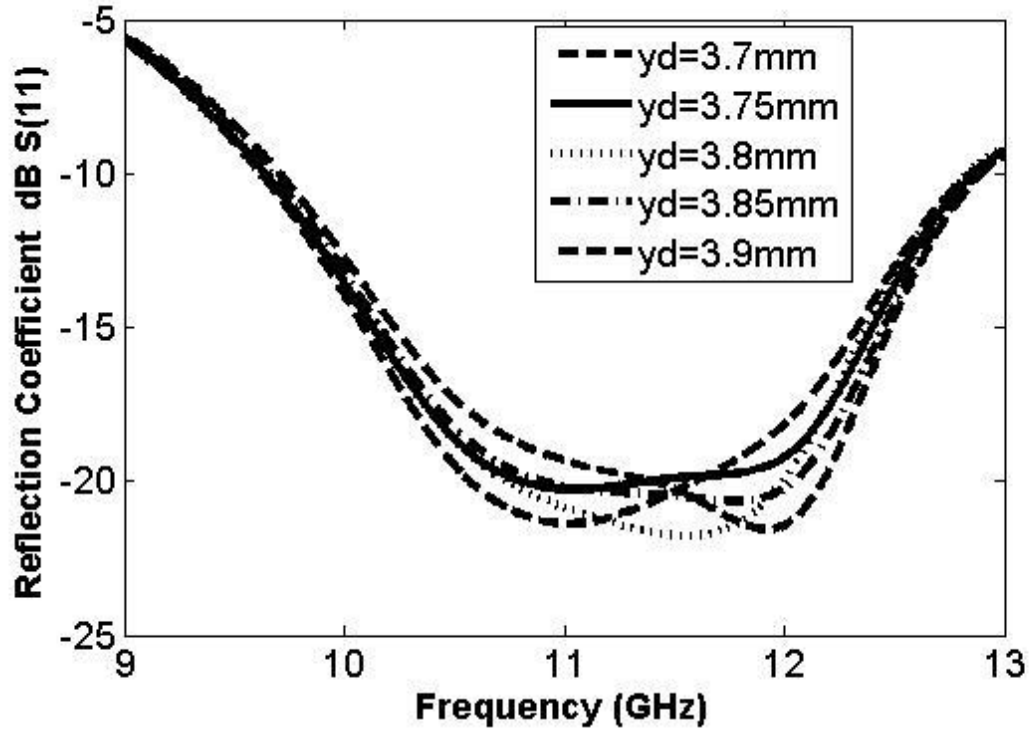


Figure 5.5: Simulated reflection coefficient as a function of frequency for various stub lengths y_d with $s_l=6.6\text{mm}$, $s_w=1.2\text{mm}$, $l_{\text{stub}}=4\text{mm}$, $y_{d1}=-2.1\text{mm}$.

Figure 5.6 shows that moving the lower DR's along the length of the slot affects the bandwidth and matching, and a good compromise has been obtained for the position $y_{d1}=-2.3\text{ mm}$. Thus the off-set positioning has given one more degree of freedom for the design optimization. The two values ($y_d = 3.75\text{mm}$ and $y_{d1} = -2.3\text{mm}$) have been chosen as they give best response in bandwidth and matching as well as resulting in the same resonance frequency of 10.832GHz .

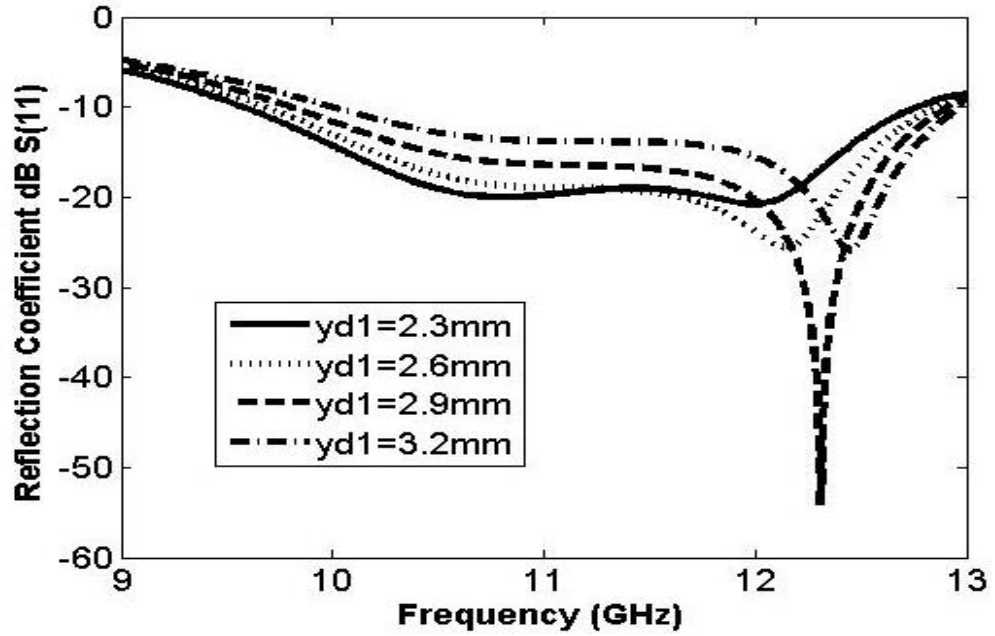


Figure 5.6: Simulated reflection coefficient as a function of frequency for varying position of lower DR y_{d1} with $s_l=6.6\text{mm}$, $s_w=1.2\text{mm}$, $l_{\text{stub}}=4\text{mm}$, $y_d=3.75\text{mm}$.

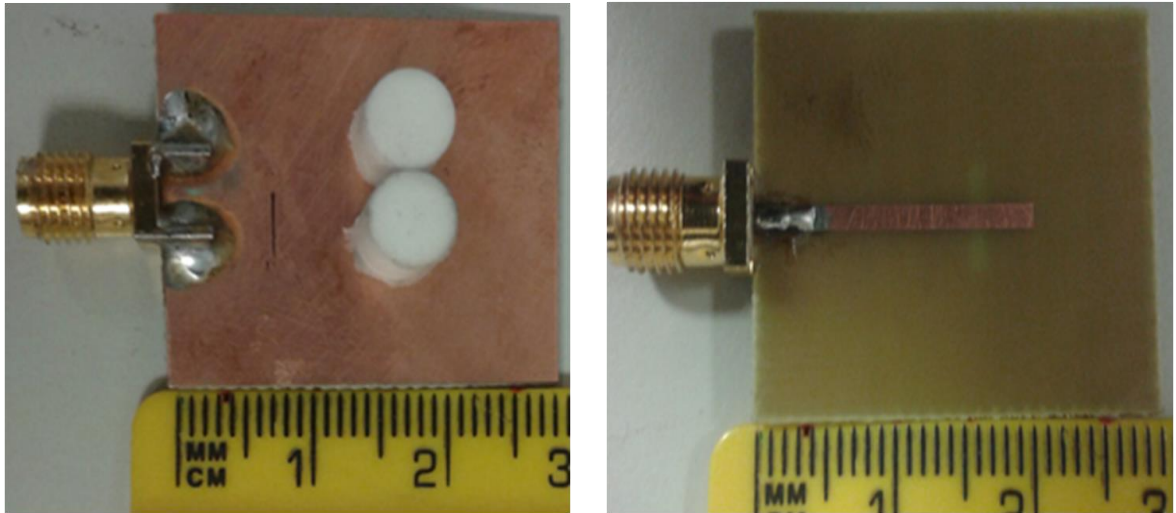
5.4 The Optimized Antenna Design and Measurement Results

Based on the detailed parametric studies, the optimum dimensions obtained for the antenna are listed in Table 5-1. These values are used in the fabrication of the antenna shown in Figure 5.7. The antenna performance was measured with HP8510C vector network analyzer. The measured and simulated reflection

coefficients of the proposed antenna are shown in Figure 5.8. The differences between the measured and simulated results, seen as a shift to higher frequency and general increase in S_{11} , may be attributed to the effects of the use of glue used to fix the DRA and fabrication inaccuracies, as has been noticed previously [51]. The presented antenna here achieves an impedance matching ($S_{11} < -10\text{dB}$ band) from 9.62GHz to 12.9GHz, that is around 29% relative bandwidth.

Table 5-1 Dimensions of the optimized antenna.

parameter	L_g	W_g	L_f	W_f	D	h
Optimum value (mm)	30	25	21	1.5	6	9
parameter	S_l	S_w	L_{stub}	yd	yd1	
Optimum value (mm)	6.6	1.2	4	3.75	-2.3	



(c)

Figure 5.7: Photograph of the fabricated antenna (a) front view and (b) back view.

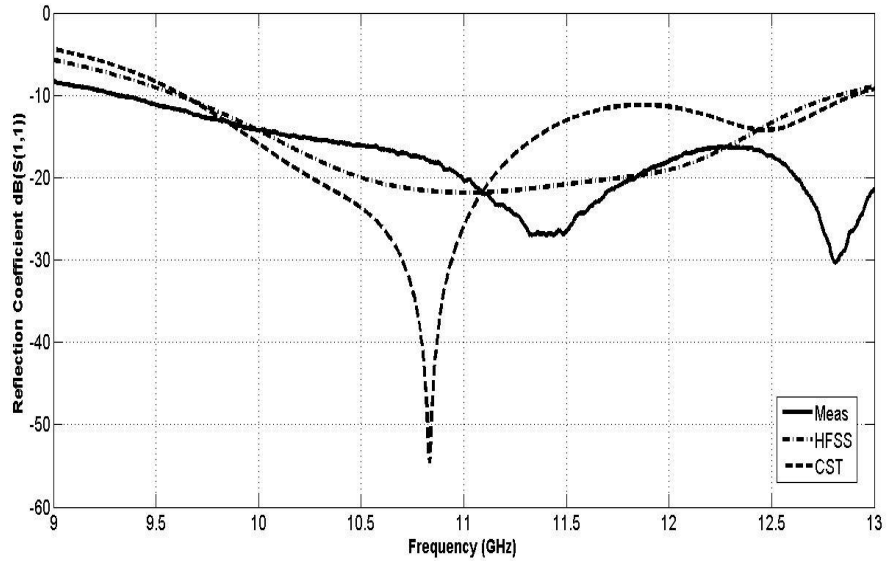


Figure 5.8: Simulated and measured reflection coefficients (S_{11}) of the proposed DRA

The simulated and measured antenna gain in the broadside direction of the proposed antenna is illustrated in

Figure 5.9. It should be noted that the simulated gain curve assumes an ideal feeding network, whereas the measured results include the insertion loss of the feeding network used, hence there are local discrepancies. The figure shows that the calculated gain varies between 5.47dBi and 8dBi with a maximum of 8dBi at 12.8GHz, while the measured gain varies between 6.34dBi and 7.72dBi across the pass band of 9.62-12.9GHz can be said that on average the measurements are comparable with the prediction.

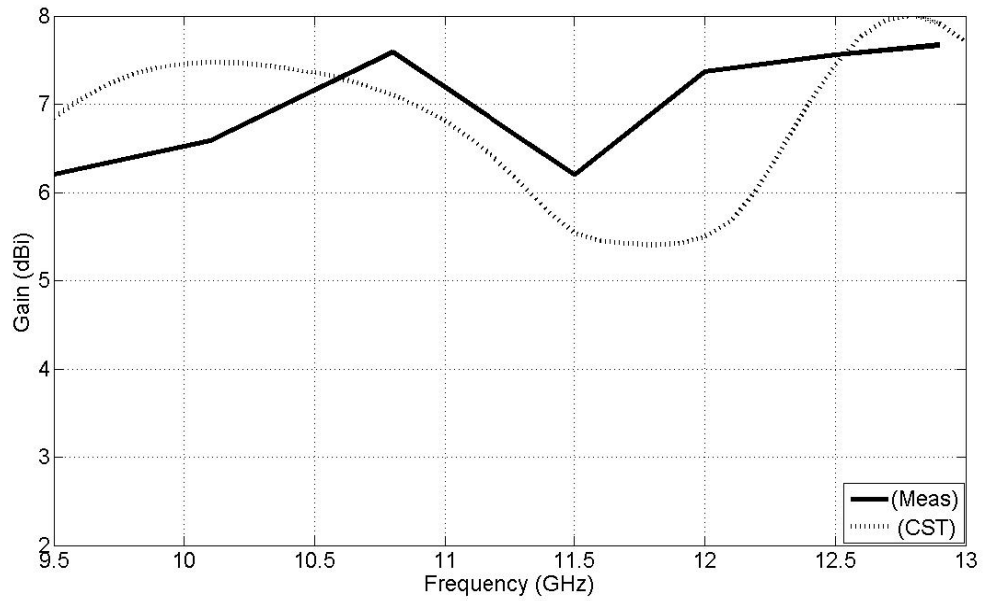


Figure 5.9: Comparison of simulated and measured antenna gain of the proposed antenna

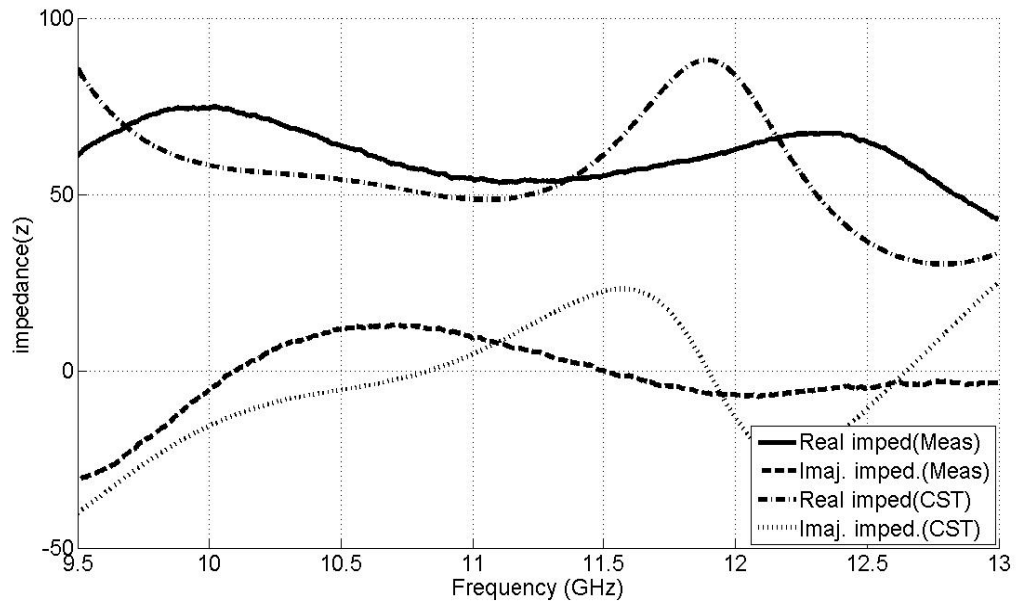
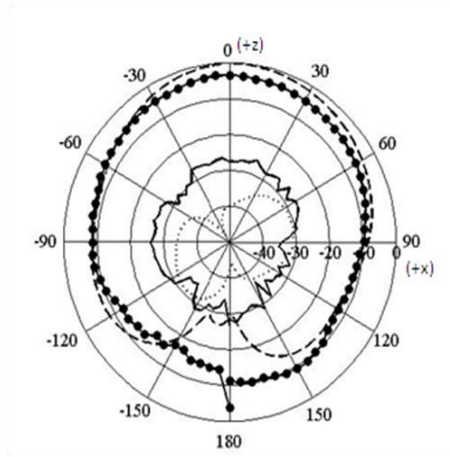


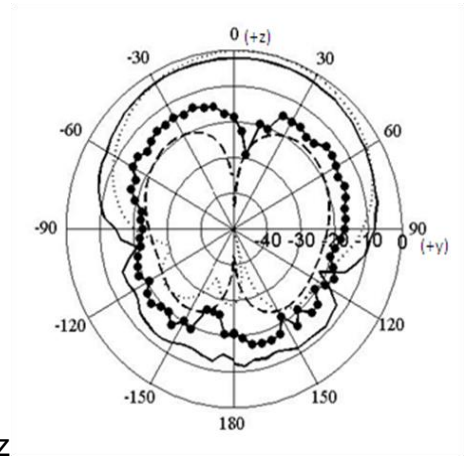
Figure 5.10: Simulated and measured impedance of the proposed antenna

Figure 5.10 shows the simulated and measured impedance for the proposed antenna. The real parts are close to $50\ \Omega$, while the imaginary parts fluctuate around zero. The slight differences between the simulated and measured impedances are due to the fabrication inaccuracies.

Measurements of the far-field radiation patterns of the prototype antenna were carried out in an anechoic chamber using an elevation-over-azimuth positioner, with the elevation axis coincident with the polar axis ($\theta = 0^\circ$) of the antenna's coordinate system. The azimuth drive thus generates cuts at constant ϕ . The fixed transmitting antenna was a broadband horn (EMCO type 3115) positioned 4 m from the antenna being tested. The azimuth positioner was rotated from $\theta = -180$ to 180 at increments of 5 for the selected measurement. Two patterns cuts, $\phi = 0^\circ$ and 90 , were taken at two selected operating frequencies for which the matching was optimal. Figure 5.11 shows the simulated and measured normalized radiation patterns at resonance frequencies of 10.8 and 12 GHz. This shows the antenna has a wide radiation field covering half of space. The field has a low cross-polarization component and is mainly linearly polarized. The back lobe in the radiation pattern is due to a small amount of radiation from the slot.

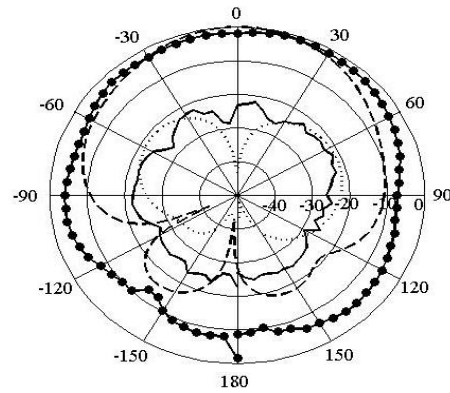


(a)

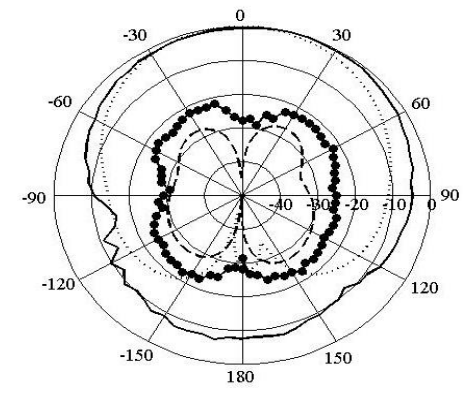


(b)

10.8GHz



(c)

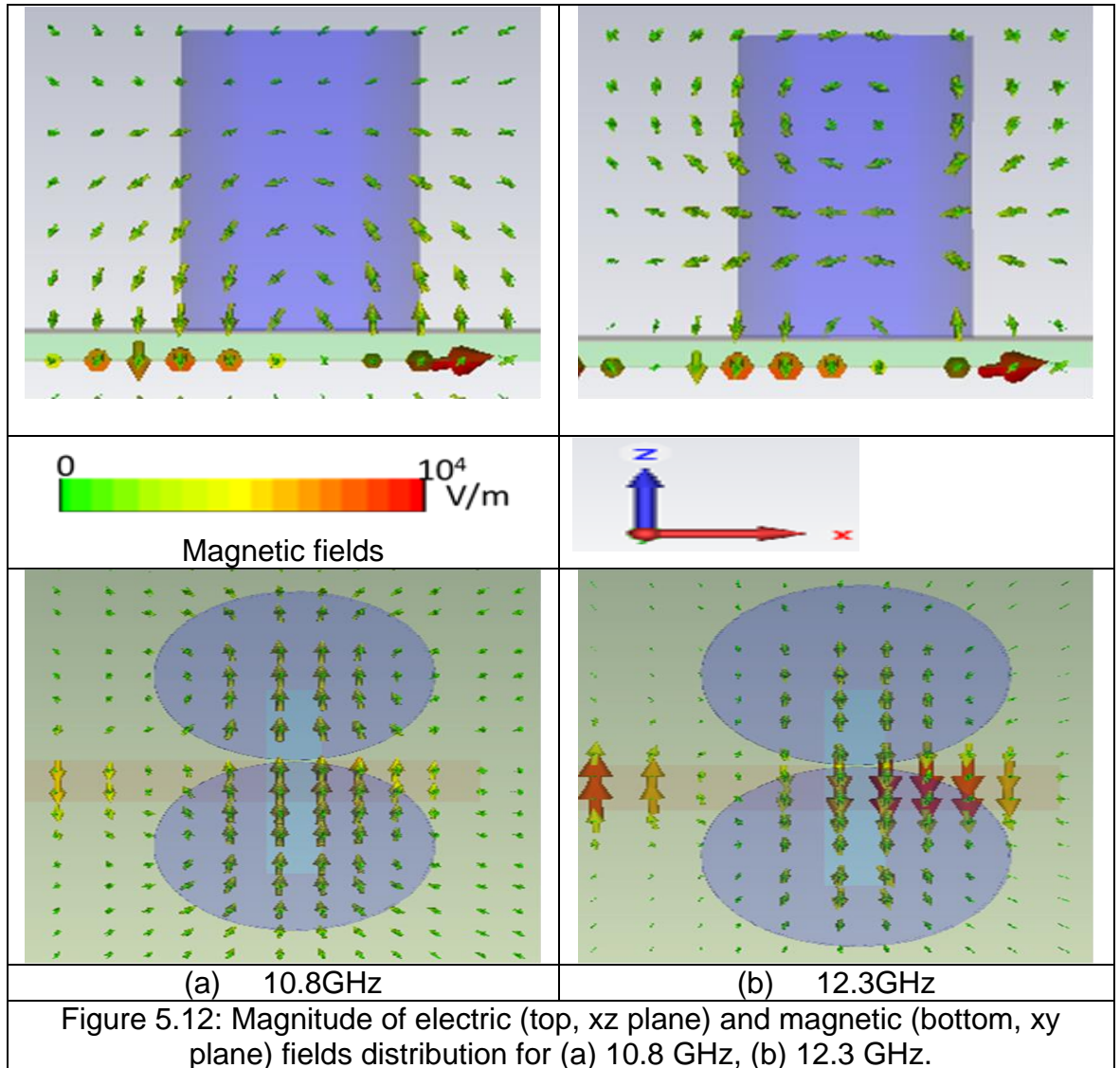


(d)

12.3GHz

Figure 5.11: Simulated and measured radiation pattern; (a) and (c) at xz plane, (b) and (d) at yz plane; simulated E_θ : dashed line, simulated E_ϕ : dotted line, measured E_θ : 'o-o-o', measured E_ϕ : solid line.

The magnitude of the electric and magnetic fields at 10.8 GHz and 12.3 GHz are shown in Figure 5.12. The electric and magnetic fields distributions are plotted on the xz and xy planes respectively.



It is observed that the magnetic field variations at 10.8 GHz and 12.3GHz along specific azimuth direction at the base of each DRA, look quite similar but the intensity increases at higher frequency. Hence, looking carefully at the variations of electric fields one can conclude that there is significant evidence of the appearance of a $TM_{110}/HE_{M11\delta}$ mode of weakly uniform distribution at lower frequency 10.8 GHz and a TM_{111}/HE_{M112} mode of cycling field distribution at the

higher frequency of 12.3 GHz. The asymmetry of such DRAs including the smallest ratio of radius-to-height ratio ($D/2h=1/3$) supports the existence of close modes to work over a wide bandwidth [128].

5.5 Conclusions

A compact DRA for wideband applications has been developed. The asymmetric location of the pair of DR can add another parameter for the designer to optimize the antenna geometry to add another variable dimension of freedom to achieve best spectrum performance. In this study, an impedance bandwidth of about 29%, covering the frequency range from 9.62GHz to 12.9 GHz, and realized gain of 8dBi are obtained. Design details of the proposed antenna and the results of both simulation and experiment were presented and discussed and show a reasonable agreement. It is believed that the compact design due to the asymmetrically located DRAs with respect to single rectangular coupling aperture could enhance closely resonant modes to achieve wider spectrum bandwidth. On the other hand it also confirms the possible operation of two DRs Elements within a small confined feeding network to operate into antenna array concept.

Next chapter further bandwidth enhancement was achieved through optimization of the aperture structure in exciting more resonance modes to cover wider bandwidth.

CHAPTER 6

OFFSET APERTURE-COUPLED TWO CYLINDRICAL DIELECTRIC RESONATORS ANTENNA FOR EXTENDED-WIDEBAND APPLICATIONS

6.1 Introduction

Frequency selective properties of defected ground structures (DGS) have been extensively utilised in printed circuits and antenna applications for more than a decade. DGS was first proposed for antenna applications in 2005 [129]. Among other benefits, the concept can be employed to reduce cross-polarization, which otherwise can be a major limitation for some wideband antennas. Defected ground structures have been used for the control of active microstrip antennas and bandwidth enhancement technique in patch antennas, and shaped defects, such as rectangular, square, or semi-circular arc with varying dimensions, can bring additional improvements [129, 130]. In [130], a DGS annular ring was examined. The application was extended to dielectric resonator antennas (DRAs): the stop-band property of this configuration is used to suppress mutual

coupling between two circular microstrip patches. Moreover, DRAs with various geometries such as conical [79], cylindrical [131] where it was first used as a radiating element [124], asymmetrical T-shaped [132], tetrahedral [35], ring shape [130], elliptical [133], and hybrid hemispherical-conical-shaped [134], were all proposed structures for bandwidth enhancement.

Recently, the operating DRA bandwidth has been improved further for ultra wideband applications [134, 135]. In [126], a single cylindrical DR was excited by two crossed slots, where the centres of the slots were set at different positions and the slot modes were considered partially independent from the DRA mode, in which a wider band was attained. In [131], a novel wideband slot-fed asymmetric DRA was proposed, with two adjacent cylindrical DRs placed asymmetrically with respect to the feeding rectangular aperture. The asymmetric location of the pair of DR constitutes an additional optimization parameter for the designer. The features of the proposed antenna are improved; an impedance bandwidth of about 29%, covering the frequency range from 9.62GHz to 12.9 GHz, and realized gain of 8 dBi are obtained [131]. In this work, for the same aperture concept this ratio is increased up to 100%.

In this chapter, a novel compact Dielectric Resonator Antenna for ultra-wideband applications is proposed, in which, two cylindrical dielectric resonators, asymmetrically located with respect to the centre of an offset

rectangular coupling aperture, are fed through this aperture. The design parameters, such as, impedance bandwidth covering the dual-band frequency range from 6.02 GHz to 7.32 GHz and from 8.72 GHz to 16.57 GHz, and an average gain of 8 dBi are fully optimised to achieve these specific results. The measured results of a prototype antenna sample are compared and discussed with simulation.

6.2 Proposed Antenna Geometry

The proposed asymmetric ultra-wide band antenna was designed and simulated using HFSS V. 14 [123] on an FR4 substrate of thickness 0.8 mm. The final configuration of the antenna is shown in Figure 6.1.

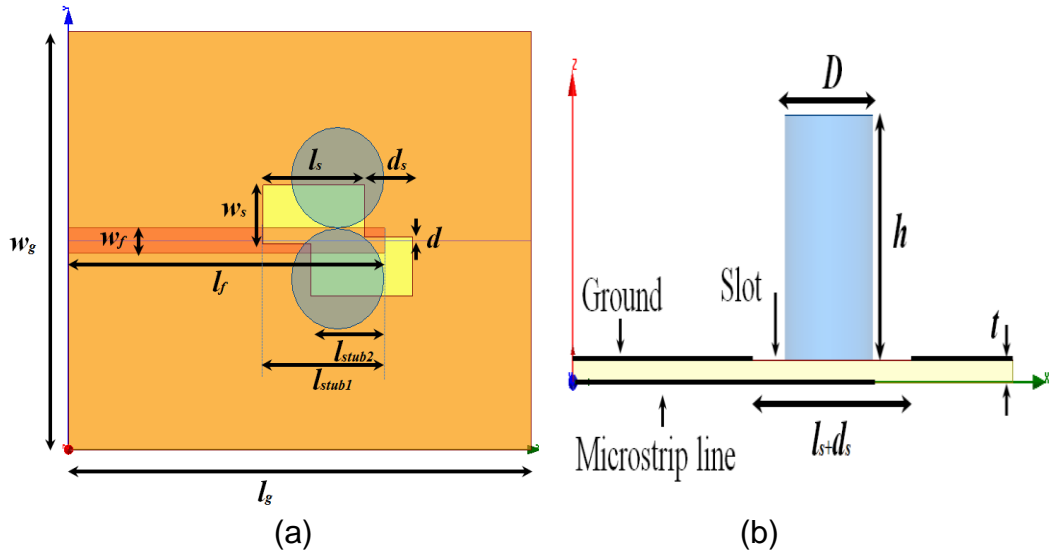


Figure 6.1: Aperture-coupled asymmetric DRA; (a) top view and (b) side view with design dimensions and parameters.

The prototype antenna is fabricated on an FR4 substrate with a relative permittivity of $\epsilon_{rs} = 4.5$, a loss tangent of 0.017 and a thickness $t = 0.8$ mm. The feed microstrip line is placed symmetrically with respect to the coupling aperture. The microstrip line dimensions were calculated using empirical formulas given in [126, 131] resulting in length $l_f = 20.5$ mm and width $w_f = 1.5$ mm. Two rectangular apertures (slots) of length s_l and width s_w are etched on the ground plane, and are shifted from the center by a distance d . Practical experience has shown that the stub length should be close to $\lambda_g/4$ [8]. The values of all the parameters shown in Figure 6.1 and used in the final antenna configuration are in Table 6-1.

Table 6-1: Dimensions of the optimized antenna

parameter	w_g	l_g	w_f	w_s	l_s
Optimum value(mm)	25	30	1.5	3.5	6.6
parameter	d_s	d	L_{stub1}	L_{stub2}	l_f
Optimum value(mm)	3.1	0.2	7.9	4.5	20.5

Based on the previous work in [131], the originality of this work resides in the creation of an offset rectangle slot to excite other modes, where “shifting the zigzag” gives design scope (we can consider this as double attached slots) as shown in Figure 6.2. This original antenna presents an enhancement of S_{11} , as illustrated in Figure 6.3. An alumina material alumina-96pct, with $\epsilon_{rd} = 9.4$,

diameter $D = 6$ mm and a height $h = 9$ mm is used for the DR structure. The resonant frequency of a single segment CDRA excited in $HE_{M11\delta}$ mode can be given by [123, 136]

$$f_r (GHz) = \frac{c}{2\pi a \sqrt{\epsilon_r}} \left(1.71 + \frac{a}{h} + 0.1578 \left(\frac{a}{2h} \right)^2 \right) \quad (6.1)$$

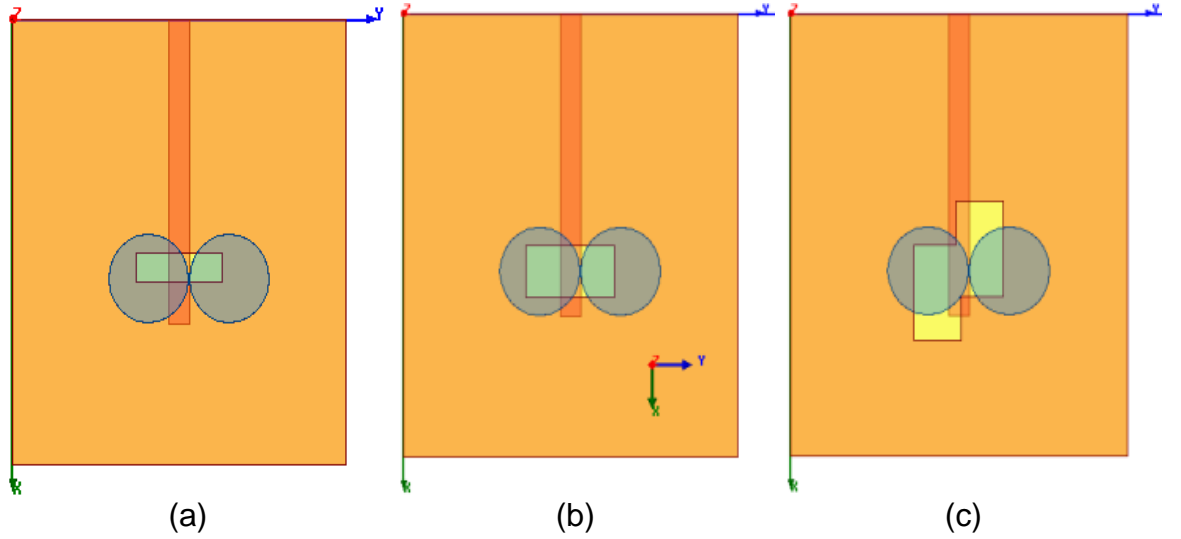


Figure 6.2: Aperture-coupled asymmetric DRA top view with steps of the designed antenna. (a) Antenna proposed in [4], (b) a second proposed antenna and (c) our proposed antenna.

where $a=D/2$ (in cm), c is the velocity of light, with the other values given above. For these dimensions, and with the given DRA properties, the calculated resonance frequency is 10.410 GHz [131]. The slot length and the permittivity of the substrate and DRA determine the resonance frequency of the slot. Since the DRAs are asymmetrically located with respect to the asymmetrical slots, we

have two stub lengths l_{stub1} and l_{stub2} , where the DRA modes depend on the DR dimensions, the permittivity, as well on as the feeding mechanism. Thus several resonant frequencies are excited leading to a wideband operation.

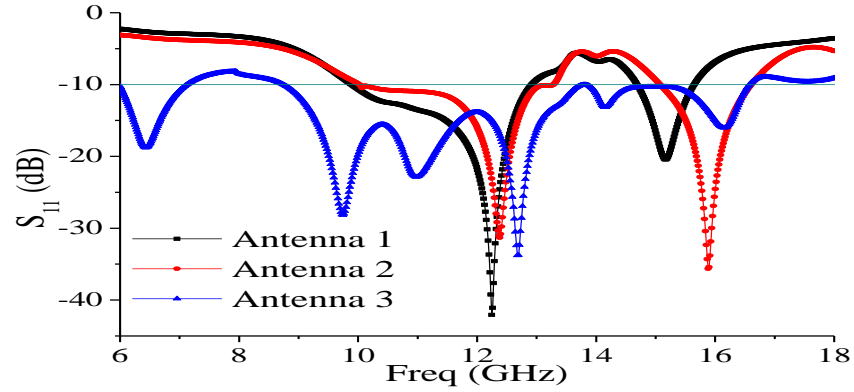


Figure 6.3: Simulated return loss of the three different DRAs shown in Figure 6.2.

6.3 Results and Discussion

Based on the detailed parametric study in [131], the obtained optimum dimensions for the antenna given above are used in the fabrication of the antenna shown in **Error! Reference source not found..** The antenna performance was measured with an HP8510C vector network analyzer, and the measured and simulated return losses of the proposed antenna are shown in Figure 6.4. The differences between the measured and simulated results, seen in a shift towards higher frequencies and a general increase in S_{11} may be attributed to the combined effects of the use of glue in fixing the DRA and

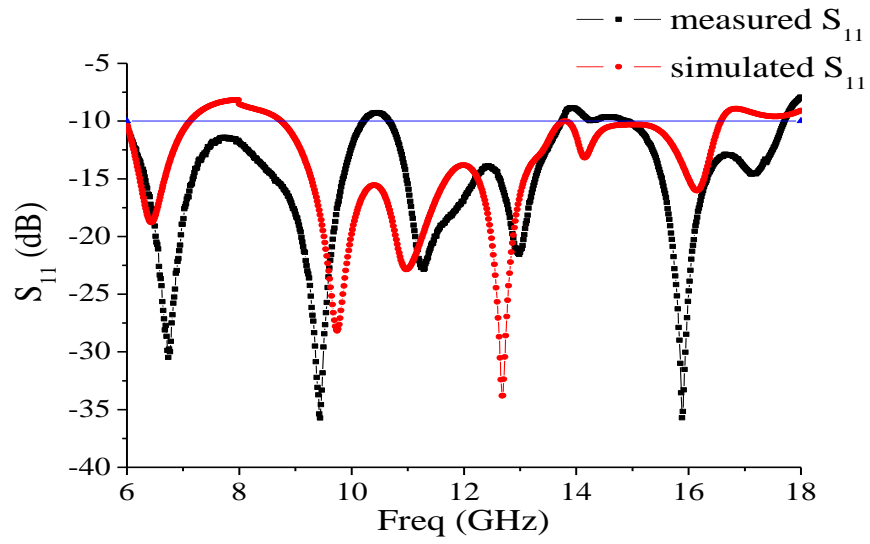


Figure 6.4: Simulated and measured return loss of the proposed DRA.

fabrication errors. The antenna realizes an impedance matching ($S_{11} < -10$ dB band) extending from 8.72 GHz to 16.57 GHz, i.e. 62%.

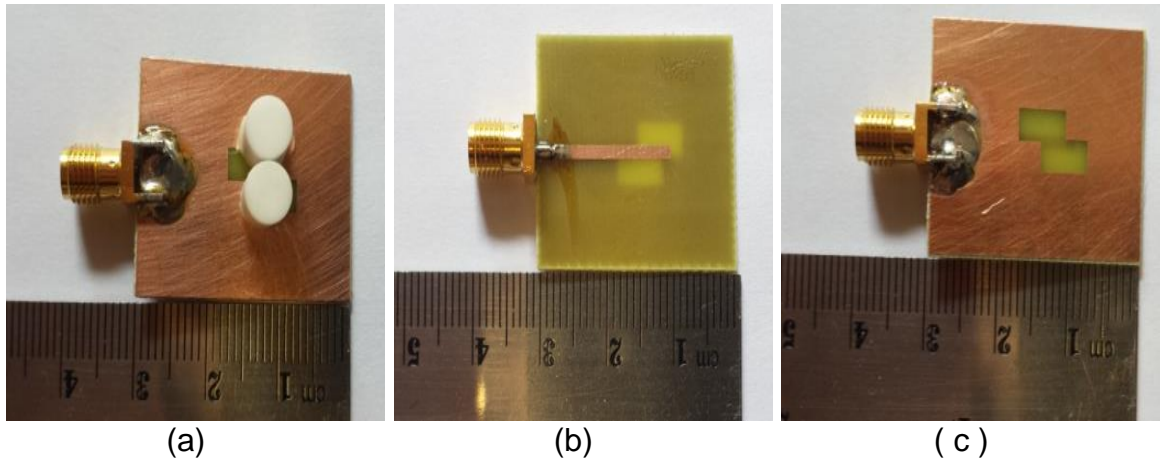


Figure 6.5: Photograph of the fabricated antenna (a) front view, (b) back view and (c) with DRs.

Figure 6.6 shows the simulated and measured impedance for the proposed antenna. The real parts are round 50 Ohms, while the imaginary parts fluctuate around zero.

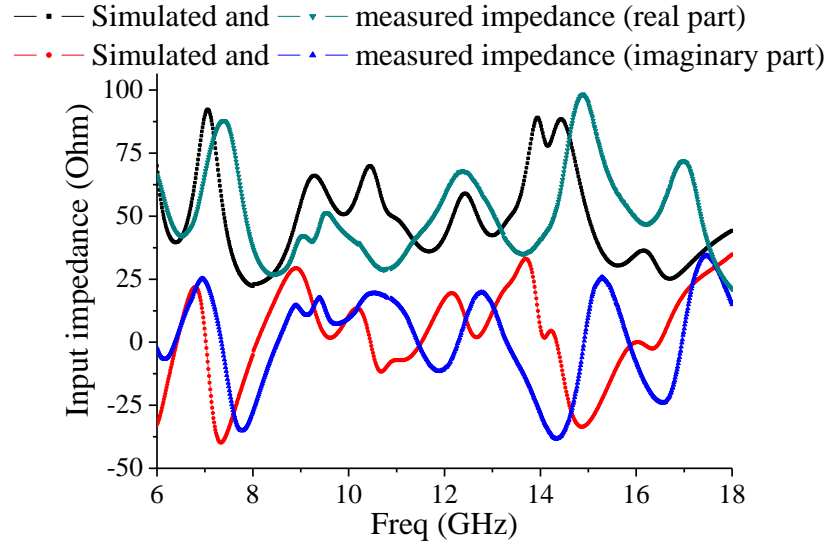


Figure 6.6: Simulated and measured impedance of the proposed antenna

The slight differences between the simulated and measured impedances are mainly due to the fabrication errors. Therefore, it note can be that several modes are excited and this is due to the shape of the slot.

Figure 6.7 illustrates the simulated and measured antenna gains in the broadside direction of the proposed antenna. It is worth noting that the simulated gain assumes an ideal feeding network, whereas the measured result includes the insertion loss of the feeding network used, hence there are local discrepancies. The illustration shows that the calculated gain varies between

6.46 dBi and 12.95 dBi with a maximum of 12.95 dBi at 17.64 GHz, while the measured gain varies between 5.56 dBi and 12 dBi across the passband of 6-17 GHz and it can be noted that on average the measurements are quite comparable with the predictions.

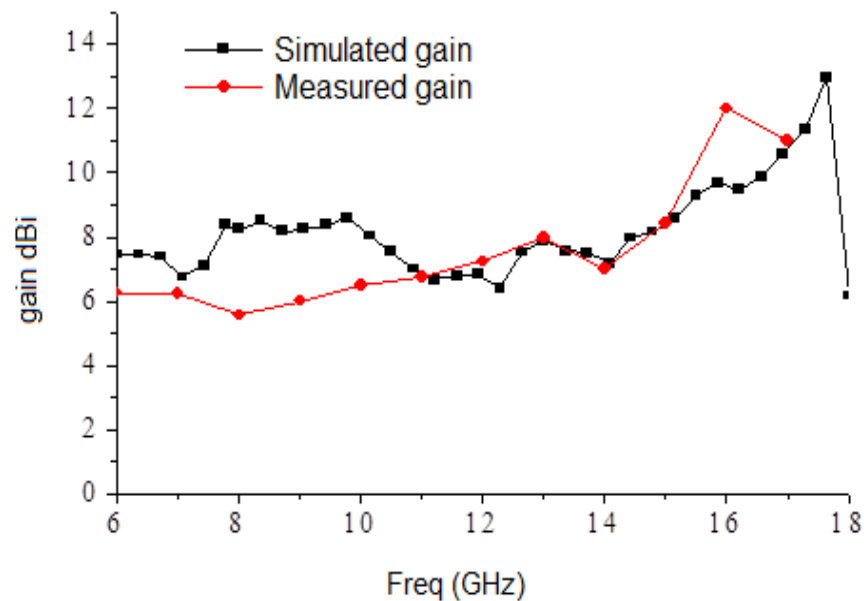


Figure 6.7: Simulated and measured antenna gain of the proposed antenna

Figure 6.8 shows the normalized measured radiation patterns at frequencies of 6, 10 and 15GHz. This shows that the antenna has a wide radiation range covering half space, and in some cases an almost omnidirectional radiation pattern is obtained. This is due to the shape and the dimensions of the slot

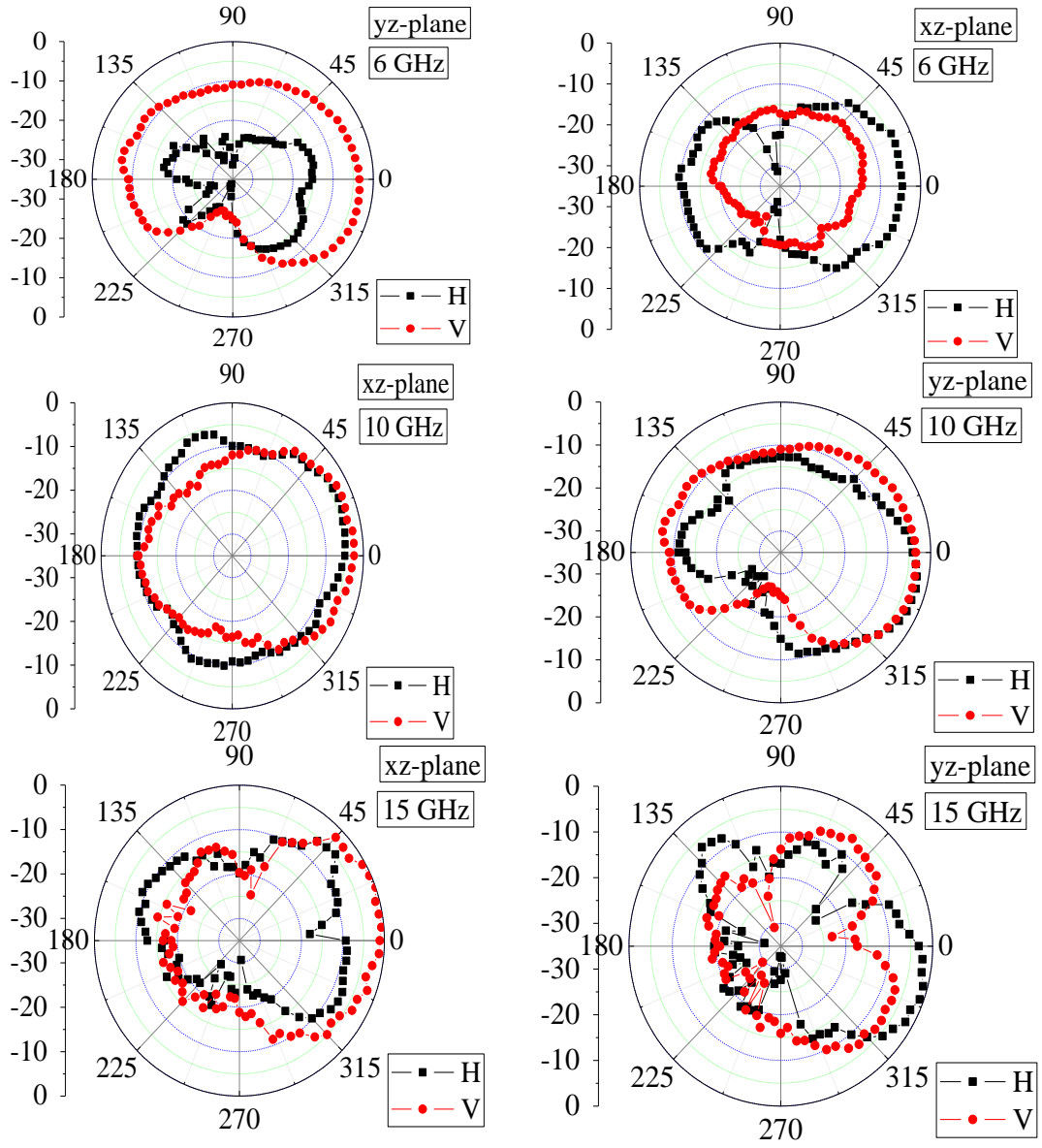


Figure 6.8: Measured radiation patterns (a) in xz-plane, (b) in yz-plane.

6.4 Conclusions

A compact dielectric resonator antenna for ultra-wideband applications has been designed, manufactured and are used showing the use of two DRs can enhance the operational performances of the antenna. The asymmetric locations of the DR pair, the dimensions and the shape of the aperture where “shifting the zigzag” gives design scope together constitute another parameter for the designer to optimize the design process. In this study, an impedance bandwidth of over 62%, covering the dual-band frequency range from 6.02 GHz to 7.32 GHz and from 8.72 GHz to 16.57 GHz, and a gain of 8 dBi were achieved compared to the author previous work presented in [4]. The next chapter provides new aperture feeding network for new type of wireless communications applications.

CHAPTER 7

DUAL SEGMENT S-SHAPED APERTURE- COUPLED CYLINDRICAL DIELECTRIC RESONATOR ANTENNA FOR X-BAND APPLICATIONS

7.1 Introduction

A new dual-segmented dielectric resonator antenna with internal S-slot coupling is proposed for use in X-band communications. One of the fundamental differences between dielectric resonator antennas (DRA) and conventional radiators is that the main loss in the DRA is dielectric loss, and with modern ceramic materials this can be very low [128, 137]. It can also remain very low for high permittivity ceramics, so there is not the same penalty for miniaturization that one would expect with metal, or metalized, radiators. Nevertheless, DRA are still believed to be subject to the fundamental size/bandwidth trade-off [50, 131, 132, 138-146]. There is some potential for overlap between filter and antenna design, particularly in establishing multi-mode solutions, although this approach is not adopted here. The design presented here is semi-empirical, with the analysis being carried out using CST Microwave Studio and Ansys HFSS software[123]. The bandwidth is controlled through the selection of the dielectric constant, and geometry of the DRA layout

through manipulation of the structural parameters for the resonators, coupling path (slot) and feed line. The realization also exploits some well-known techniques developed for physically small, low profile, mobile handset and terminal antenna designs.

In this chapter, a new low cost dual-segmented S-slot coupled dielectric resonator antenna design is proposed for wideband applications in the X-band region. The antenna performance characterized in terms of the reflection coefficient, gain and radiation pattern are investigated. Various placements of the two DR segments located on the same side, or on opposite sides, of the substrate are examined to improve radiation performance. Experimental testing of the antenna prototype was compared with the modelling results.

7.2 Antenna Design Concepts and Structure

The general layout of the DRA assembly is given in Figure 7.1, two identical dielectric resonators are mounted on a 30.0 mm × 25.0 mm substrate backed ground plane. The resonators are 6.0 mm (D) × 9.0 mm (h) cylindrical posts of Rogers thermoset TMM4 laminate ($\epsilon_{dr} = 9.4$), and the substrate is a Rogers thermoset TMM4 laminate ($\epsilon_{subs} = 4.5$, $\tan \delta = 0.017$) of thickness 0.8 mm (t). The resonators are excited in the dual

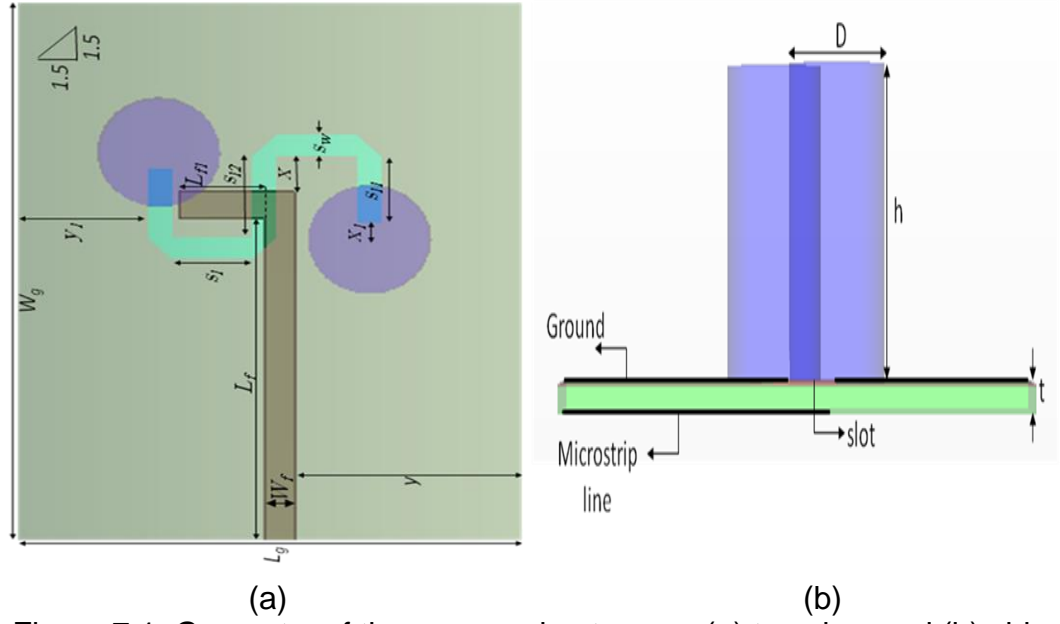


Figure 7.1: Geometry of the proposed antennas. (a) top view and (b) side view with design dimensions and parameters

HEM₁₁₀ mode, for which the structure parameters and target frequency are related through the curve-fitted equation,

$$f(GHz) = \frac{30}{2\pi a \epsilon_r^{0.42}} (1.6 + 0.513 z + 1.392 z^2 - 0.575 z^3 + 0.088 z^4) \quad (7.1)$$

where $a = D/2$ (cm) and $z = a/2h$ [1].

The antenna assembly is excited using an L-shaped strapline, with dimensions $L_f = 19.5$ mm, $L_{f1} = 4.2$ mm, and $W_f = 1.5$ mm calculated using the standard formulae [16]. The internal coupling mechanism is provided by an S-shaped slot. This configuration acts to influence the resonant structure, and the amount

of undesired radiation in the backward direction. It also acts to control the coupling between the radiator and the feeding network.

7.3 Parametric Design Studies and Optimized Design

The following parametric study is useful because it provides a comprehensive picture of the antenna characteristics. A detailed model of the antenna performance is constructed using ANSYS HFSS software and systematic parameter sweeps are made on each of the principal structure parameters governing the S-shaped slot coupling in turn, while the others are held constant. The antenna performance is characterized in terms of the gain, reflection coefficient, and radiation pattern; these are summarized in Figures 7.2 to 7.5.

Figure 7.2 shows the variation of reflection coefficient versus frequency (S_{11}) with frequency for various vertical slot lengths (S_l) with $S_{l1}=3.5\text{mm}$, $S_w=1.1\text{mm}$ and $x=1.5\text{mm}$. It can be seen that as the vertical slot length increases, the resonant frequency decreases, altering the bandwidth. The optimal value for the vertical slot lengths appears to be 3.75 mm, as can be seen from the wider impedance bandwidth, and minimum reflection coefficient (-10 dB) across the frequency range.

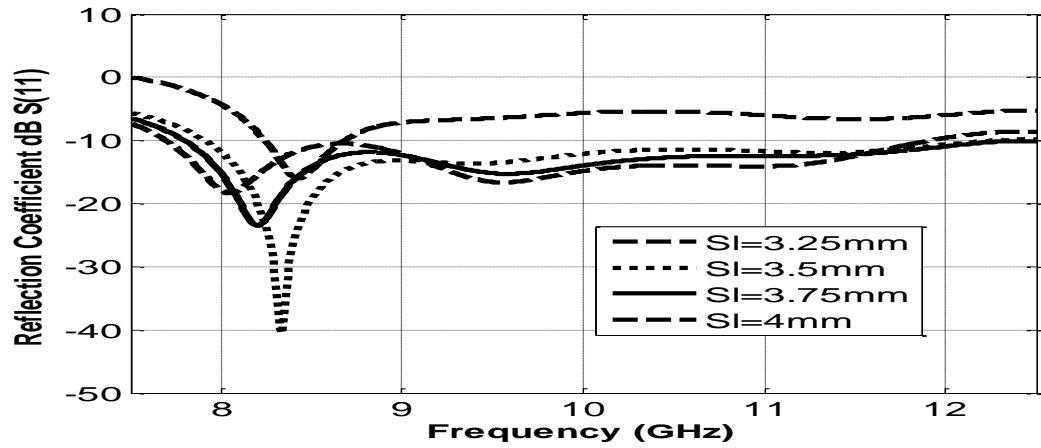


Figure 7.2: Simulated reflection coefficient versus frequency for different vertical slot lengths s_l ; $s_l=3.25\text{mm}$ (solid), $s_l=3.5\text{mm}$ (dashed), $s_l=3.75\text{mm}$ (dotted), $s_l=4\text{mm}$ (dash-dotted).

Figure 7.3 shows the variation of the reflection coefficient with frequency for different values of the horizontal slot length (Sl_1) with $S_l = 3.75\text{ mm}$, $S_w = 1.1\text{ mm}$, and $x = 1.5\text{ mm}$. It can be seen that the resonant frequency and impedance bandwidth reduce with decreasing values of Sl_1 ; the optimal value for Sl_1 is 4 mm .

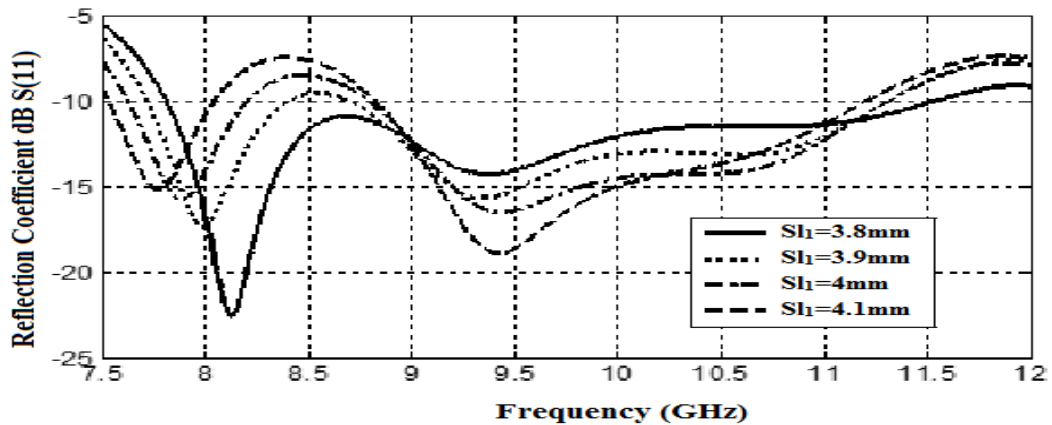


Figure 7.3: Simulated reflection coefficient versus frequency for various horizontal slot lengths of the two slot ends sl_1 ; $sl_1=3.8\text{mm}$ (solid), $sl_1=3.9\text{mm}$ (dotted), $sl_1=4.0\text{mm}$ (dashed) and $sl_1=4.1\text{mm}$ (dash-dotted).

Figure 7.4 shows the variation of the reflection coefficient with slot width (S_w), with $S_l = 3.75$ mm, $S_{l1} = 4$ mm, and $x = 1.5$ mm. The primary effect is with the reflection coefficient, and a slight change in the impedance bandwidth can be observed on the upper band-edge, the optimal slot width appears to be 1.2 mm.

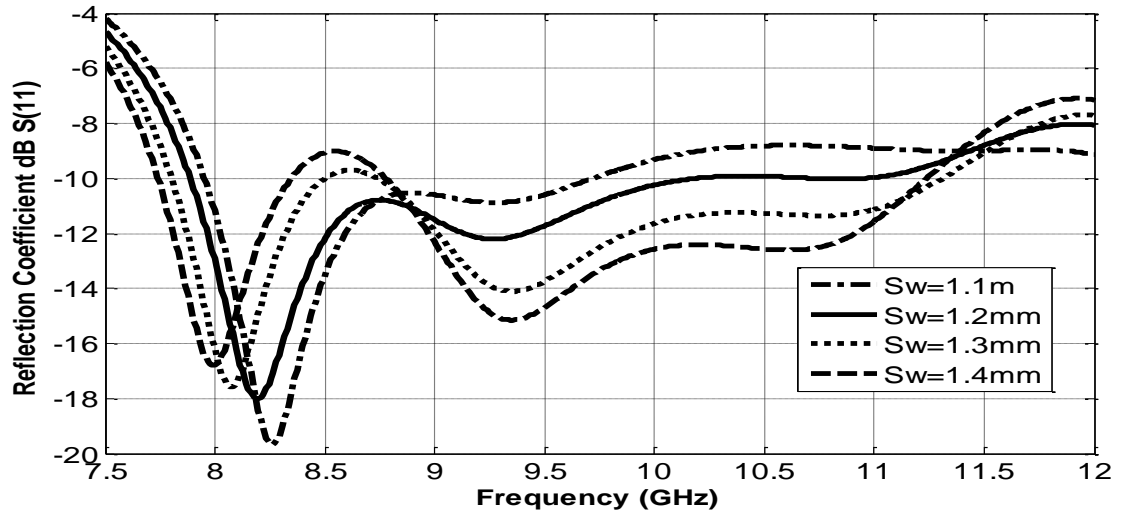


Figure 7.4: Simulated reflection coefficient verses frequency for various slot widths S_w ; $S_w=1.1$ mm (solid), $S_w =1.2$ mm (dashed) and $S_w =1.3$ mm (dotted). Figure 7.5 monitors the effect of the relative positioning of the S-slot with respect

to the feed line on the reflection coefficient, this is the x-parameter in Figure 1 (in this case $S_l = 3.75$ mm, $S_{l1} = 4$ mm and $S_w = 1.2$ mm). The optimum position is given by $x = 1.2$ mm. This has some effect on tuning the impedance bandwidth.

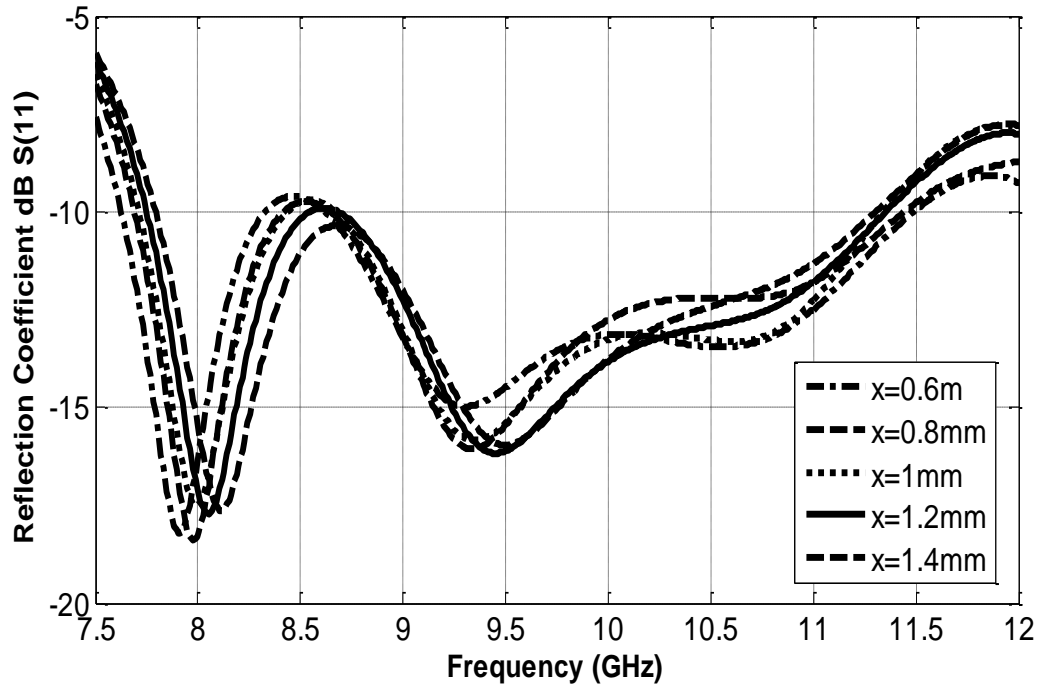


Figure 7.5: Simulated reflection coefficient versus frequency with varying position of S-slot along feeding line x ; $x=0.6\text{mm}$ (solid), $x=0.8\text{mm}$ (dashed), $x=1.0\text{mm}$ (dotted), $x=1.2\text{mm}$ (dash-dotted) and $x=1.4\text{mm}$ (circles)

7.4 Results and Discussion

Based on the detailed parametric studies, the optimum dimensions were found, and listed in Table 7-1. The substrate dielectric characterized by relative permittivity $\epsilon_{rs} = 4.5$ and tangent loss $\tan\delta = 0.017$, whereas the relative dielectric of the DR is $\epsilon_{rdr} = 9.4$. A prototype DRA assembly was constructed using the parameter values derived from parametric study.

Table 7-1: Optimum dimensions (in mm) for the prototype antenna assembly.

parameter	W_g	L_g	D	h	L_f	W_f	L_{f1}	X_1
Optimum value(mm)	30	25	6	9	19.5	1.5	4.2	0.9
parameter	y	S_l	S_{l1}	S_{l2}	X	y_1	S_w	
Optimum value(mm)	11.25	4	3.75	4.5	1.2	6.5	1.2	

The proposed antenna with those parameters was fabricated, and Figure 7.6 shows a photograph for the fabricated antenna. The reflection coefficient was measured using a vector network analyser (HP8510C) and results for antenna assemblies with and without DR posts present are summarized in Figure 7.7, alongside the corresponding simulation data. When there are no resonant posts on the slot side, the measured impedance bandwidth, for $S_{11} \leq -10$ dB, is extended from 11.2 GHz to 12.6 GHz, i.e. the relative impedance bandwidth is 11%. Introduction of two DR posts on the slot side produces a bandwidth from 7.8 GHz to 11.85 GHz, a relative bandwidth of 41%. In simulation the corresponding values were found to be 9% and 37%. The addition of the DR posts act to improve the reflection coefficient and impedance bandwidth. The simulated and measured data show multiple resonances which account for this wide bandwidth performance. Some variations may be observed, this follows from the fact that the parametric analysis is not fully optimized, leading to some

uncertainties in the final cut values for some of the structural parameters used on the prototype. This may be iteratively improved.

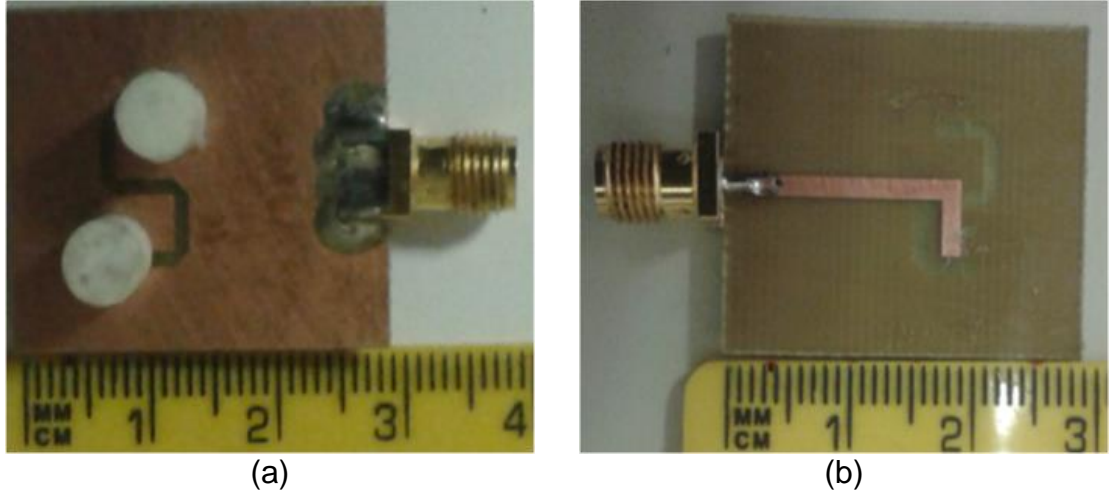


Figure 7.6: Fabricated antenna (a) front view (b) back view

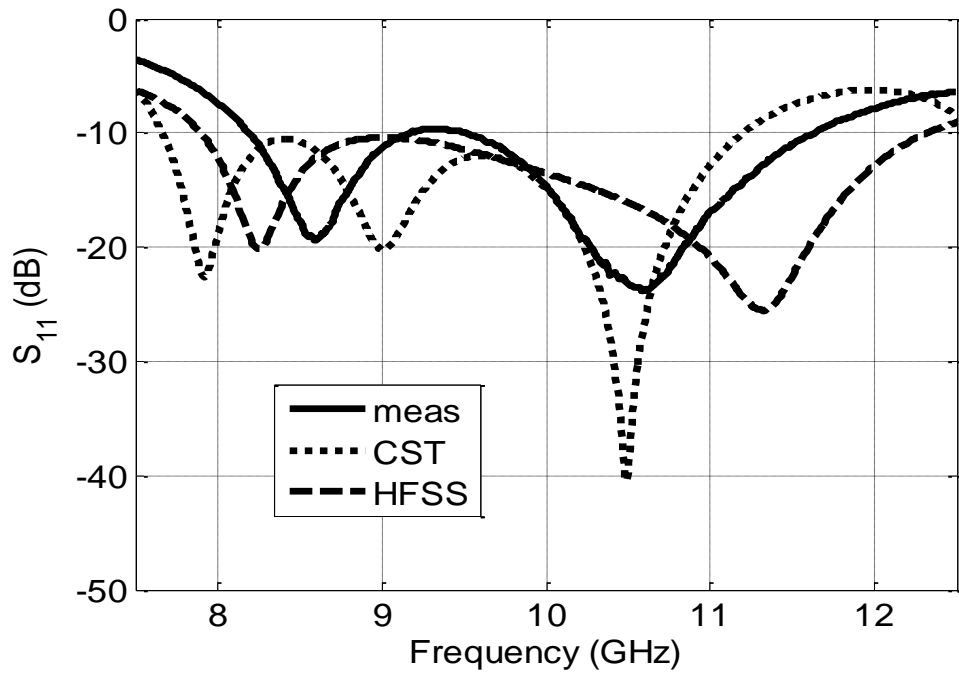
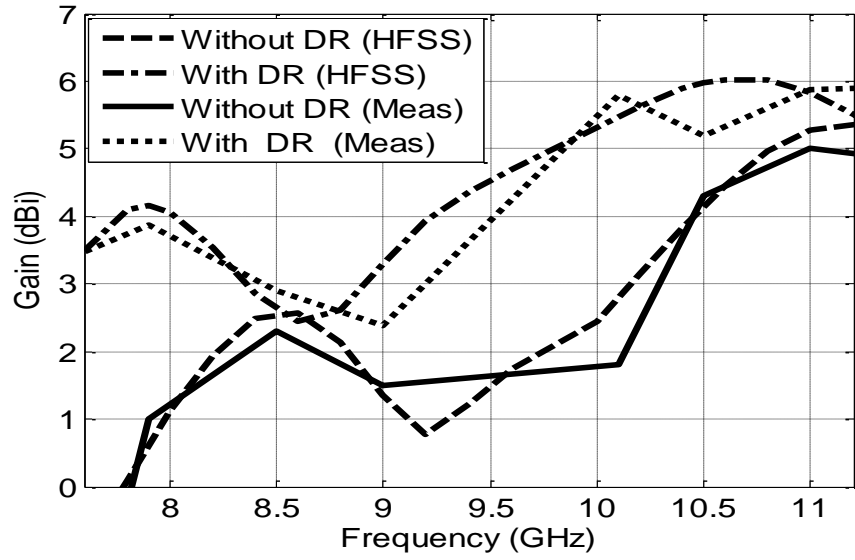
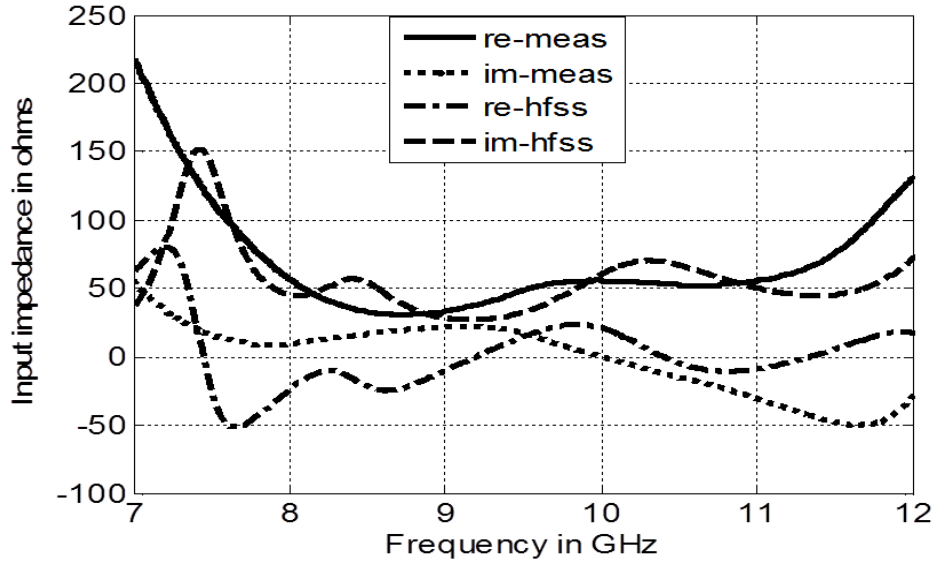


Figure 7.7: Simulated and measured reflection coefficient versus frequency for the proposed antenna.

Figure 7.8 (a) illustrates the simulated and measured antenna gain in the broadside direction of the proposed antenna for two cases with and without the two DR's. It should be noted that the simulated gain curve assumes an ideal feeding network, whereas the measured results include the insertion loss of the feeding network used, hence there are local discrepancies. It is clear from the figure that the calculated max gain with no DR is 5.3dBi at 11.2GHz, and with two DR's on the slot side it is 6.16dBi at 10.6GHz, while the measured max gain with no DR's on slot side is 5dBi at 11GHz and 5.8dBi at 11.2GHz with two DR's on the slot side. On average, it can be said that the results of measurements are comparable with the predicted one. Also, it is clear from figure that across most of the operation band there is about 4 dB improvement in gain. This can be attributed to the use of two DR's which are fed in balance. The difference between the simulated and measured gain values at some places is around 1dB which can be attributed to the alignment errors. The impedance response of the proposed is shown in Figure 7.8 (b). It can be seen that in the desired frequency range real part of impedance is close to 50Ω while imaginary part is almost negligible. This shows that proper impedance matching is achieved between feeding slot and aperture slot because of proper selection of feeding slot length and aperture slot position provided while deciding the aperture slot location.



(a)



(b)

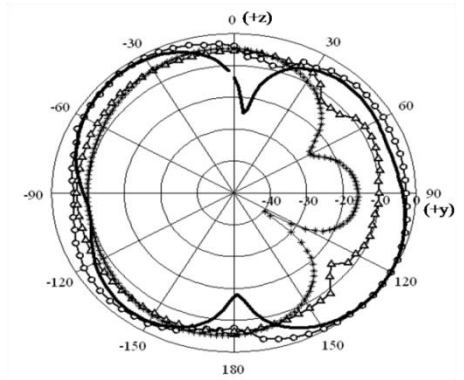
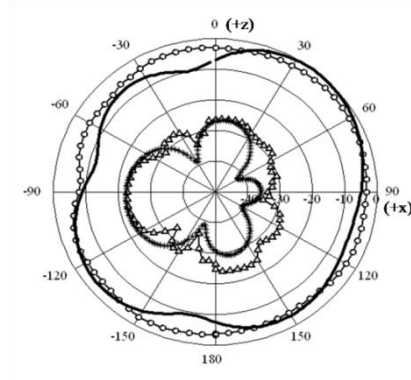
Figure 7.8: (a) Comparison of simulated and measured antenna gain of the proposed antenna, (b) Impedance Vs. Frequency plot of the proposed antenna

The Far-field radiation patterns of the prototype antenna were measured in a far-field anechoic chamber using an elevation-over-azimuth positioner, with the elevation axis coincident with the polar axis $\theta = 0^\circ$, of the antenna's coordinate

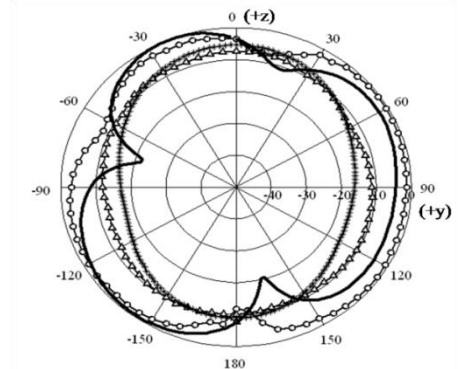
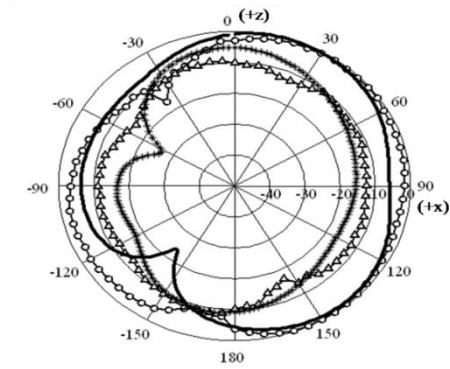
system. The reference antenna was a broadband horn (EMCO type 3115) positioned at 3.5 m from the antenna under test. Two pattern cuts (i.e. the xz and yz planes) were taken at three selected operating frequencies (8.2 GHz, 9 GHz and 10.45 GHz), covering the complete designated bandwidth. The simulated and measured radiation pattern data are shown in Figure 7.9. The results show that the radiation patterns are nearly omnidirectional with minimal distorted characteristics. The computed radiation patterns are in a reasonable agreement and consistent with measurements.

7.4.1 Magnitudes of Electric and Magnetic Fields

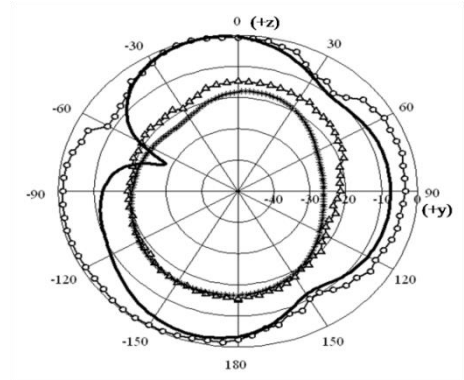
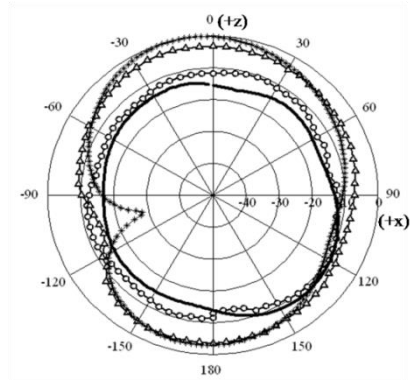
The magnitude variations in the electric and magnetic fields were calculated in simulation and plotted for the optimized antenna model at 7.92 GHz, 9.00 GHz and 10.49 GHz, these characteristics are summarized in Figure 7.10. When close to resonance at 10.49 GHz, the electric fields displays strongly transverse characteristics, and mixed axial and transverse characteristics at the other lower frequencies, where there are no resonances. The magnetic field lines are essentially transverse, parallel to the DR base. This is in line with the prediction of the base mode frequency (10.695 GHz) from equation (1). The dominant mode at this frequency is the $HEM_{11\delta}$.



7.92GHz



9GHz



10.49GHz

(a)

(b)

Figure 7.9: Far-field radiation patterns at (a) xz-plane and (b) yz-plane; E_{θ} Meas.(solid-circles), E_{ϕ} Meas.(triangle), E_{θ} HFSS (solid) and E_{ϕ} HFSS (solid-*).

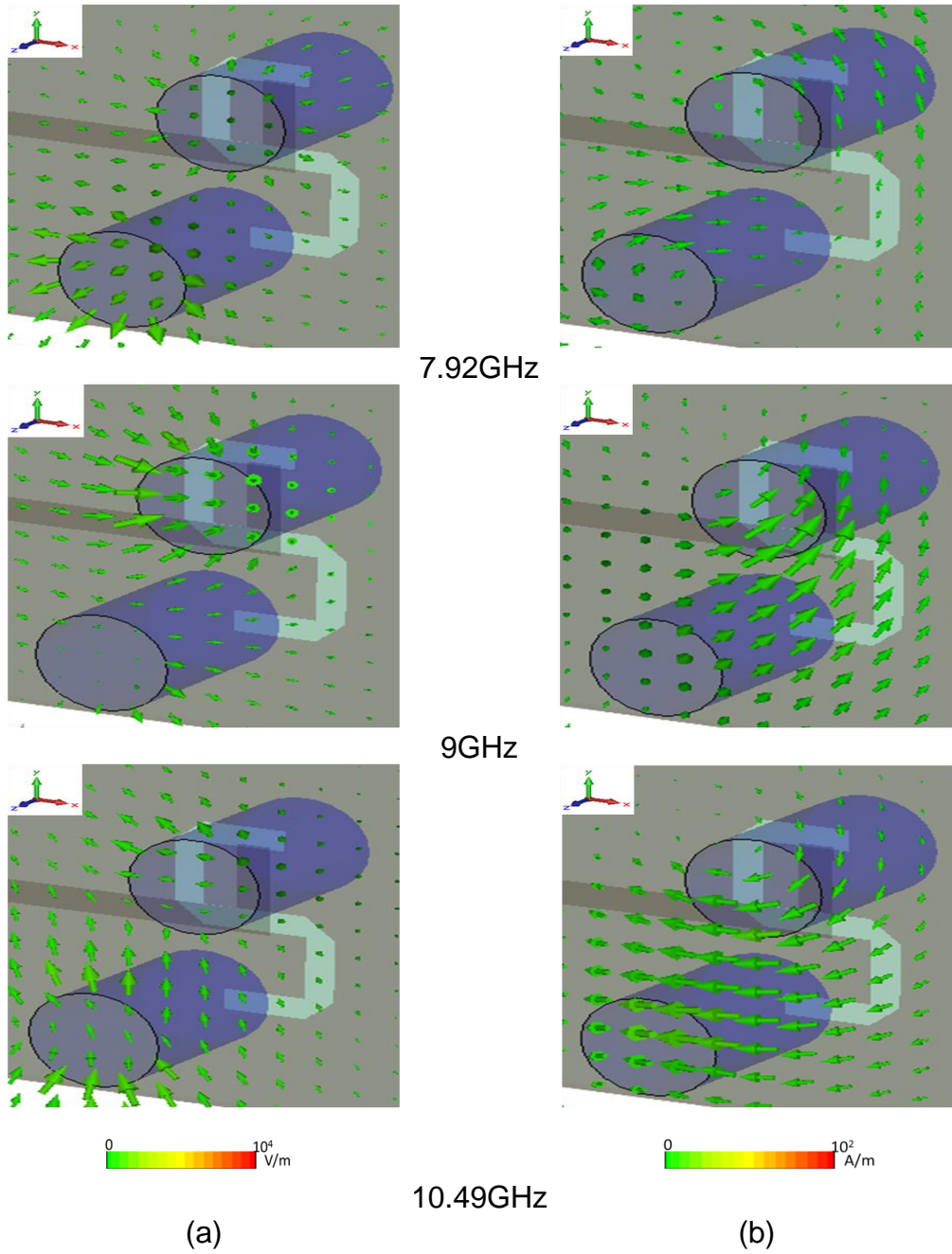
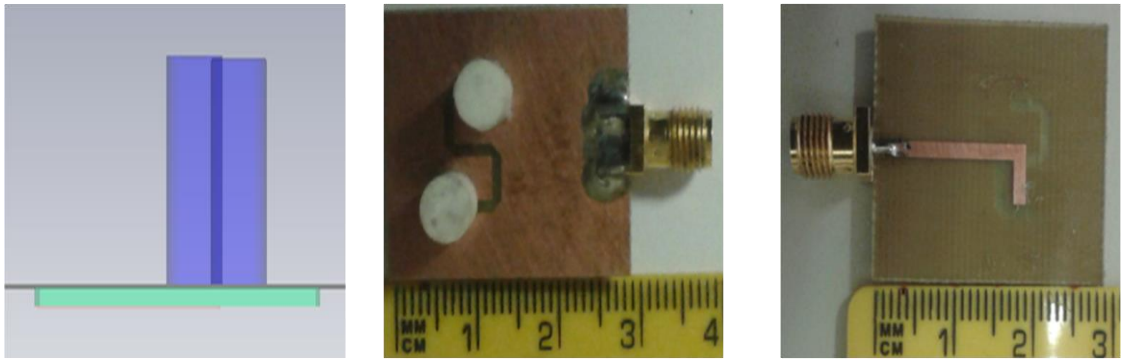


Figure 7.10 : Magnitude of (a) Electric and (b) Magnetic fields distribution of the proposed dual segment S-shaped aperture coupled CDRA antenna at 7.92GHz, 9GHz and 10.49GHz.

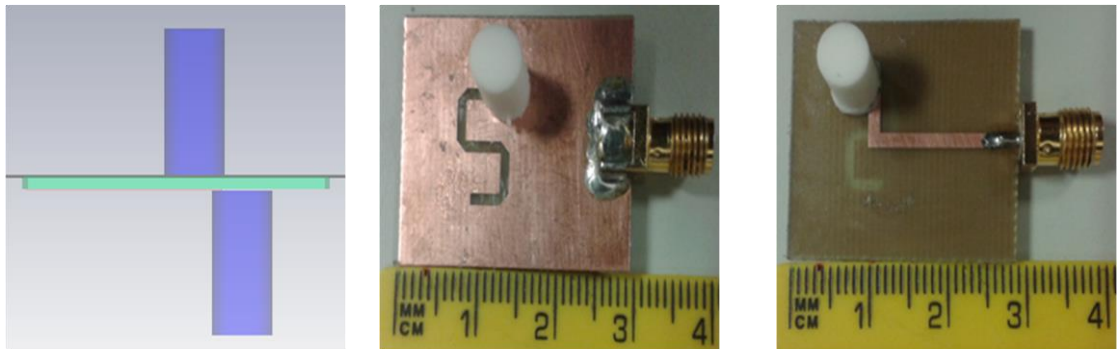
7.4.2 Positioning of the Dielectric Resonators

The relative positioning of the DR posts needs to be considered in more detail. A refinement of the parametric study in Section 7.3 was made by considering the following configurations (Figure 7.11): (i) both resonators on the slot side, (ii) upper resonator on the slot side and lower resonator on the feed side, and (iii) upper resonator on the feed side and lower resonator on the slot side.

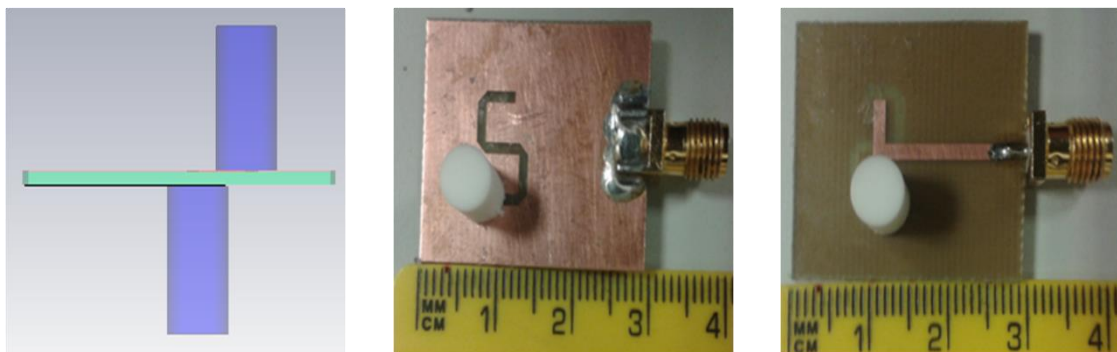
The performances of the three configurations are shown in Figure 12, for the simulated model and the prototype DRA. In Figure 7.13 (a), it can be seen that case (i) delivers the largest impedance bandwidth with improved impedance matching. The actual working bandwidth of the DRA is found to extend from 7.66GHz to 11.2GHz. In Figure 7.12 (b), the gain performance for case (iii) indicates the best response for the difference between the maximum and minimum gain states.



(a) Two DR's on the slot side



(b) Lower DR on the slot side and upper DR on feed side



(c) Upper DR on the slot size and lower DR on feed side

Figure 7.11: Investigated positions of DR's (a) Simulated with HFSS, (b) fabricated antenna with lower DR on the slot side and upper DR on feed side and (c) fabricated antenna with upper DR on the slot size and lower DR on feed side.

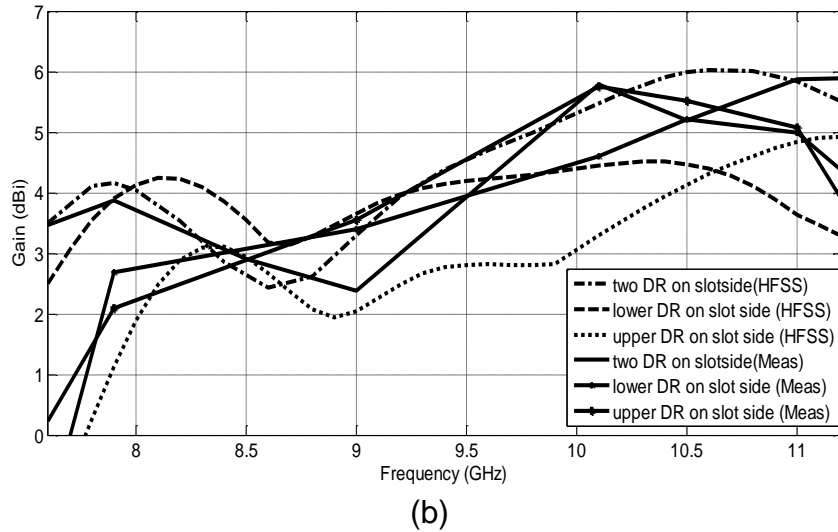
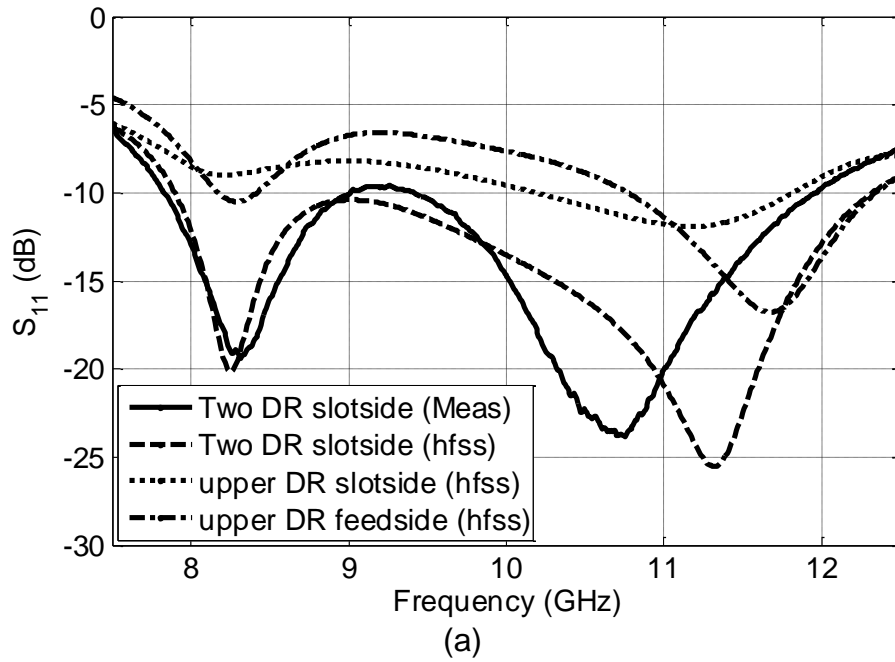


Figure 7.12: Simulated and measured (a) Reflection coefficient magnitude (S_{11}) and (b) Gain (dBi) vs. frequency plots with different DR's positions.

The simulated far field radiation patterns at a distance of 1m, for the three different cases are presented in Figure 7.13, for two operating frequencies, 9.5GHz and 10.5GHz. Case (iii) appears to give the best diversity pattern at these frequencies.

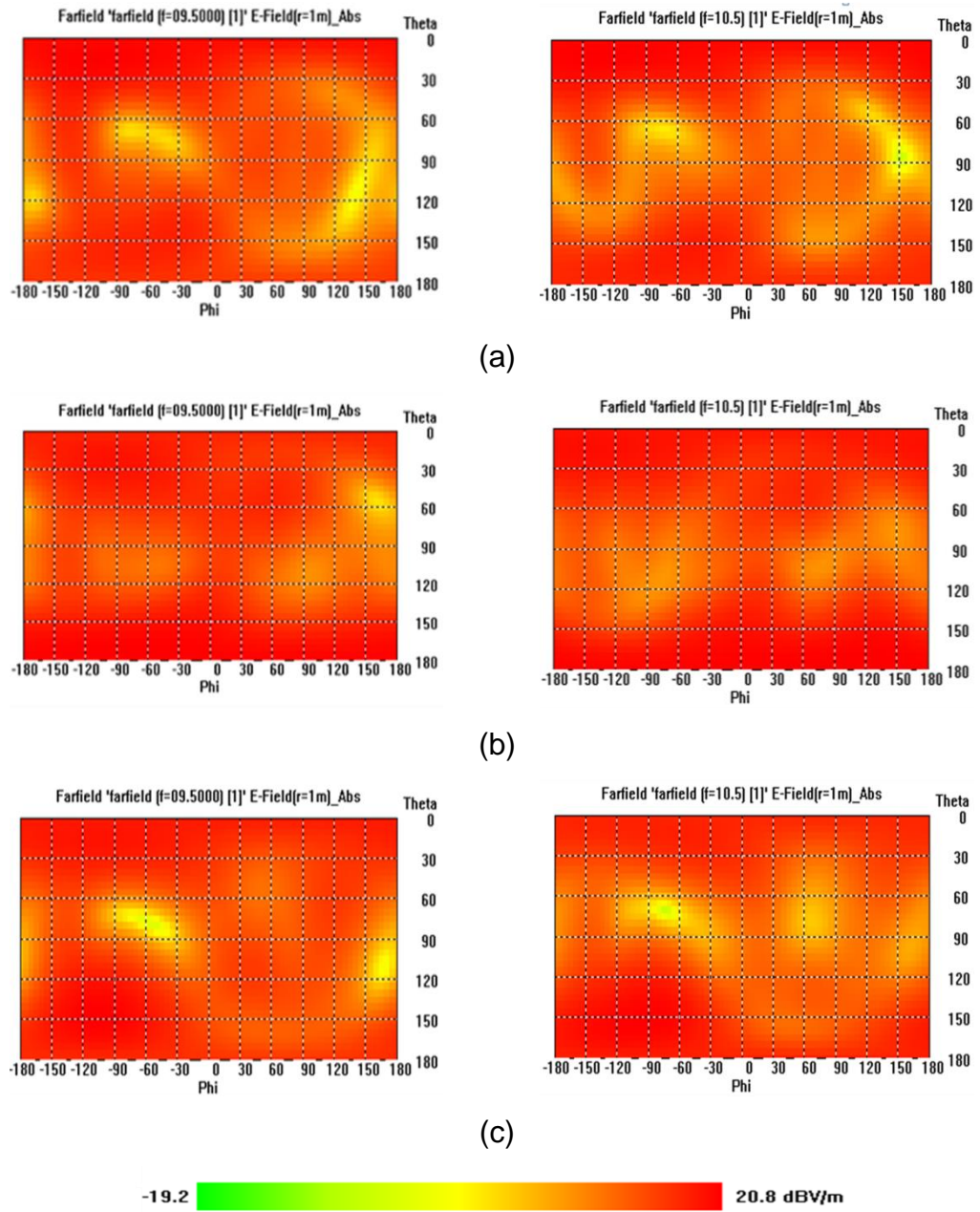


Figure 7.13: 2D E-field radiation patterns at 9.5GHz and 10.5GHz (a) Two DR's on the slot side, (b) lower DR on the slot side and upper DR on feed side, (c) upper DR on the slot size and lower DR on feed side.

7.5 Conclusions

A new physically compact aperture-coupled dual-segment DRA has been proposed for use in X-band communications. Identical cylindrical DR posts of permittivity 9.4 are mounted on a substrate backed ground plane. The antenna was excited using an L-shaped feed line, and internal antenna coupling was achieved using an S-shaped slot. The effective antenna volume after optimisation process was found around $30.0 \times 25.0 \times 0.8 \text{ mm}^3$. The measured prototype performance shows an average gain of 6.0 dBi over the frequency range 7.66 GHz to 11.2 GHz, with stable radiation patterns. The DR posts may be arranged in two distinct configurations: (i) occupying space on one side of the substrate, and (ii) on opposing sides. The first configuration results in a higher gain performance, whilst the second results in approximated uniform radiation pattern within 1m radial distance from the antenna.

CHAPTER 8

BALANCED DUAL-SEGMENT CYLINDRICAL DIELECTRIC RESONATOR ANTENNA FOR ULTRA-WIDEBAND APPLICATIONS

8.1 Introduction

UWB antennas are one of the key devices in many UWB systems, such as broadband wireless communications, electronic warfare, medical imaging and radar systems, etc. UWB antennas offer many desirable features, and at the same time often with a simple RF front-end [147, 148]. Generally, an UWB antenna has a broad frequency range larger than $(f_h/f_l) > 1.22$ (where f_h is the upper frequency edge and f_l is the lower frequency edge) in order to be 'ultra wide' but actually it depends on the system requirements and the centre frequency of the bandwidth [148]. There are mainly four types of UWB antennas having:

- scaled structure (such as Bow-Tie dipoles, biconical dipoles and log-periodic dipole arrays),
- self-complementary structure (self-complementary spiral antennas),
- traveling wave structure (Vivaldi antennas), and

- multiple reflection (or resonance) structure (dielectric resonator antenna) [149, 150].

Based on the feed configuration antennas can be categorized as balanced and unbalanced. In an unbalanced antenna, the ground plane is used as part of the radiator, with radiating currents induced on both of the ground plane and the radiating element. This situation degrades the antenna's radiation characteristics and introduces losses and uncertainty in its matching. A balanced structure is a genuine alternative to avoid this degradation in performance. In a balanced structure, currents mutually cancel their effects, with net current flowing only on the antenna radiating element and not on the ground plane, so that the performance of the antenna is not affected [151].

Dielectric Resonator Antennas (DRAs) have been extensively studied owing to their numerous advantages such as high radiation efficiency, low weight, and small size due to the high permittivity of their constructing material. DRAs can be excited by various feeding methods, such as slot, coaxial feed, microstrip line and coplanar lines [87, 152].

The DR feedline geometry has been utilized for the extension of the antenna bandwidth [85]. Other techniques to achieve UWB operation employ monopole geometries, composite DRAs using composite shapes and/or composite materials, modified ground plane shapes and use of defected ground

plane[153]. Other techniques to achieve UWB operation employ monopole geometries, composite DRAs using composite shapes and/or composite materials, modified ground plane shapes and use of defected ground plane [52, 153]. The use of dual segments of different dielectric constant fed by the same line showed improved bandwidth [125, 152]. Moreover, it has been shown recently that dual similar dielectric resonators (DRs) placed asymmetrically with respect to the feeding aperture can bring an increase in bandwidth as well as more design flexibility [131, 154].

In this chapter, a balanced dual segment cylindrical dielectric antenna (CDRA) with ultra wide-band operation is reported. A T-shaped slot and L-shaped microstrip feeding line are suggested to furnish a balanced coupling mechanism for feeding two DRAs. Performance of the proposed antenna was analyzed and optimized against the target frequency band. The proposed antenna was then modified by adding a C-shaped strip to increase the gain.

The performances of the two balanced antennas were characterized and optimized in terms of antenna reflection coefficient, radiation pattern, and gain. The designed antennas covered the frequency range from 6.4 GHz to 11.736 GHz that is 58.7% bandwidth. A maximum gain of 2.66 dB was achieved at frequency of 7 GHz, and a further 2.25 dB increase in the maximum gain was attained using the added C-shaped strip. For validation, prototypes of the two antennas were fabricated and tested. The characteristics of these balanced

antennas are analyzed and optimized using the CST microwave studio suite that is an electromagnetic simulator based on the finite integration technique [155].

8.2 Frist Design: Without a C-shape Strip

8.2.1 Antenna Geometry

The geometry of the proposed DRA antenna is shown in Figure 8.1(a). The ground plane, with an area of $(23 \times 12) \text{ mm}^2$, is etched on the substrate bottom to constitute a copper-coated baseboard. Two opposing L-shaped sections with a vertical L-section length $f_1 = 3.4 \text{ mm}$, vertical L-section width $W_{f2} = 1.5 \text{ mm}$, horizontal L-section length $L_{f2} = 4.5 \text{ mm}$, and horizontal L-section width $W_{f1} = 2.25 \text{ mm}$ are added to the ground plane to form the balanced two-arm structure. Two cylindrical DRAs (CDRAs) of relative permittivity $\epsilon_{\text{rdr}} = 9.4$, diameter $D = 6.0 \text{ mm}$ and height $h = 9.0 \text{ mm}$ are symmetrically fixed on the two opposite L-shaped sections of the ground plane. The substrate is Rogers TMM4tm with a thickness $t = 0.8 \text{ mm}$, relative permittivity $\epsilon_{\text{rs}} = 4.5$, and loss tangent of 0.017, with dimensions $(23 \times 23) \text{ mm}^2$. As a feeding mechanism, a T-shaped slot with vertical length $y = 3.5 \text{ mm}$, vertical width $x = 1.25 \text{ mm}$, horizontal length $s_l = 4.0 \text{ mm}$ and horizontal width $s_w = 0.35 \text{ mm}$ is etched on the ground plane. The dimensions of the aperture influence the resonant frequency of the structure

and the amount of undesired radiation in the back direction, and also determine the coupling between the radiating element and the microstrip line. The microstrip line dimensions can be calculated using empirical formulas given in [127]: accordingly, a $50\ \Omega$ L-shaped microstrip feed line with vertical length $L_f = 10.5\text{ mm}$, horizontal length $L_{f3} = 6.5\text{ mm}$ and width $W_f = 1.5\text{ mm}$ is used for impedance matching. At the tip of microstrip feed line, a $50\ \Omega$ coaxial SMA connector is connected for feeding microwave power.

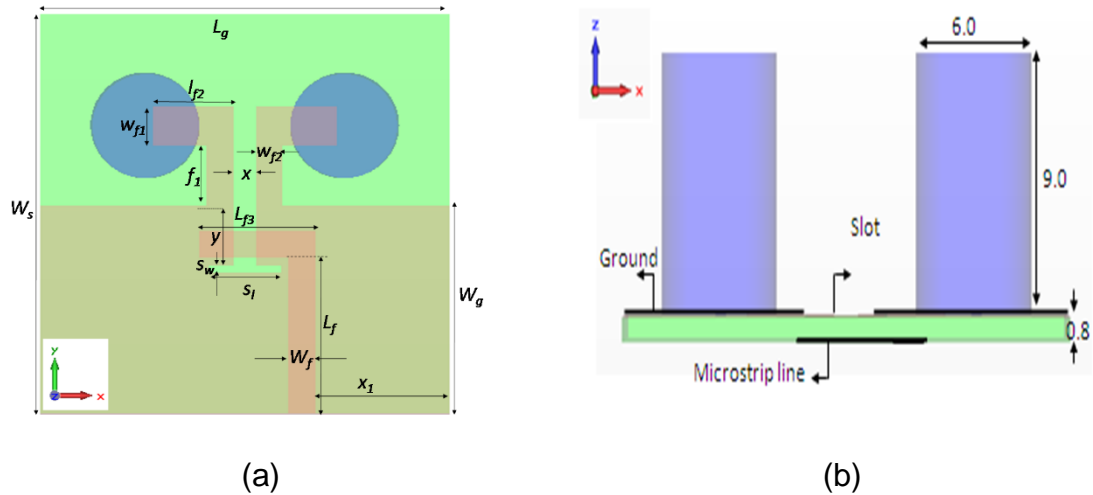


Figure 8.1: Balanced dual-segment cylindrical dielectric resonator antenna; (a) top view and (b) side view with design dimensions and parameters.

Figure 8.1 shows that the two inverted L-sections work as a half wavelength dipole that is fed by the inverted T-shaped slot. The length of the dipole is given by:

$$L_D = 2 L_{f2} + x \quad (8.1)$$

This printed dipole is not adequately thin ($L_D / W_{f1} \leq 10$), and thus its resonance can be considered to occur at 0.45 effective wavelength. It can be shown that dipole resonates at frequency f_{r1} given by:

$$f_{r1} = c / (2.22 L_D \sqrt{\epsilon_{re}}) \quad (8.2)$$

$$\epsilon_{re} = (\epsilon_{rs} + 1) / 2 \quad (8.3)$$

where ϵ_{re} is the effective relative permittivity of the substrate.

The resonant frequency of an isolated DR cylinder is calculated by [51]:

$$f_{r2} = \frac{c}{2\pi a \sqrt{\epsilon_{rdr}}} \left[1.71 + 2 \left(\frac{a}{2h} \right) + 0.1578 \left(\frac{a}{2h} \right)^2 \right] \quad (8.4)$$

Here $a = D/2$ (in cm), D and h are respectively the diameter and the height of each DR, the relative permittivity of the DR material, and c is the speed of light. For the DR used here, the resonance frequency according to Eq 8.4 is 10.629GHz.

Thus, the expected range of frequency can approximately found from Eq8.3 for the lower limit, and from Eq 8.4 for the upper limit. The two limits will obviously be influenced by the corresponding design parameters. The effects of various design parameters on the antenna performance are investigated in the following sections.

8.2.2 Parametric Study

This section reports a parametric study to investigate the effects of various parameters on the response of the proposed antenna. The antenna structure was analyzed and optimized using Computer Simulation Technology (CST) Microwave Studio Suite™ 2014[156]. The parametric analysis was carried out by varying one parameter while holding the remaining ones fixed. The optimized dimensions are presented in Table 8-1. The investigations start with the effect of the T-slot parameters then proceed to explore the effects of the dimensions of the two inverted L-sections.

Table 8-1: Detailed parameters of the proposed antenna (all dimensions are in millimetres)

D	h	W_g	L_g	W_s	L_s	l_f	W_f	L_{f3}	x_1
6	9	12	23	23	23	10.5	1.5	6.5	7.5

The influence of the horizontal slot length s_l on the reflection coefficient is shown in Figure 8.2 With increasing the horizontal slot length, there is a slight increase in impedance bandwidth, a shift in the resonance frequency towards the right and a slight reduction in reflection coefficient. An optimum horizontal slot length of $s_l = 4$ mm was chosen.

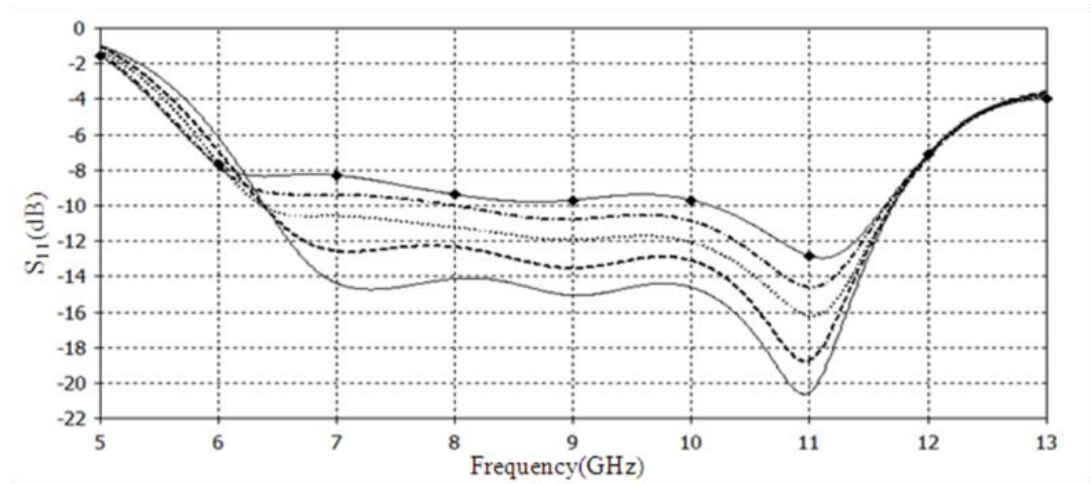


Figure 8.2 S Simulated effects on reflection coefficient of the horizontal slot length s_l ; $s_l=3.0$ (solid), $s_l=3.5$ (dashed), $s_l=4.0$ (dotted), $s_l=4.5$ (dash-dotted), $s_l=5.0$ (circles).

Figure 8.3 shows the simulated reflection coefficient of the DRA with variation of the vertical slot length (y) from 2.5 mm to 4 mm. The optimum impedance bandwidth is achieved at vertical slot length of 3.25 mm with minimum reflection coefficient across the spectrum bandwidth.

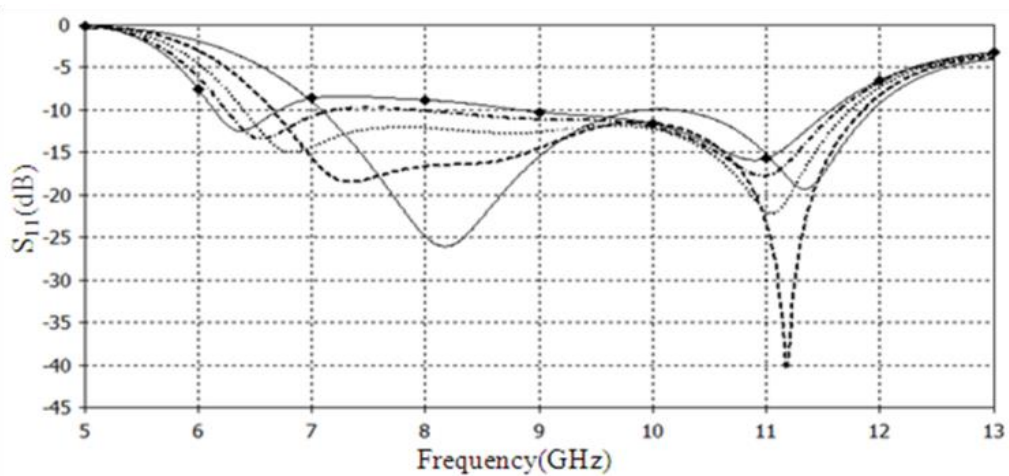


Figure 8.3: Simulated reflection coefficient versus frequency for various vertical slot lengths y ; $y=2.5$ (solid), $y=2.875$ (dashed), $y=3.25$ (dotted), $y=3.625$ (dash-dotted) and $y=4.0$ (circles).

Figure 8.4 shows simulated results of the reflection coefficient of the DRA obtained by varying the horizontal slot width (s_w) of the DRA from 0.2 mm to 0.5 mm. It is clear that a slot width of 0.35 mm gives an optimum ($S_{11} < -10$ dB) impedance bandwidth. Figure 8.5 shows the simulated reflection coefficient of the DRA for varying vertical slot width (x) of the DRA from 0.5 mm to 1.5 mm. It is clear that the vertical slot width of 1.25 mm gives an optimum ($S_{11} < -10$ dB) impedance bandwidth.

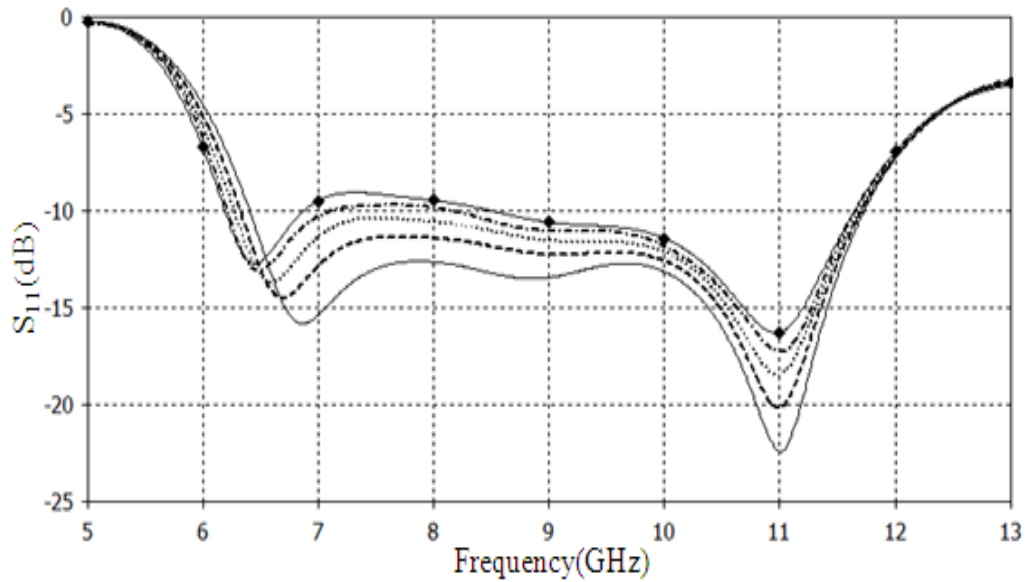


Figure 8.4: Simulated reflection coefficient versus frequency for various horizontal slot width s_w ; $s_w=0.2$ mm(solid), $s_w=0.275$ mm(dashed), $s_w=0.35$ mm(dotted), $s_w=0.425$ mm(dash-dotted) and $s_w=0.5$ mm(circles).

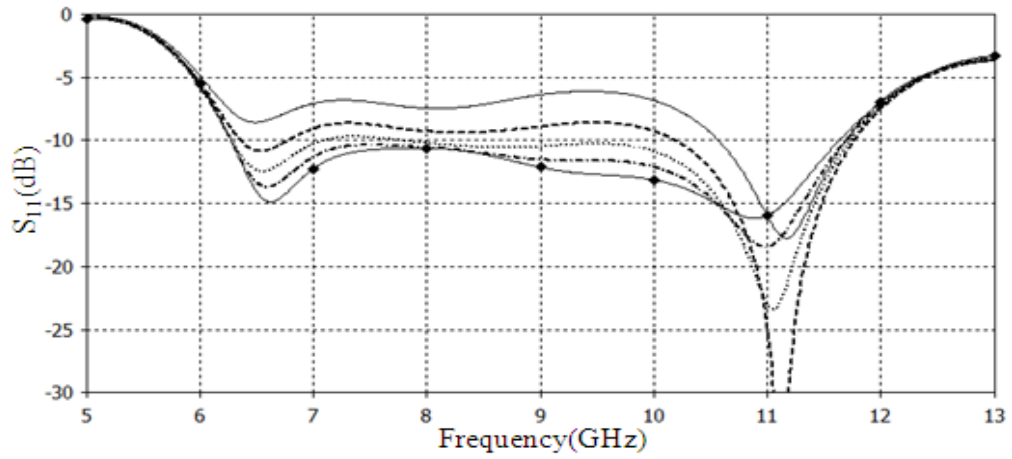


Figure 8.5: Simulated reflection coefficient versus frequency for different vertical slot width x ; $x = 0.5$ mm (solid), $x = 0.75$ mm (dashed), $x = 1.0$ mm (dotted), $x = 1.25$ mm (dash-dotted) and $x = 1.5$ mm (circles).

Figure 8.6 shows the simulated reflection coefficient of the DRA for varying the length of the vertical L-section, f_1 , from 2.5 mm to 4.0 mm. The results show that a longer section leads to a lower value of the upper edge of the band. A vertical L-section length of 2.5 mm gives a maximum impedance bandwidth.

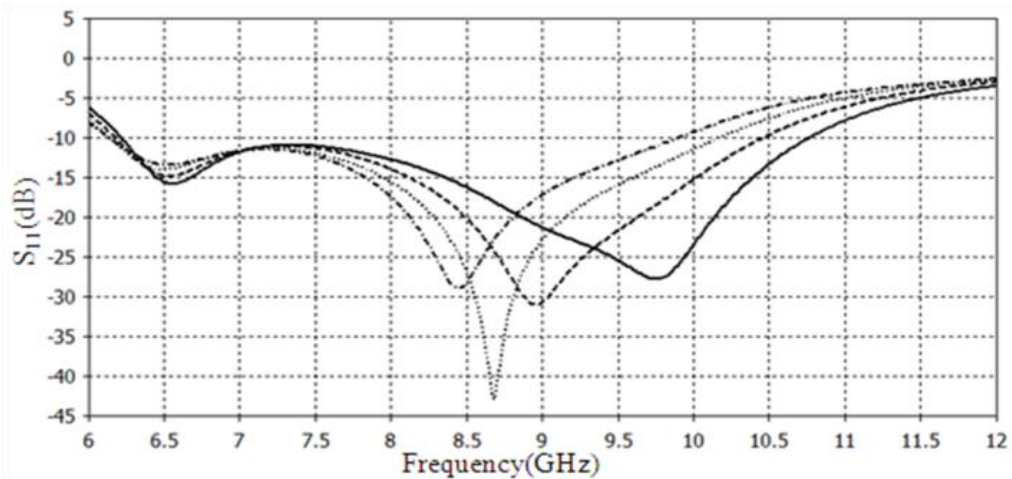


Figure 8.6: Simulated reflection coefficient versus frequency for various vertical L-section lengths f_1 ; $f_1 = 2.5$ mm (solid), $f_1 = 3$ mm (dashed), $f_1 = 3.5$ mm (dotted) and $f_1 = 4$ mm (dash-dotted).

Figure 8.7 shows the simulated reflection coefficient of the DRA when varying the vertical L-section width (W_{f2}) from 1 mm to 1.5 mm. The vertical L-section width has a slight effect on the reflection coefficient and an optimum ($S_{11} < -10$ dB) impedance bandwidth is achieved with $W_{f2} = 1.25$ mm.

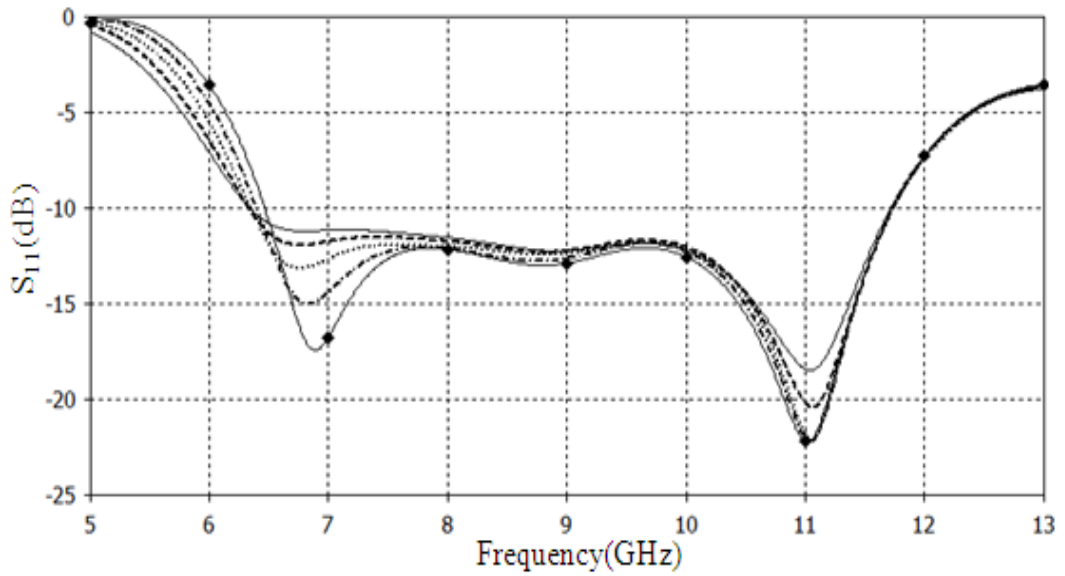


Figure 8.7: Simulated reflection coefficient versus frequency for different vertical L-section width W_{f2} ; $W_{f2} = 0.5$ mm (solid), $W_{f2} = 0.75$ mm (dashed) and $W_{f2} = 1.0$ mm (dotted) $W_{f2} = 1.25$ mm (dash-dotted) and $W_{f2} = 1.5$ mm (circles).

Figure 8.8 shows the simulated reflection coefficient of the DRA for variable horizontal L-section length, L_{f2} , from 3 mm to 5 mm. The figure shows that increased length L_{f2} shifts the lower edge of the band towards lower frequencies. The bandwidth is also affected by varying the parameter L_{f2} . This finding can be explained by noting that the two inverted-L sections work as a $\lambda_g/2$ dipole whose resonance frequency was given by Equ. 3. This frequency

influences the lower edge of the operation bandwidth. For the dimensions shown in Table 1, the parameters ($x=1.25\text{mm}$, $L_{f2}=4.5$), and using Equ. 3 the resonance frequency f_{r1} was found to be 8.023 GHz. A vertical L-section length of 4.5 mm was found to give a good compromization between band width and value of the reflection coefficient.

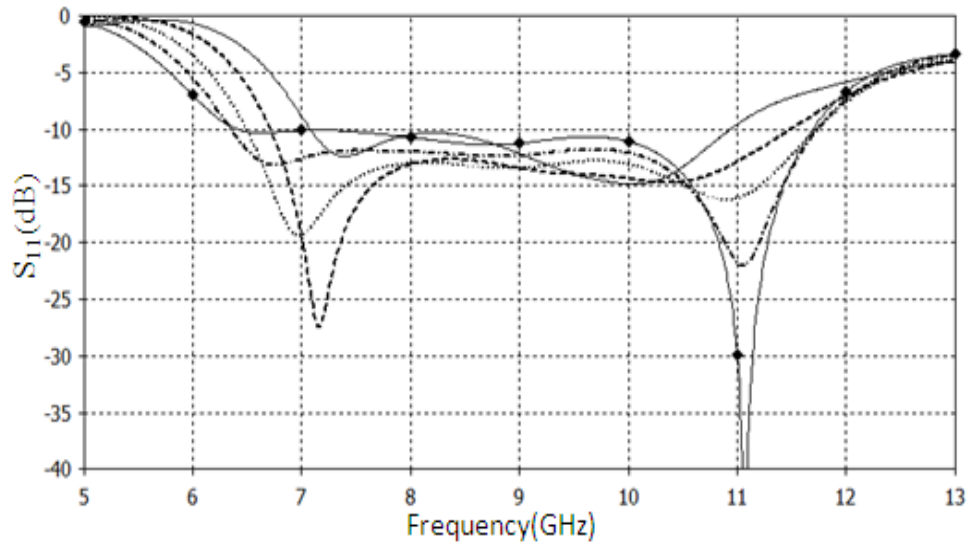


Figure 8.8: Simulated reflection coefficient versus frequency for various horizontal L-section lengths L_{f2} ; $L_{f2} = 3$ mm (solid), $L_{f2} = 3.5$ mm (dashed), $L_{f2} = 4.0$ mm (dotted), $L_{f2} = 4.5$ mm (dash-dotted) and $L_{f2} = 5.0$ mm (circles).

Figure 8.9 displays the simulated reflection coefficient of the DRA against horizontal L-section width W_{f1} from 1.5 mm to 3 mm. The figure shows that a vertical L-section width of 1.0 mm is the optimum width for a large impedance bandwidth

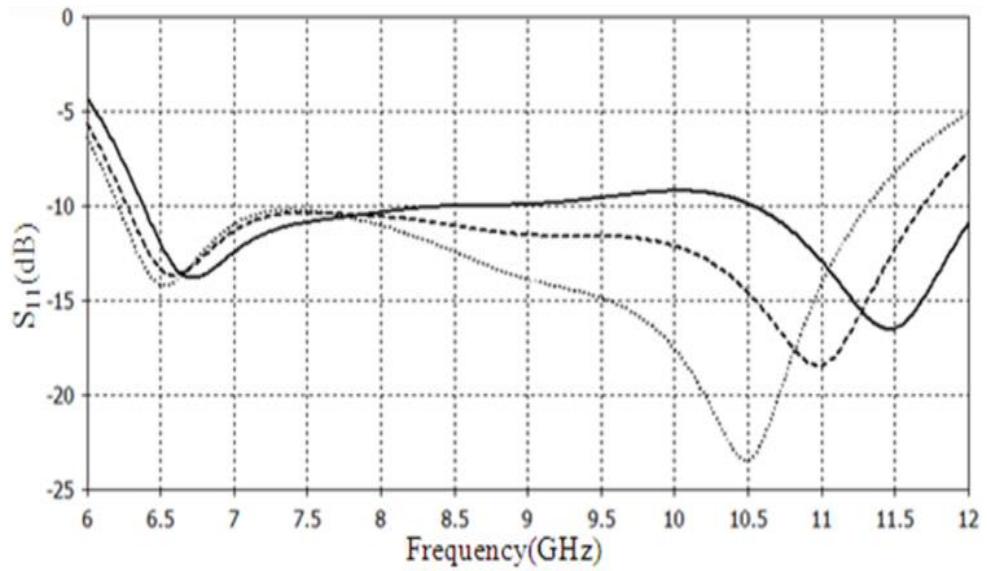


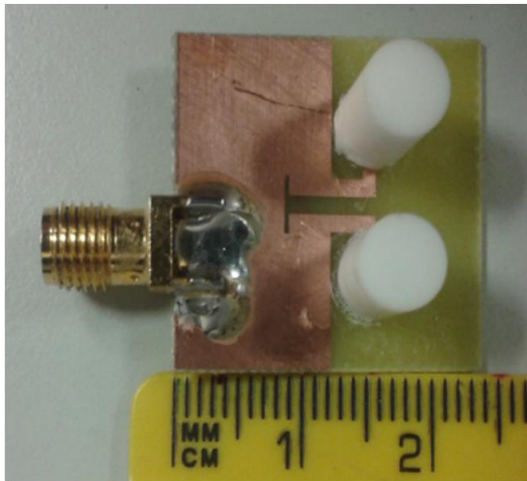
Figure 8.9: Simulated reflection coefficient versus frequency for various horizontal L-section width W_{f1} ; $W_{f1} = 0.5$ mm (solid), $W_{f1} = 1.0$ mm (dashed) and $W_{f1} = 1.5$ mm (dotted).

8.2.3 Experimental Results and Discussions

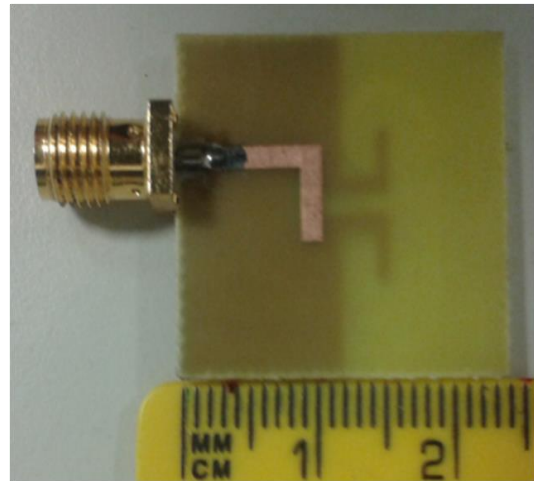
To validate the proposed design, a prototype of the DRA antenna shown in Figure 8.1 with the optimized dimensions listed in Table 8-2 was fabricated and measured. The substrate parameters were $\epsilon_{rs} = 4.5$ with loss tangent = 0.017, and for the DRA $\epsilon_{rdr} = 9.4$. The fabricated antenna is shown in Figure 8.10.

Table 8-2: Optimum parameters of the proposed antenna. (All dimensions are in millimetres).

D	h	W_g	L_g	W_s	L_s	l_f	f_1	l_{f2}	l_{f3}
6	9	12	23	23	23	10.5	2.5	4.5	6.5
W_f	W_{f1}	W_{f2}	s_w	s_l	x	x_1	y		
1.5	1.0	1.25	0.35	4.0	1.25	7.5	3.25		



(a)



(b)

Figure 8.10: Photo of the proposed antenna; (a) front view and (b) rear view.

The prototype was tested using an HP8510C vector network analyser, with the measured and simulated reflection coefficients shown in Figure 8.11. These results show that the simulated antenna here achieves an impedance matching ($S_{11} < -10$ dB) from 6.4 GHz to 11.736 GHz, which represents a 58.7% bandwidth whereas the measured antenna achieves impedance matching from

7.15 GHz to 12.3 GHz, 52.9% bandwidth. The differences between the measured and simulated results, seen in a shift to higher frequency and the general increase in S_{11} , may be attributed to the combined effects of the use of the glue to fix the DRA and fabrication errors.

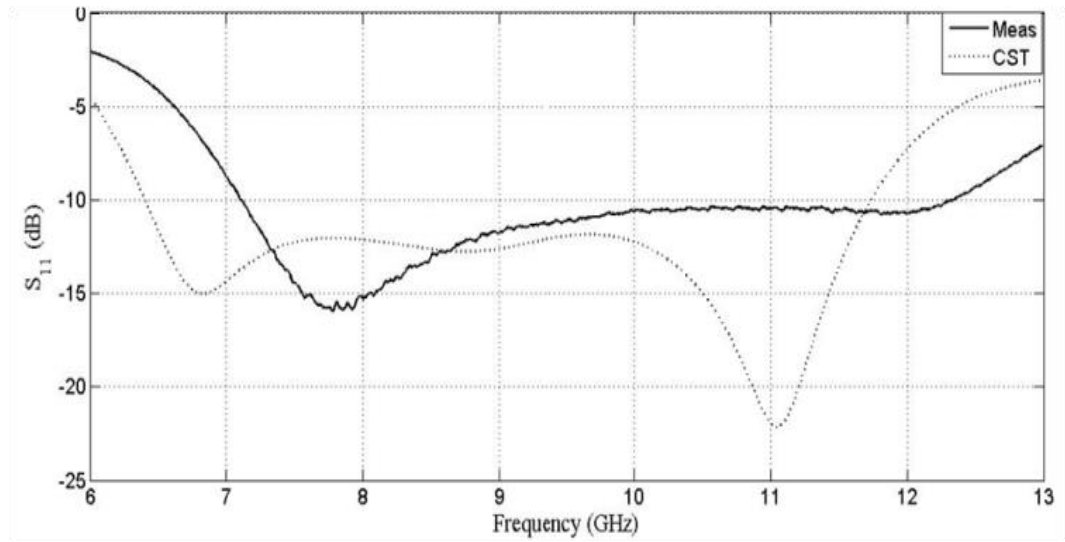


Figure 8.11: Simulated and measured reflection coefficients versus frequency for the proposed antenna.

Figure 8.12 plots the measured and simulated peak gains of the proposed antenna, showing that the simulated antenna has a gain that varies between 2.66dBi and 1.86dBi across the pass band (6.4 GHz to 11.736 GHz) and is a maximum at 7.0 GHz. The measured gain varies between 2.79dBi and 2.63dBi, and has a maximum at 7.89 GHz. The relatively small gain of the proposed antenna is attributed to its small dimensions of $23 \times 23 \text{ mm}^2$, which are only 0.69×0.69 wavelengths at a centre frequency of 9 GHz.

Examination of the results shown in Figs. 2 to 9 and the experimental results of Figs. 11 and 12 were shows that the reflection coefficient has dips at frequencies ranging from 10 GHz to 11 GHz. These are in good agreement with the resonance frequency (10.629 GHz) of the isolated DR predicted by Equ. 4. The peak gain also shows a maximum at about this frequency. Although the DR is a resonating element, the wide band performance demonstrated in the Figs. 2 to 9 and Figs. 11 and 12 can be attributed to the existence of two frequencies. The lower one is dedicated by the $\lambda_g/2$ dipole which can be found from Equs.1 to 3. The upper frequency is controlled by resonance frequency of the DR which is given by Equ. 4.

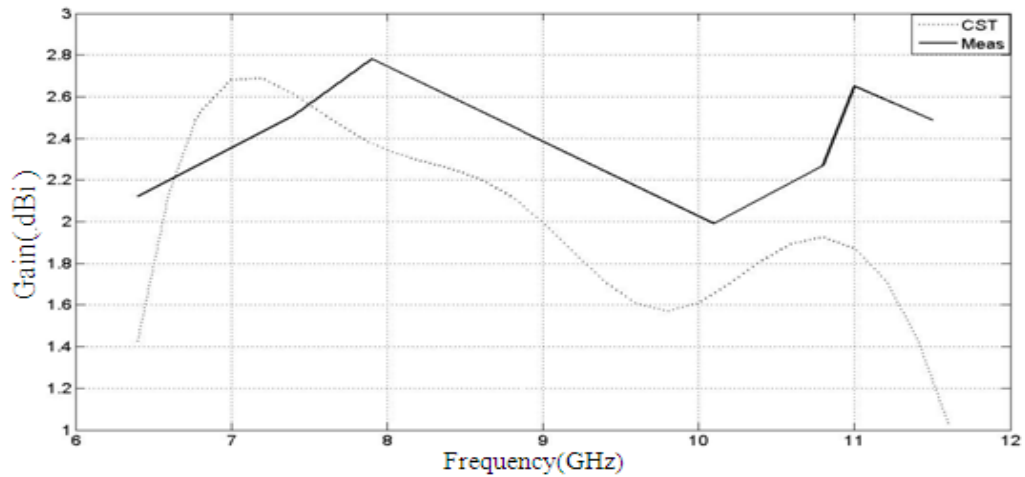


Figure 8.12: Measured and simulated peak gains of the proposed DRA.

The proposed DR antenna was also measured in the far-field using an anechoic chamber with an elevation-over-azimuth positioner, with the elevation axis

coincident with the polar axis ($\theta = 0^\circ$) of the antenna's co-ordinate system. The azimuth drive thus generated cuts at constant ϕ .

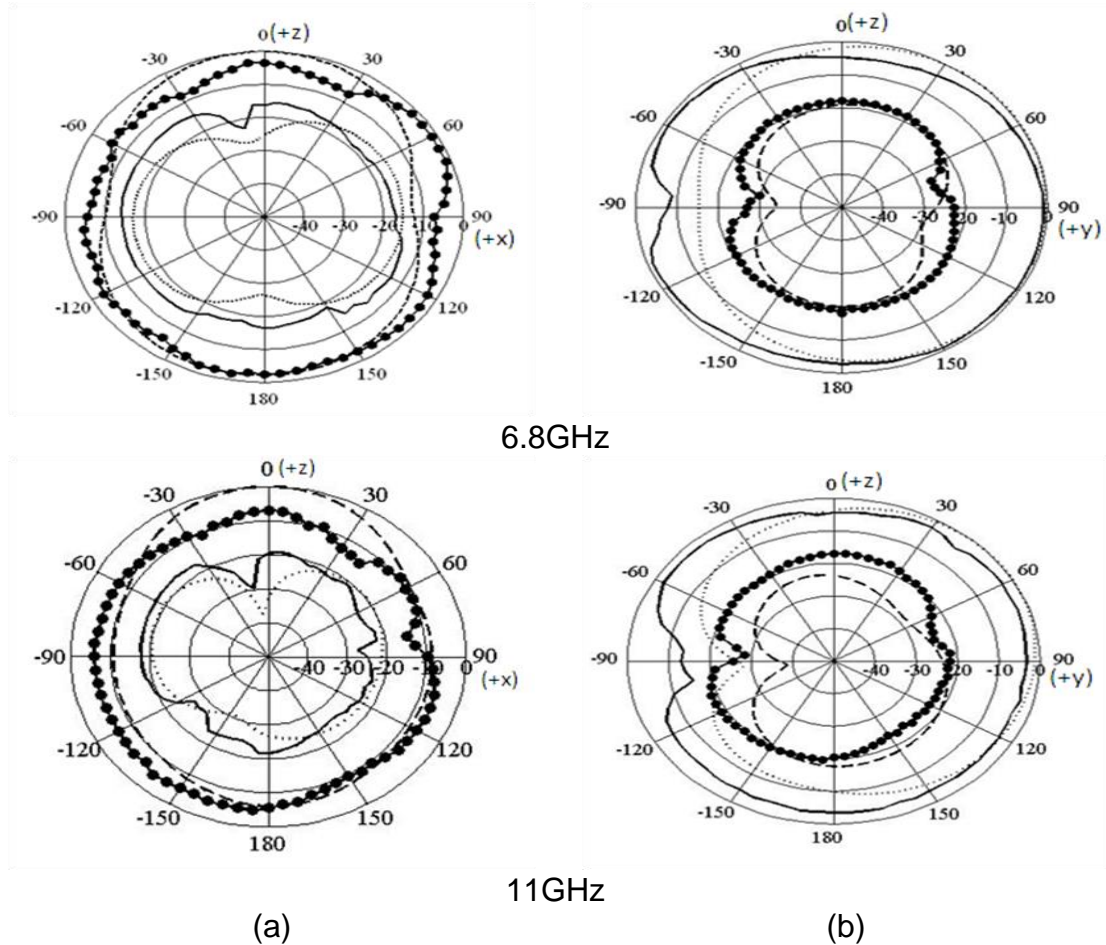


Figure 8.13: Simulated and measured radiation patterns; (a) at xz plane, (b) at yz plane; simulated E_θ : dashed line, simulated E_ϕ : dotted line, measured E_θ : 'o-o-o', measured E_ϕ : solid line.

The fixed antenna (transmitting antenna) was a broadband horn (EMCO type 3115), positioned 4 m from the antenna being tested. The azimuth positioner was rotated from $\theta = -180^\circ$ to 180° at increments of 5° for the selected

measurement. Two pattern cuts (i.e. $\phi = 0$ and 90°) were taken at two selected operating frequencies for which the matching was best.

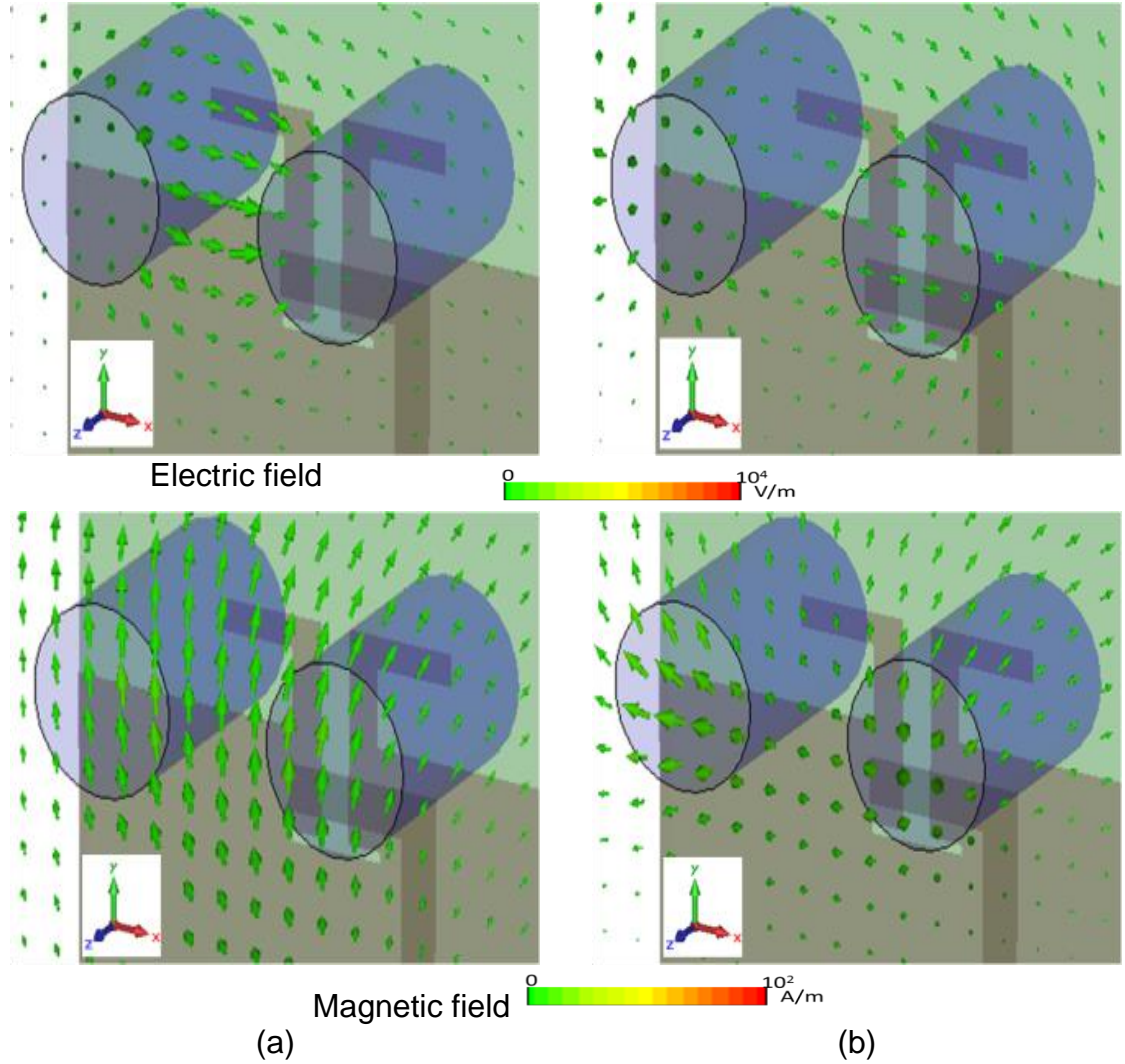


Figure 8.14: Magnitude of electric and magnetic field distributions of the proposed T-slot fed balanced dual segment CDRA at (a) 6.8 GHz, (b) 11 GHz.

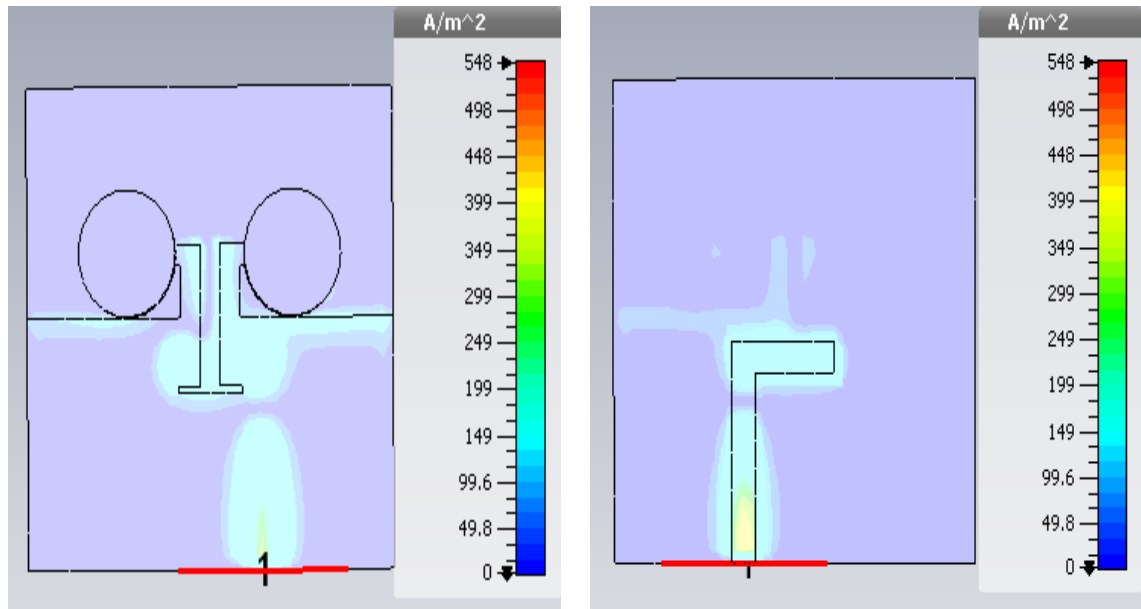
Figure 8.13 depicts the simulated and measured radiation patterns at the two frequencies (6.8 GHz and 11 GHz) for which the matching was best. It is clear

that the pattern has quasi-omnidirectional shape, and maximum antenna radiation is in the positive y-direction.

The distributions of the electric and magnetic fields for the optimized antenna at two frequencies of 6.8 GHz and 11 GHz were calculated using CST software and the results are shown in Figure 8.14. It is observed that the magnetic and electric field lines are parallel to the DR base, i.e. they are transverse to DR axis. This result justifies the use of Equ.4 for predicting the resonance frequency of the DRs. The variations of the electric field indicate that at 11GHz the electric field is higher at the surface of the cylinder. This finding is supported by the fact that at a frequency of 6.8 GHz there is no resonance in the DR since the lowest mode has a frequency of 10.629GHz as predicted by Equ.1. However, at 11GHz, the DRs are very near to resonance in the dominant mode HEM_{110} .

The current distribution on the ground plane was studied in the simulation model, using the two specified frequencies, 6.8 GHz and 9.0 GHz. The results are shown in Figure 8.15, where most of the induced current on the ground can be seen to be concentrated in the region of beneath radiator feeding network and negligible induced surface currents were shown to exist on the rest of the ground. As a results this balanced antenna design will be insensitive to the

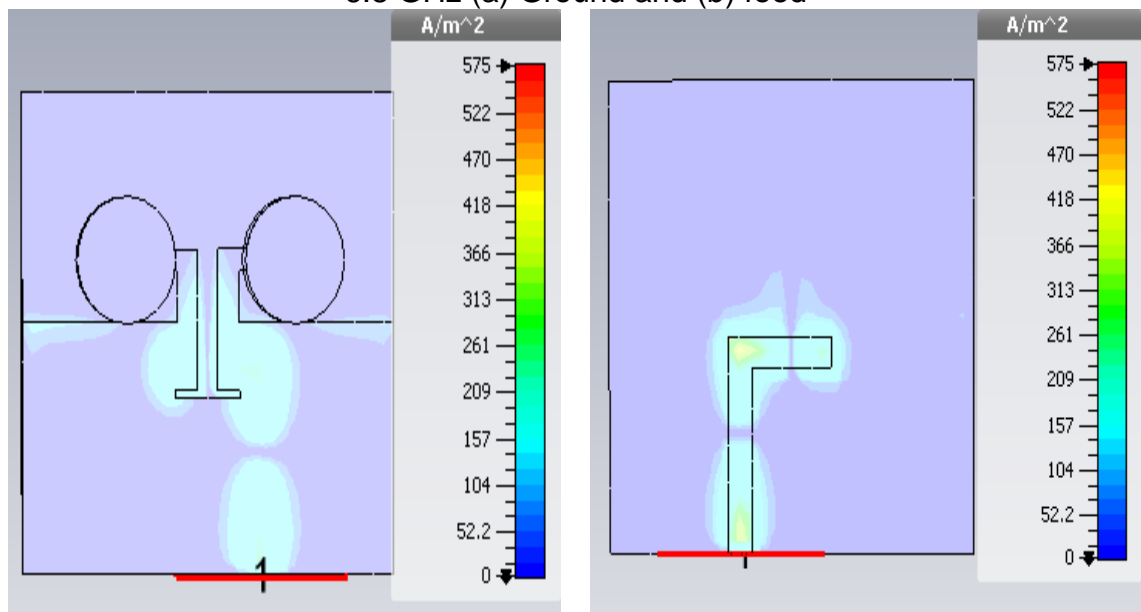
loading and coupling effects on possible circuits mounted on or near the ground surface.



(a)

(b)

6.8 GHz (a) Ground and (b) feed



(a)

(b)

9 GHz (a) Ground and (b) feed

Figure 8.15: current distribution on the ground plane

8.3 Second Design: Adding a C-shape Strip

The proposed antenna of Figure 8.1, was modified to increase its gain by adding a parasitic flipped C-shaped strip on the same side of the DRA with radius r_c and width W_c . The width of the substrate W_s was also increased as shown in Figure 8.16. The added strip can be considered to work as a guide to the transmitted wave leading to increased gain. The strip length is given by:

$$\text{strip length} = \frac{n^\circ}{360^\circ} \times 2\pi (\text{average radius of the strip}) \quad (8.5)$$

where n° is the sector angle of the strip.

The dimensions and position of this strip were optimized using parametric analysis. It was found that $W_s = 35$ mm, $r_c = 7$ mm, $W_c = 1$ mm, and a separation of $y_c = 13.5$ mm between the ground plane and the centre of the parasitic C- shaped strip gave the best results. The improvement in gain of the proposed antenna can be controlled by properly adjusting the parameters of the parasitic strip.

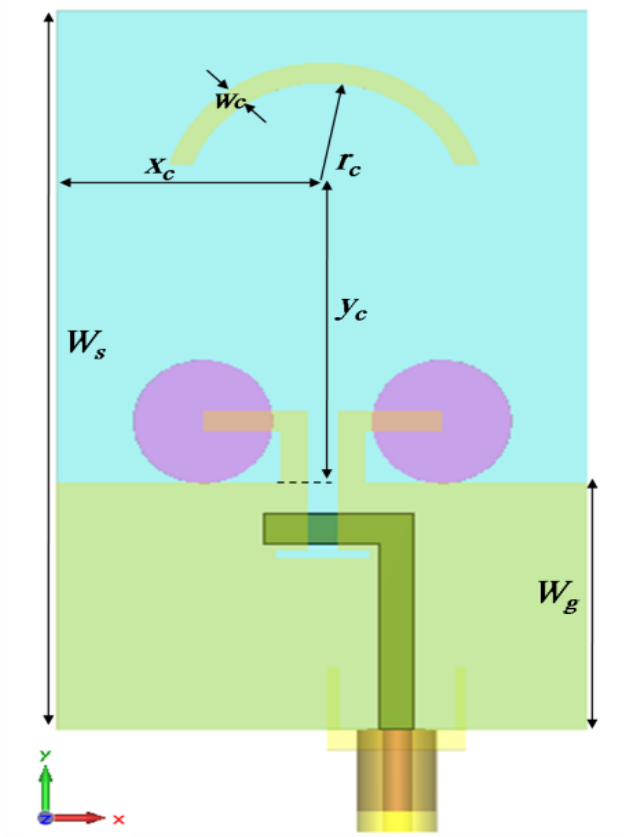


Figure 8.16: Geometry of the modified antenna with a C-shaped strip.

8.3.1 Antenna Performance

The performance of the modified antenna was analyzed and optimized using the full-wave electromagnetic simulator CST Microwave Studio suit 2011. Figure 8.17 shows the variation of realized gain of the modified antenna with frequency for strip widths W_c from 0.5 mm to 1.5 mm. It is clear that increasing the width of the strip caused a slight increase in the realized gain in the lower edge of the frequency band and shifted the lower edge to the right.

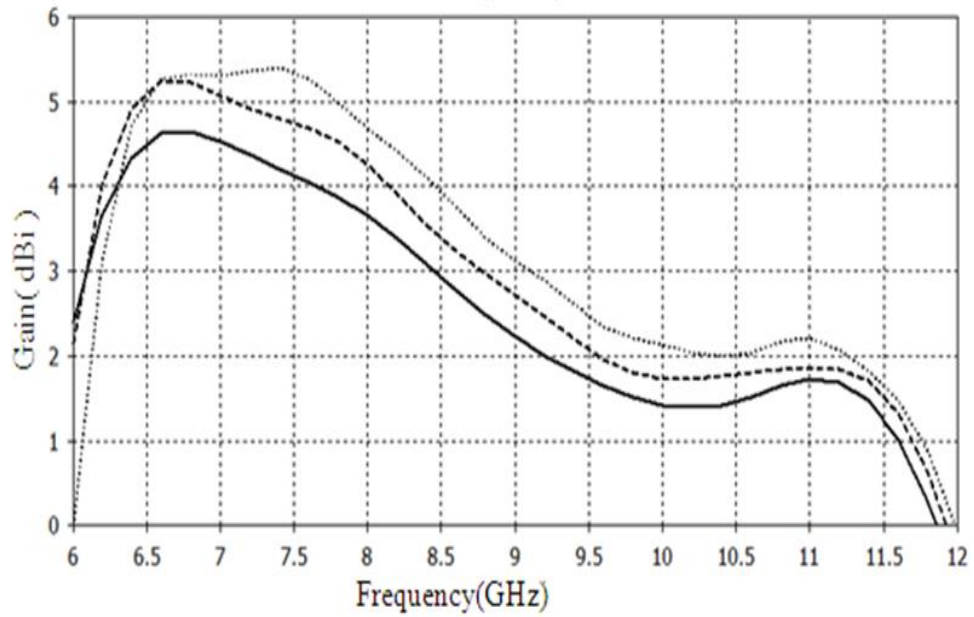


Figure 8.17: Simulated realized gain versus frequency for various widths W_c of the C-shaped strip; $W_c = 0.5$ mm (solid), $W_c = 1.0$ mm (dashed) , $W_c = 1.5$ mm (dotted).

Figure 8.18 shows the variation of realized gain of the modified antenna with frequency for different values of the vertical separation between ground plane and center of the C-shaped strip y_c . There is a slight reduction in realized gain and a shift towards the left near the lower end of the frequency band with increasing separation between the ground plane and the center of the strip. However, no change towards the upper end of the frequency band was noticed

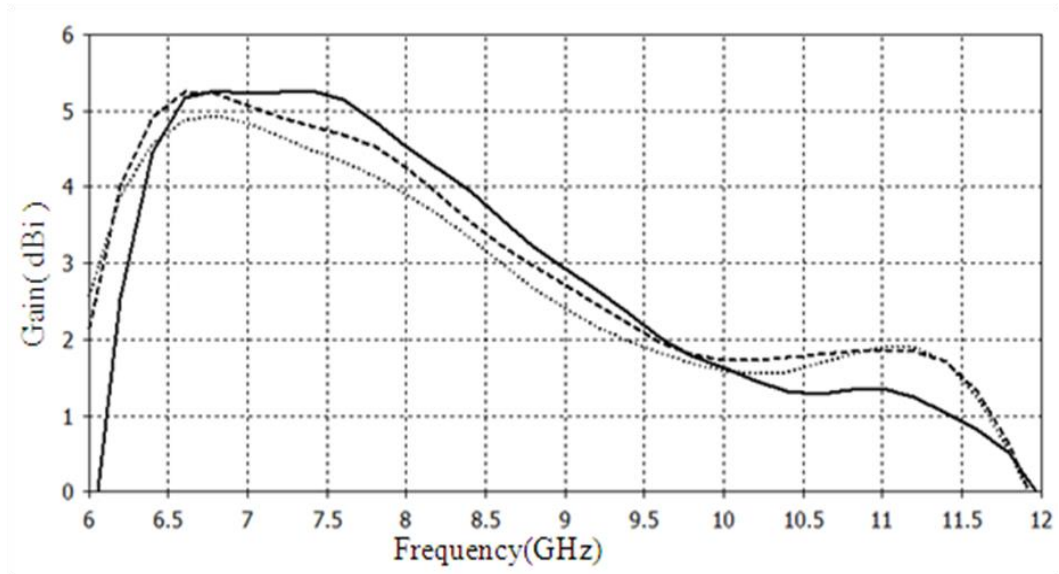


Figure 8.18: Simulated realized gain verses frequency for various vertical separation between ground plane and center of C-shaped strip y_c ; $y_c = 13$ mm (solid), $y_c = 13.5$ mm (dashed), $y_c = 14.0$ mm (dotted).

Figure 8.19 shows the variation of realized gain with frequency of the modified antenna for different values of horizontal separation between the edge of the substrate and center of the C-shaped strip x_c . The horizontal separation has a slight effect on the realized gain, thus the center of parasitic strip is put at the center of the horizontal axis of the substrate so that $x_c = 11.5$ mm.

Based on the detailed parametric studies of the flipped C-shaped strip parameters, the optimum geometry for the modified antenna was simulated, and then fabricated, and Figure 8.20 shows a photograph of the implemented antenna. The antenna performance was measured using an HP8510C vector network analyzer. The measured and simulated reflection coefficients of the

proposed antenna with and without the added strip are shown in Figure 8.20(a). The matching properties of the antenna were only slightly affected by the addition of the strip as this is relatively far from the DRs.

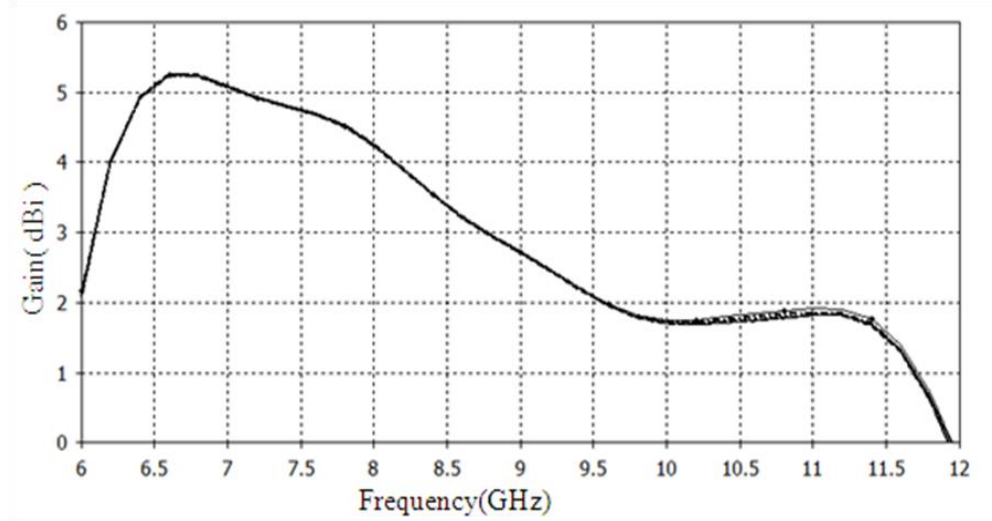


Figure 8.19: Simulated realized gain versus frequency for various horizontal separations between the center of the C-shaped strip and the edge of the substrate x_c ; $x_c = 10.5$ mm (solid), $x_c = 11.5$ mm (dashed), $x_c = 12.5$ mm (dotted), $x_c = 14.5$ mm (dash-dotted), $x_c = 16.5$ mm (solid-circle).

Based on the detailed parametric studies for the flipped C-shaped strip parameters, the optimum geometry for the modified antenna was simulated. The modified antenna was fabricated with the optimum dimensions of the flipped C-shaped strip and the photograph of the implemented antenna with the parasitic strip is shown in Figure 8.19. The antenna performance was measured using HP8510C vector network analyzer. The measured and simulated reflection coefficients of the proposed antenna without strip and with the addition of strip are shown in Figure 8.20 (a). The measured and simulated gain for the two considered cases is shown in Figure 8.20(b).

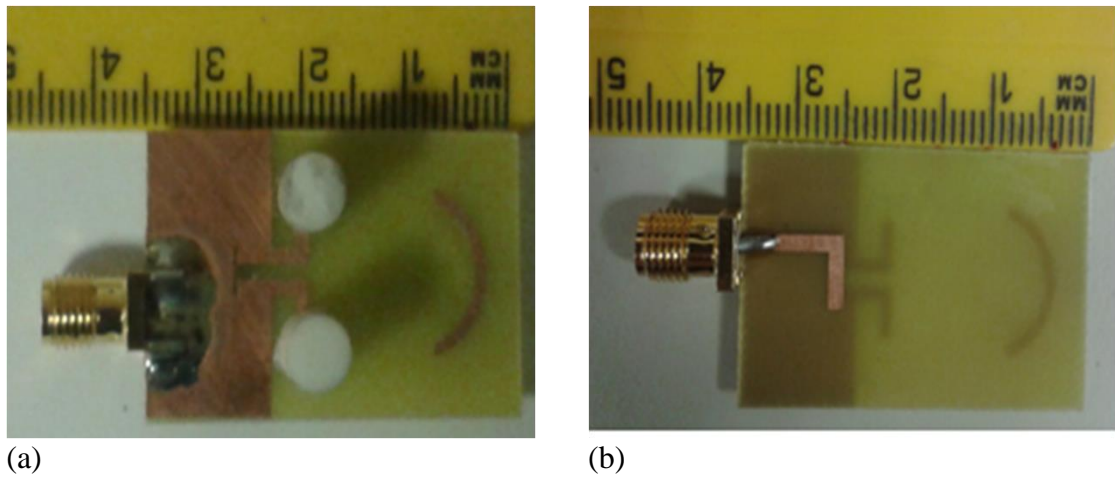
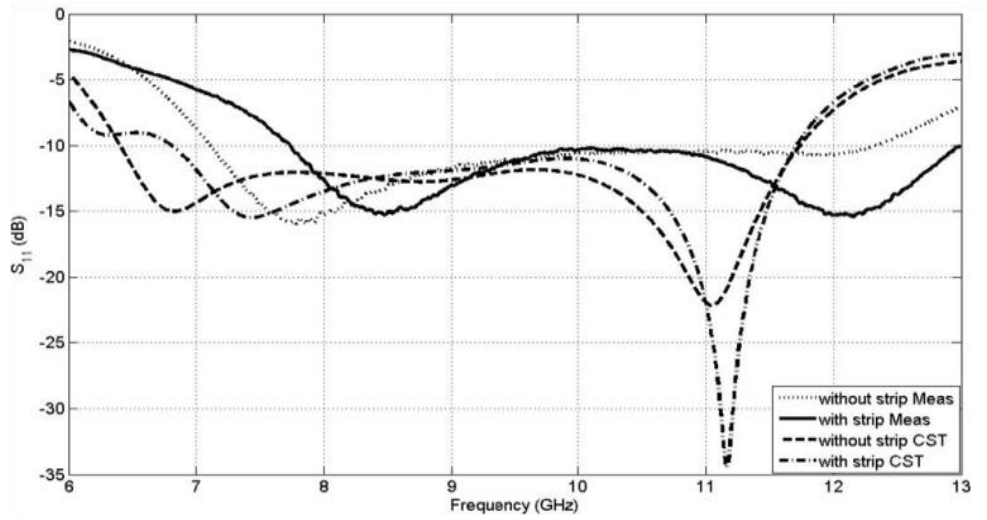
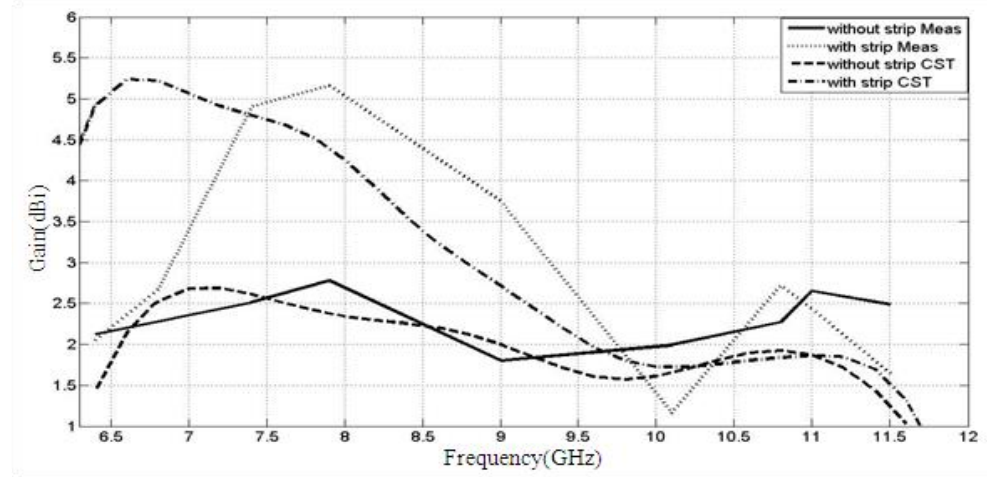


Figure 8.20: Fabricated antenna (a) front view and (b) rear view

The measured and simulated gains, for the two designs with and without the C-shaped strip, are shown in Figure 8.21(b). It can be seen that the addition of the strip has increased the antenna gain by about 2.25 dB at the lower half of the operation band, while there is marginal improvement in the upper half of the band. The C-shaped strip with a radius of 7 mm, width of 1 mm and a strip angle of 140° has an average physical length of 18.326 mm. This strip length can resonate at half wavelength as well as unity wavelength. For the used substrate, the two resonating modes have frequency of 4.94 GHz and 9.87 GHz. However, the gain of the antenna will be affected by the two L-section dipole and well as the C-shaped strip.



(a)



(b)

Figure 8.21: Simulated and measured (a) reflection coefficient and (b) gain versus frequency for the proposed antenna with strip and without strip.

The previous results of Figure 8.12 show that the dipole has a peak gain at about 7GHz and 8GHz for the simulation and measured results. The C-shaped strip has resonance at predicted frequency of 9.87. It should be noted here that the obtained gain is a result of the combined effects of many factors: the added

strip, the two DRs, and the two arms of the inverted L-shaped lines that feed the two DRs. The combined effect on the antenna has resulted in maximum gains which show peaking at lower frequencies, around 6.5 to 7 GHz for the CST results and 7.5 to 8 GHz for the measured results.

8.4 Conclusions

A DRA antenna consisting of a balanced dual segment CDR antenna excited by T- Shaped slot as coupling mechanism for feeding power to dual segment DRAs through L-shaped feeding line is proposed. Parametric studies have been carried out to optimize the antenna design. The designed antenna offered good impedance bandwidth from 6.4GHz to 11.734 GHz (58.7% for $S_{11} \leq -10$ dB). It also provides a maximum gain of 2.66dBi at 7GHz. The modified design, by adding a C-shaped strip and increasing the width of the substrate, resulted in a 2.24 dB increase in the maximum gain while maintaining nearly the same impedance bandwidth. The measurements showed good agreement between simulated and measured results. The measured radiation patterns, and peak gains of the proposed antennas validate using of the proposed antenna for UWB applications.

CHAPTER 9

CONCLUSIONS AND RECOMMENDATIONS FOR FUTURE WORK

9.1 Conclusions

Research in the area of DRA is still required to design and develop antennas capable of operating in all the major wireless services and standard; and thus the proposed work in this thesis has been carried out. The aim of this research was to introduce new concepts in the design process of a printed monopole dielectric loaded antenna and Dielectric Resonator Antennas (DRAs) in which a sufficient operating bandwidth can be achieved for wireless communication applications. Several new compact designs have been presented and investigated.

Research should add to the fundamental knowledge of the field, generate useful analytic and design techniques, and provide practical experience to the researcher. These criteria were successfully achieved. Practical experience was gained through extensive testing of the antennas on a vector network analyser, and in an anechoic chamber. Several experimentally reported design techniques were verified as results of these tests; and independent verifications of various design studies have been added new values to the general

knowledge base of this exciting research field. Hence the conclusions of this research work can be summarized as follows:

Chapter 2: the research background and overview of Dielectric Resonator Antennas (DRA) were introduced in this chapter. The history of DRA and practical applications of the DRAs are introduced including brief comments about Compact DRA design, Multiband DRA and Wideband DRA. The advantages of the DRA features and different geometries were also discussed. Several popular feeding methods (ex. coaxial feed, slot aperture, microstrip line feed, proximity coupled microstrip line feed, co-planar feed and dielectric image guide) for DRAs were also described. Some equivalent circuits of feed line and transmission line modelling for microstrip feed design were reviewed. Finally, Q-factor and bandwidth predictors were developed for all the modified DRA structures.

Chapter 3: a low-profile multi-frequency band DRA antenna was presented. The realized antenna structure has shown a relative bandwidth of 135.7% and an average gain of 2.2 dBi over the frequency interval from 1.15 GHz to 6.0 GHz at return loss better than 10 dB. The radiation pattern was a broad-beam type, of approximately dumbbell shape, that is appropriate for a mobile terminal application. The antenna size was optimized at 57 mm × 37.5 mm × 5.8 mm³,

which is suitable for integration with a variety of mobile terminals operating over DCS, PCS, UMTS, Bluetooth and IEEE 802.11a/b/g wireless standards.

Chapter 4: a small quasi-omni-directional DRA has been proposed for the lower UWB band that is suitable for a variety of body area network and IEEE802.11a/WiMAX applications. The antenna was constructed from a low permittivity ceramic as a rectangular block, with microstrip feed and broadband matching lines on FR4. The radiation patterns were quite stable with an average gain of around 3dBi covering the lower ultra-wideband (UWB) spectrum bandwidth. The radiation efficiency was reasonable over the total bandwidth and do confirm the advantage of using such antenna structures.

Chapter 5: a compact DRA for wideband applications was demonstrated. The use of multiple DRs was able to enhance the performance of the antenna radiation performance. The asymmetric location of the pair of DRs was also added another parameter for the designer to optimize the antenna geometry to add another variable dimension of freedom to achieve best spectrum performance. In this study, an impedance bandwidth of about 29%, covering the frequency range from 9.62GHz to 12.9 GHz, and realized gain of 8dBi were obtained. Design details of the proposed antenna and the results of both simulation and experiment were presented and discussed and show a reasonable agreement. It is believed that the compact design due to the

asymmetrically located DRAs with respect to single rectangular coupling aperture could enhance closely resonant modes to achieve wider spectrum bandwidth. On the other hand it also confirms the possible operation of two DRs elements within a small confined feeding network to operate within antenna array concept.

Chapter 6: a compact DRA for UWB applications has been demonstrated. The use of two DRs can enhance the operational performances of the antenna. The asymmetric locations of the DR pair, the dimensions and the shape of the aperture where “shifting the zigzag” gives design scope together constitute another parameter for the designer to optimize the design process. In this study, an impedance bandwidth of over 62%, covering the dual-band frequency range from 6.02 GHz to 7.32 GHz and from 8.72 GHz to 16.57 GHz, and a gain of 8 dBi were achieved compared to the author work discussed in Chapter 5.

Chapter 7: a new physically compact aperture-coupled dual-segment DRA has been proposed for use in X-band communications. Identical cylindrical DR posts of permittivity 9.4 are mounted on a substrate backed ground plane. The antenna was excited using an L-shaped feed line, and internal antenna coupling was achieved using an S-shaped slot. The effective antenna volume after optimisation process was found around $30.0 \times 25.0 \times 0.8 \text{ mm}^3$. The measured prototype performance shows an average gain of 6.0 dBi over the frequency

range 7.66 GHz to 11.2 GHz, with stable radiation patterns. It was proposed that the DR posts may be arranged in two distinct configurations: (i) occupying space on one side of the substrate, and (ii) on opposing sides. The first configuration results in a higher gain performance, whilst the second results in approximated uniform radiation pattern within 1m radial distance from the antenna.

Chapter 8: a DRA consisting of a balanced dual segment CDR antenna excited by T-shaped slot as coupling mechanism for feeding power to dual segment DRAs through L-shaped feeding line was proposed. Parametric studies have been carried out to optimize the antenna design. The designed antenna offered good impedance bandwidth from 6.4GHz to 11.734 GHz (58.7% for $S_{11} \leq -10$ dB). It also provides a maximum gain of 2.66dBi at 7GHz. The modified design, by adding a C-shaped strip and increasing the width of the substrate, resulted in a 2.24 dB increase in the maximum gain while maintaining nearly the same impedance bandwidth. The measurements showed good agreement between simulated and measured results. The measured radiation patterns, and peak gains of the proposed antennas were validated using of the proposed antenna for UWB applications.

9.2 Future Work

The future work plan could be constructed to extend the trends established in this report, resulting in detailed design strategies for the antennas and their response to the target operational environment. The following points have been selected as being the most likely threads for future development:

1. Further development of the design process in Chapter 3 is required. In particular the trade-off between antenna volume and target bandwidth needs to be fully characterised. This could be achieved by reducing the size of both the radiating patch and ground plane to accommodate a small volume antenna that is more suitable for developing mobile handset applications.
2. Investigation of low – profile and compact DRA antenna. It would be envisaged that can be achieved more bandwidth suitable for developing wireless applications.
3. Investigation of application of DRA antennas to MIMO systems. It would be envisaged that suitable control mechanisms will be embedded into the antenna structure [157, 158].

4. Design and measurement of better matched antenna to provide an optimum design for LP and CP polarized DRA antenna [159-162].
5. One further possible study that might be considered relates to the DRA antennas in chapter 6, 7 and 8. These antennas could be operated on single and multi-band facilities on different frequencies which are not necessarily harmonically related [163-166].
6. The possible use of EBG material and meta-material with DRA that could add considerable value in studies to improve antenna performance such as that in MIMO systems or antenna arrays [167-170].

REFERENCES

- [1] R. D. Richtmyer, "Dielectric resonators," *Appl. Phys*, vol. 10, pp. 391-398, June 1939.
- [2] H. Y. Yee, "Natural Resonant Frequencies of Microwave Dielectric Resonators (Correspondence)," *Microwave Theory and Techniques, IEEE Transactions on*, vol. 13, pp. 256-256, 1965.
- [3] A. Karp, H. J. Shaw, and D. K. Winslow, "Circuit Properties of Microwave Dielectric Resonators," *Microwave Theory and Techniques, IEEE Transactions on*, vol. 16, pp. 818-828, 1968.
- [4] J. Van Bladel, "On the Resonances of a Dielectric Resonator of Very High Permittivity," *Microwave Theory and Techniques, IEEE Transactions on*, vol. 23, pp. 199-208, 1975.
- [5] J. Van Bladel, "The Excitation of Dielectric Resonators of Very High Permittivity," *Microwave Theory and Techniques, IEEE Transactions on*, vol. 23, pp. 208-217, 1975.
- [6] E. A. J. Marcatili, "Dielectric Rectangular Waveguide and Directional Coupler for Integrated Optics," vol. 48, pp. 2071-2102, 1969.
- [7] P. Guillon and Y. Garault, "Accurate Resonant Frequencies of Dielectric Resonators," *Microwave Theory and Techniques, IEEE Transactions on*, vol. 25, pp. 916-922, 1977.

- [8] R. K. Mongia, "Half-split dielectric resonator placed on metallic plane for antenna applications," *Electronics Letters*, vol. 25, pp. 462-464, 1989.
- [9] J. F. Legier, P. Kennis, S. Toutain, and J. Citerne, "Resonant Frequencies Of Rectangular Dielectric Resonators," *IEEE Transactions on Microwave Theory and Techniques*, vol. MTT-28, pp. 1031-1034, 1980.
- [10] D. Kajfez and P. Guillon, *Dielectric Resonators*: Artech House, 1986.
- [11] J. K. Plourde and R. Chung-Li, "Application of Dielectric Resonators in Microwave Components," *Microwave Theory and Techniques, IEEE Transactions on*, vol. 29, pp. 754-770, 1981.
- [12] S. Long, M. McAllister, and S. Liang, "The resonant cylindrical dielectric cavity antenna," *Antennas and Propagation, IEEE Transactions on*, vol. 31, pp. 406-412, 1983.
- [13] M. W. McAllister, S. A. Long, and G. L. Conway, "Rectangular dielectric resonator antenna," *Electronics Letters*, vol. 19, pp. 218-219, 1983.
- [14] M. W. McAllister and S. A. Long, "Resonant hemispherical dielectric antenna," *Electronics Letters*, vol. 20, pp. 657-659, 1984.
- [15] A. Ittipiboon, R. K. Mongia, Y. M. M. Antar, P. Bhartia, and M. Cuhaci, "Aperture fed rectangular and triangular dielectric resonators for use as magnetic dipole antennas," *Electronics Letters*, vol. 29, pp. 2001-2002, 1993.

- [16] K. W. Leung, K. M. Luk, and E. K. N. Yung, "Spherical cap dielectric resonator antenna using aperture coupling," *Electronics Letters*, vol. 30, pp. 1366-1367, 1994.
- [17] R. K. Mongia, A. Ittipiboon, P. Bhartia, and M. Cuhaci, "Electric-monopole antenna using a dielectric ring resonator," *Electronics Letters*, vol. 29, pp. 1530-1531, 1993.
- [18] K. W. Leung, K. Y. Chow, K. M. Luk, and E. K. N. Yung, "Excitation of dielectric resonator antenna using a soldered-through probe," *Electronics Letters*, vol. 33, pp. 349-350, 1997.
- [19] A. Petosa, A. Ittipiboon, Y. M. M. Antar, D. Roscoe, and M. Cuhaci, "Recent advances in dielectric-resonator antenna technology," *Antennas and Propagation Magazine, IEEE*, vol. 40, pp. 35-48, 1998.
- [20] G. P. Junker, A. A. Kishk, A. W. Glisson, and D. Kajfez, "Effect of an air gap around the coaxial probe exciting a cylindrical dielectric resonator antenna," *Electronics Letters*, vol. 30, pp. 177-178, 1994.
- [21] G. P. Junker, A. A. Kishk, A. W. Glisson, and D. Kajfez, "Effect of air gap on cylindrical dielectric resonator antenna operating in TM_{01} mode," *Electronics Letters*, vol. 30, pp. 97-98, 1994.
- [22] W. M. Abdel-Wahab, S. Safavi-Naeini, and D. Busuioc, "Modeling and Design of Millimeter-Wave High Q-Factor Parallel Feeding Scheme for Dielectric Resonator Antenna Arrays," *Antennas and Wireless Propagation Letters, IEEE*, vol. 10, pp. 53-55, 2011.

- [23] A. A. Kishk, B. Ahn, and D. Kajfez, "Broadband stacked dielectric resonator antennas," *Electronics Letters*, vol. 25, pp. 1232-1233, 1989.
- [24] K. M. Luk, K. W. Leung, and K. Y. Chow, "Bandwidth and gain enhancement of a dielectric resonator antenna with the use of a stacking element," *Microwave and Optical Technology Letters*, vol. 14, pp. 215-217, 1997.
- [25] A. Sangiovanni, J. Y. Dauvignac, and C. Pichot, "Embedded dielectric resonator antenna for bandwidth enhancement," *Electronics Letters*, vol. 33, pp. 2090-2091, 1997.
- [26] W. Huang and A. A. Kishk, "Compact wideband multi-layer cylindrical dielectric resonator antennas," *IET Microwaves, Antennas and Propagation*, vol. 1, pp. 998-1005, 2007.
- [27] R. N. Simons and R. Q. Lee, "Effect of parasitic dielectric resonators on CPW/aperture-coupled dielectric resonator antennas," *Microwaves, Antennas and Propagation, IEE Proceedings H*, vol. 140, pp. 336-338, 1993.
- [28] Z. Fan, Y. M. M. Antar, A. Ittipiboon, and A. Petosa, "Parasitic coplanar three-element dielectric resonator antenna subarray," *Electronics Letters*, vol. 32, pp. 789-790, 1996.
- [29] K. L. Wong, N. C. Chen, and H. T. Chen, "Analysis of a hemispherical dielectric resonator antenna with an airgap," *Microwave and Guided Wave Letters, IEEE*, vol. 3, pp. 355-357, 1993.

- [30] A. Ittipiboon, A. Petosa, D. Roscoe, and M. Cuhaci, "An investigation of a novel broadband dielectric resonator antenna," in *Antennas and Propagation Society International Symposium, 1996. AP-S. Digest, 1996*, pp. 2038-2041 vol.3.
- [31] S. M. Shum and K. M. Luk, "Characteristics of dielectric ring resonator antenna with an air gap," *Electronics Letters*, vol. 30, pp. 277-278, 1994.
- [32] K.-L. Wong and N.-C. Chen, "Analysis of a broadband hemispherical dielectric resonator antenna with a dielectric coating," *Microwave and Optical Technology Letters*, vol. 7, pp. 73-76, 1994.
- [33] N.-C. Chen, H.-C. Su, K.-L. Wong, and K.-W. Leung, "Analysis of a broadband slot-coupled dielectric-coated hemispherical dielectric resonator antenna," *Microwave and Optical Technology Letters*, vol. 8, pp. 13-16, 1995.
- [34] Y. Ge, K. P. Esselle, and T. S. Bird, "A wideband probe-fed stacked dielectric resonator antenna," *Microwave and Optical Technology Letters*, vol. 48, pp. 1630-1633, 2006.
- [35] A. A. Kishk, "Wide-band truncated tetrahedron dielectric resonator antenna excited by a coaxial probe," *Antennas and Propagation, IEEE Transactions on*, vol. 51, pp. 2913-2917, 2003.
- [36] A. A. Kishk, Y. Yin, and A. W. Glisson, "Conical dielectric resonator antennas for wide-band applications," *IEEE Transactions on Antennas and Propagation*, vol. 50, pp. 469-474, 2002.

- [37] L. Xian-Ling and T. A. Denidni, "Wideband Rectangular Dielectric Resonator Antenna With a Concave Ground Plane," *Antennas and Wireless Propagation Letters, IEEE*, vol. 8, pp. 367-370, 2009.
- [38] L. C. Y. Chu, D. Guha, and Y. M. M. Antar, "Conformal Strip-Fed Shaped Cylindrical Dielectric Resonator: Improved Design of a Wideband Wireless Antenna," *Antennas and Wireless Propagation Letters, IEEE*, vol. 8, pp. 482-485, 2009.
- [39] G. Almpanis, C. Fumeaux, and R. Vahldieck, "Semi-trapezoidal dielectric resonator antenna for wideband applications," in *2007 IEEE Antennas and Propagation Society International Symposium, AP-S, June 10, 2007 - June 15, 2007*, Honolulu, HI, United states, 2007, pp. 4877-4880.
- [40] R. Chair, A. A. Kishk, K. F. Lee, and C. E. Smith, "Wideband flipped staired pyramid dielectric resonator antennas," *Electronics Letters*, vol. 40, pp. 581-582, 2004.
- [41] A. S. Al-Zoubi and A. A. Kishk, "Wide band strip-fed rectangular dielectric resonator antenna with improved radiation patterns," in *Antennas and Propagation Society International Symposium, 2009. APSURSI '09. IEEE*, 2009, pp. 1-4.
- [42] L. Xian-Ling, T. A. Denidni, and Z. Li-Na, "Wideband L-Shaped Dielectric Resonator Antenna With a Conformal Inverted-Trapezoidal Patch Feed," *Antennas and Propagation, IEEE Transactions on*, vol. 57, pp. 271-274, 2009.

- [43] Z. Li-Na, Z. Shun-shi, S. Wenhui, and Y. Xuexia, "Wideband U-shaped dielectric resonator antenna," in *Antennas and Propagation, 2009. EuCAP 2009. 3rd European Conference on*, 2009, pp. 2361-2364.
- [44] R. K. Mongia, A. Ittipiboon, and M. Cuhaci, "Measurement of radiation efficiency of dielectric resonator antennas," *Microwave and Guided Wave Letters, IEEE*, vol. 4, pp. 80-82, 1994.
- [45] A. Petosa and A. Ittipiboon, "Dielectric Resonator Antennas: A Historical Review and the Current State of the Art," *Antennas and Propagation Magazine, IEEE*, vol. 52, pp. 91-116, 2010.
- [46] R. K. Mongia and P. Bhartia, "Dielectric Resonator Antennas – A Review and General Design Relations for Resonant Frequency and Bandwidth," *International Journal of Microwave and Millimeter-Wave Computer-Aided Engineering*, vol. 4, pp. 230-247, 1994.
- [47] K. Pliakostathis and D. Mirshekar-Syahkal, "A novel enclosed cylindrical dielectric resonator antenna," in *Antennas and Propagation Society International Symposium, 2002. IEEE, 2002*, pp. 474-477 vol.4.
- [48] M. Gastine, L. Courtois, and J. L. Dormann, "Electromagnetic Resonances of Free Dielectric Spheres," *Microwave Theory and Techniques, IEEE Transactions on*, vol. 15, pp. 694-700, 1967.
- [49] O. Sager and F. Tisi, "On eigenmodes and forced resonance-modes of dielectric spheres," *Proceedings of the IEEE*, vol. 56, pp. 1593-1594, 1968.

- [50] R. Kumar Mongia and A. Ittipiboon, "Theoretical and experimental investigations on rectangular dielectric resonator antennas," *Antennas and Propagation, IEEE Transactions on*, vol. 45, pp. 1348-1356, 1997.
- [51] A. A. Kishk, A. Ittipiboon, Y. M. M. Antar, and M. Cuhaci, "Slot excitation of the dielectric disk radiator," *Antennas and Propagation, IEEE Transactions on*, vol. 43, pp. 198-201, 1995.
- [52] D. Soren, R. Ghatak, K. Mishra, and D. R. Poddar, " Dielectric Resonator Antennas: Designs and Advances " *Progress In Electromagnetics Research B*, vol. 60, pp. 195-213, 2014.
- [53] R. D. M. a. M. T. K. Tam, "Chapter 7 -Compact Circular Sector And Annular Sector Dielectric Resonator Antennas for Wireless Communication Handsets," in *Dielectric Resonator Antennas*, K. W. L. by K.M. Luk, Ed., ed uk: Research Studies Press Ltd., 2003.
- [54] G. P. Junker, A. A. Kishk, and A. W. Glisson, "Numerical analysis of dielectric resonator antennas excited in quasi-TE modes," *Electronics Letters*, vol. 29, pp. 1810-1811, 1993.
- [55] M. T. K. Tam and R. D. Murch, "Half volume dielectric resonator antenna designs," *Electronics Letters*, vol. 33, pp. 1914-1916, 1997.
- [56] S. G. O'Keefe, S. P. Kingsley, and S. Saario, "FDTD simulation of radiation characteristics of half-volume HEM and TE-mode dielectric resonator antennas," *Antennas and Propagation, IEEE Transactions on*, vol. 50, pp. 175-179, 2002.

- [57] M. T. K. Tam and R. D. Murch, "Compact circular sector and annular sector dielectric resonator antennas," *Antennas and Propagation, IEEE Transactions on*, vol. 47, pp. 837-842, 1999.
- [58] M. T. K. Tam and R. D. Murch, "Circularly polarized circular sector dielectric resonator antenna," *Antennas and Propagation, IEEE Transactions on*, vol. 48, pp. 126-128, 2000.
- [59] A. W. G. A. A. Kishk, and G. P. Junker, "Bandwidth Enhancement for Split Cylindrical Dielectric Resonator Antennas," *Progress In Electromagnetics Research, PIER* 56, vol. 33, pp. 97-118, 2001.
- [60] D. Cormos, A. Laisne, R. Gillard, F. Le Bolzer, and C. Nicolas, "Compact dielectric resonator antenna for WLAN applications," *Electronics Letters*, vol. 39, pp. 588-590, 2003.
- [61] G. Yuehe, "Size-reduced dielectric resonator antenna for UWB applications," in *Antennas and Propagation (APCAP), 2012 IEEE Asia-Pacific Conference on*, 2012, pp. 45-46.
- [62] Z. Fan and Y. M. M. Antar, "Slot-coupled DR antenna for dual-frequency operation," *Antennas and Propagation, IEEE Transactions on*, vol. 45, pp. 306-308, 1997.
- [63] A. Sangiovanni, J. Y. Dauvignac, and C. Pichot, "Stacked dielectric resonator antenna for multifrequency operation," *Microwave and Optical Technology Letters*, vol. 18, pp. 303-306, 1998.

- [64] C. Nannini, J. M. Ribero, J. Y. Dauvignac, and C. Pichot, "A dual-frequency dielectric resonator antenna," *Microwave and Optical Technology Letters*, vol. 38, pp. 9-10, 2003.
- [65] Y. Sung, C. S. Ahn, and Y. S. Kim, "Microstripline fed dual-frequency dielectric resonator antenna," *Microwave and Optical Technology Letters*, vol. 42, pp. 388-390, 2004.
- [66] B. Paul, S. Mridula, P. Mohanan, P. V. Bijumon, and M. T. Sebastian, "A compact very-high-permittivity dielectric-eye resonator antenna for multiband wireless applications," *Microwave and Optical Technology Letters*, vol. 43, pp. 118-121, 2004.
- [67] L. Huitema, M. Koubeissi, M. Mouhamadou, E. Arnaud, C. Decroze, and T. Monediere, "Compact and Multiband Dielectric Resonator Antenna With Pattern Diversity for Multistandard Mobile Handheld Devices," *Antennas and Propagation, IEEE Transactions on*, vol. 59, pp. 4201-4208, 2011.
- [68] T. A. Denidni and R. Qinjiang, "Hybrid dielectric resonator antennas with radiating slot for dual-frequency operation," *Antennas and Wireless Propagation Letters, IEEE*, vol. 3, pp. 321-323, 2004.
- [69] R. Qinjiang, T. A. Denidni, and A. R. Sebak, "A hybrid resonator antenna suitable for wireless communication applications at 1.9 and 2.45 GHz," *Antennas and Wireless Propagation Letters, IEEE*, vol. 4, pp. 341-343, 2005.

- [70] R. Qinjiang, T. A. Denidni, A. R. Sebak, and R. H. Johnston, "Compact Independent Dual-Band Hybrid Resonator Antenna With Multifunctional Beams," *Antennas and Wireless Propagation Letters, IEEE*, vol. 5, pp. 239-242, 2006.
- [71] L. Yi-Fang, L. Chia-Ho, C. Hua-Ming, and P. S. Hall, "A Miniature Dielectric Loaded Monopole Antenna for 2.4/5 GHz WLAN Applications," *Microwave and Wireless Components Letters, IEEE*, vol. 16, pp. 591-593, 2006.
- [72] K. W. Leung, K. M. Luk, K. Y. Chow, and E. K. N. Yung, "Bandwidth enhancement of dielectric resonator antenna by loading a low-profile dielectric disk of very high permittivity," *Electronics Letters*, vol. 33, pp. 725-726, 1997.
- [73] A. A. Kishk, X. Zhang, A. W. Glisson, and D. Kajfez, "Numerical analysis of stacked dielectric resonator antennas excited by a coaxial probe for wideband applications," *IEEE Transactions on Antennas and Propagation*, vol. 51, pp. 1996-2006, 2003.
- [74] A. Rashidian, K. Forooraghi, and M. T. Aligodarz, "Investigations on two-segment dielectric resonator antennas," *Microwave and Optical Technology Letters*, vol. 45, pp. 533-537, 2005.
- [75] R. Qinjiang, T. A. Denidni, and A. R. Sebak, "Broadband compact stacked T-shaped DRA with equilateral-triangle cross sections,"

- Microwave and Wireless Components Letters, IEEE*, vol. 16, pp. 7-9, 2006.
- [76] T. A. Denidni, R. Qinjiang, and A. R. Sebak, "Broadband L-shaped dielectric resonator antenna," *Antennas and Wireless Propagation Letters, IEEE*, vol. 4, pp. 453-454, 2005.
 - [77] G. P. Junker, A. A. Kishk, A. W. Glisson, and D. Kajfez, "Effect of fabrication imperfections for ground-plane-backed dielectric-resonator antennas," *Antennas and Propagation Magazine, IEEE*, vol. 37, pp. 40-47, 1995.
 - [78] M. Verplanken and J. V. Bladel, "The Electric-Dipole Resonances of Ring Resonators of Very High Permittivity (Short Papers)," *Microwave Theory and Techniques, IEEE Transactions on*, vol. 24, pp. 108-112, 1976.
 - [79] A. A. Kishk, Y. Yan, and A. W. Glisson, "Conical dielectric resonator antennas for wide-band applications," *Antennas and Propagation, IEEE Transactions on*, vol. 50, pp. 469-474, 2002.
 - [80] A. A. Kishk, "Experimental study of broadband embedded dielectric resonator antennas excited by a narrow slot," *Antennas and Wireless Propagation Letters, IEEE*, vol. 4, pp. 79-81, 2005.
 - [81] A. G. Walsh, C. S. DeYoung, and S. A. Long, "An investigation of stacked and embedded cylindrical dielectric resonator antennas," *Antennas and Wireless Propagation Letters, IEEE*, vol. 5, pp. 130-133, 2006.

- [82] Y.-F. Ruan, Y.-X. Guo, and X.-Q. Shi, "Wideband dielectric resonator antenna," *Microwave and Optical Technology Letters*, vol. 48, pp. 222-226, 2006.
- [83] C. S. De Young and S. A. Long, "Wideband Cylindrical and Rectangular Dielectric Resonator Antennas," *Antennas and Wireless Propagation Letters, IEEE*, vol. 5, pp. 426-429, 2006.
- [84] R. Chair, A. A. Kishk, and K. F. Lee, "Wideband simple cylindrical dielectric resonator antennas," *Microwave and Wireless Components Letters, IEEE*, vol. 15, pp. 241-243, 2005.
- [85] P. V. Bijumon, S. K. Menon, M. N. Suma, M. T. Sebastian, and P. Mohanan, "Broadband cylindrical dielectric resonator antenna excited by modified microstrip line," *Electronics Letters*, vol. 41, pp. 385-387, 2005.
- [86] S. K. Menon, B. Lethakumary, P. Mohanan, P. V. Bijumon, and M. T. Sebastian, "Wideband cylindrical dielectric resonator antenna excited using an L-strip feed," *Microwave and Optical Technology Letters*, vol. 42, pp. 293-294, 2004.
- [87] A. A. Kishk, R. Chair, and L. Kai Fong, "Broadband dielectric resonator antennas excited by L-shaped probe," *Antennas and Propagation, IEEE Transactions on*, vol. 54, pp. 2182-2189, 2006.
- [88] R. Chair, A. A. Kishk, and K. F. Lee, "Hook- and 3-D J-shaped probe excited dielectric resonator antenna for dual polarisation applications,"

- Microwaves, Antennas and Propagation, IEE Proceedings*, vol. 153, pp. 277-281, 2006.
- [89] L. Bin and L. Kwok Wa, "Strip-fed rectangular dielectric resonator antennas with/without a parasitic patch," *Antennas and Propagation, IEEE Transactions on*, vol. 53, pp. 2200-2207, 2005.
 - [90] K. M. Luk, M. T. Lee, K. W. Leung, and E. K. N. Yung, "Technique for improving coupling between microstripline and dielectric resonator antenna," *Electronics Letters*, vol. 35, pp. 357-358, 1999.
 - [91] K. W. Leung and C. K. Leung, "Wideband dielectric resonator antenna excited by cavity-backed circular aperture with microstrip tuning fork," *Electronics Letters*, vol. 39, pp. 1033-1035, 2003.
 - [92] A. Buerkle, K. Sarabandi, and H. Mosallaei, "Compact slot and dielectric resonator antenna with dual-resonance, broadband characteristics," *Antennas and Propagation, IEEE Transactions on*, vol. 53, pp. 1020-1027, 2005.
 - [93] G. Yuan, O. Ban-Leong, E. Wei-Bin, and A. P. Popov, "A compact wideband hybrid dielectric resonator antenna," *Microwave and Wireless Components Letters, IEEE*, vol. 16, pp. 227-229, 2006.
 - [94] A. A. N. Al-Azza and F. J. Harackiewicz, "Modified ultra wideband hybrid dielectric resonator antenna," in *Antennas and Propagation Society International Symposium (APSURSI), 2014 IEEE*, 2014, pp. 1980-1981.

- [95] A. Panigrahi, Y. K. Choukiker, S. K. Behera, and R. Jyoti, "Square ring dielectric resonator antenna for wideband applications," in *Computer Communication and Informatics (ICCCI), 2014 International Conference on*, 2014, pp. 1-3.
- [96] V. Vashistha, M. V. Kartikeyan, J. Malik, and R. P. Maheshwari, "Analysis of ultra wide band dielectric resonator antenna with band notch for WLAN communication," in *Electrical, Electronics and Computer Science (SCEECS), 2014 IEEE Students' Conference on*, 2014, pp. 1-3.
- [97] R. K. Mongia, A. Ittibipoon, and M. Cuhaci, "Low profile dielectric resonator antennas using a very high permittivity material," *Electronics Letters*, vol. 30, pp. 1362-1363, 1994.
- [98] K. P. Esselle, "A low-profile rectangular dielectric-resonator antenna," *Antennas and Propagation, IEEE Transactions on*, vol. 44, pp. 1296-1297, 1996.
- [99] M. Haneishi and H. Takazawa, "Broadband circularly polarised planar array composed of a pair of dielectric resonator antennas," *Electronics Letters*, vol. 21, pp. 437-438, 1985.
- [100] K.-L. Wong and N.-C. Chen, "Analysis of a broadband hemispherical dielectric resonator antenna with a dielectric coating," *Microwave and Optical Technology Letters*, vol. 7, pp. 73-76, 1994.

- [101] S. W. Chen and K. A. Zaki, "Dielectric ring resonators loaded in waveguide and on substrate," *Microwave Theory and Techniques, IEEE Transactions on*, vol. 39, pp. 2069-2076, 1991.
- [102] H. Y. Lo, K. W. Leung, and K. M. Luk, "Slot-line-excited equilateral-triangular dielectric resonator antenna of very high permittivity," *Microwave and Optical Technology Letters*, vol. 29, pp. 230-231, 2001.
- [103] K. W. Leung, K. M. Luk, and K. Y. A. Lai, "Input impedance of hemispherical dielectric resonator antenna," *Electronics Letters*, vol. 27, pp. 2259-2260, 1991.
- [104] J. T. H. St. Martin, Y. M. M. Antar, A. A. Kishk, A. Ittipiboon, and M. Cuhaci, "Dielectric resonator antenna using aperture coupling," *Electronics Letters*, vol. 26, pp. 2015-2016, 1990.
- [105] G. P. Junker, A. A. Kishk, and A. W. Glisson, "Input impedance of dielectric resonator antennas excited by a coaxial probe," *Antennas and Propagation, IEEE Transactions on*, vol. 42, pp. 960-966, 1994.
- [106] S. Shiu-Ming and L. Kwai-Man, "FDTD analysis of probe-fed cylindrical dielectric resonator antenna," *Antennas and Propagation, IEEE Transactions on*, vol. 46, pp. 325-333, 1998.
- [107] C. Kut Yuen and L. Kwok Wa, "Theory and experiment of the cavity-backed slot-excited dielectric resonator antenna," *Electromagnetic Compatibility, IEEE Transactions on*, vol. 42, pp. 290-297, 2000.

- [108] K. Y. Chow, K. W. Leung, K. M. Luk, and E. K. N. Yung, "Input impedance of the slot-fed dielectric resonator antenna with/without a backing cavity," *Antennas and Propagation, IEEE Transactions on*, vol. 49, pp. 307-309, 2001.
- [109] K. W. Leung and K. K. So, "Rectangular waveguide excitation of dielectric resonator antenna," *Antennas and Propagation, IEEE Transactions on*, vol. 51, pp. 2477-2481, 2003.
- [110] I. A. Eshrah, A. A. Kishk, A. B. Yakovlev, and A. W. Glisson, "Theory and implementation of dielectric resonator antenna excited by a waveguide slot," *Antennas and Propagation, IEEE Transactions on*, vol. 53, pp. 483-494, 2005.
- [111] R. A. Kranenburg and S. A. Long, "Microstrip transmission line excitation of dielectric resonator antennas," *Electronics Letters*, vol. 24, pp. 1156-1157, 1988.
- [112] K. W. Leung, K. Y. Chow, K. M. Luk, and E. K. N. Yung, "Low-profile circular disk DR antenna of very high permittivity excited by a microstripline," *Electronics Letters*, vol. 33, pp. 1004-1005, 1997.
- [113] R. A. Kranenburg, S. A. Long, and J. T. Williams, "Coplanar waveguide excitation of dielectric resonator antennas," *Antennas and Propagation, IEEE Transactions on*, vol. 39, pp. 119-122, 1991.

- [114] L. Kwok Wa, "Conformal strip excitation of dielectric resonator antenna," *Antennas and Propagation, IEEE Transactions on*, vol. 48, pp. 961-967, 2000.
- [115] M. T. Birand and R. V. Gelsthorpe, "Experimental millimetric array using dielectric radiators fed by means of dielectric waveguide," *Electronics Letters*, vol. 17, pp. 633-635, 1981.
- [116] A. Petosa, "Dielectric resonator antenna handbook," 2007.
- [117] O. Lehmus, J. Ollikainen, and P. Vainikainen, "Characteristics of half-volume DRAs with different permittivities," in *Antennas and Propagation Society International Symposium, 1999. IEEE*, 1999, pp. 22-25 vol.1.
- [118] M. Ali, R. Dougal, G. Yang, and H. S. Hwang, "Wideband (5-6 GHz WLAN band) circularly polarized patch antenna for wireless power sensors," in *Antennas and Propagation Society International Symposium, 2003. IEEE*, 2003, pp. 34-37 vol.2.
- [119] L. Xian-Ling and T. A. Denidni, "H-Shaped Dielectric Resonator Antenna for Wideband Applications," *Antennas and Wireless Propagation Letters, IEEE*, vol. 7, pp. 163-166, 2008.
- [120] L. N. Zhang, S. S. Zhong, and S. Q. Xu, "Broadband U-shaped dielectric resonator antenna with elliptical patch feed," *Electronics Letters*, vol. 44, pp. 947-949, 2008.

- [121] L. Z. Thamae and W. Zhipeng, "Broadband Bowtie Dielectric Resonator Antenna," *Antennas and Propagation, IEEE Transactions on*, vol. 58, pp. 3707-3710, 2010.
- [122] S. Chan Hwang, R. A. Abd-Alhameed, Z. Dawei, L. Ting Hee, and P. S. Excell, "A Crescent-Shaped Multiband Planar Monopole Antenna for Mobile Wireless Applications," *Antennas and Wireless Propagation Letters, IEEE*, vol. 9, pp. 152-155, 2010.
- [123] "'High Frequency Structure Simulator (HFSS), Ansoft Corp", <http://www.ansoft.com>.
- [124] S. A. Long, M. McAllister, and S. Liang, "The resonant cylindrical dielectric cavity antenna," *Antennas and Propagation, IEEE Transactions on*, vol. 31, pp. 406-412, 1983.
- [125] A. Rashidian and D. M. Klymyshyn, "On the Two Segmented and High Aspect Ratio Rectangular Dielectric Resonator Antennas for Bandwidth Enhancement and Miniaturization," *Antennas and Propagation, IEEE Transactions on*, vol. 57, pp. 2775-2780, 2009.
- [126] G. Almpanis, C. Fumeaux, and R. Vahldieck, "Offset Cross-Slot-Coupled Dielectric Resonator Antenna for Circular Polarization," *Microwave and Wireless Components Letters, IEEE*, vol. 16, pp. 461-463, 2006.
- [127] D. M. Pozar, *Microwave Engineering*, 2 ed. John Wiley & Sons, New York, 1998.

- [128] K.-M. Luk and K.-W. Leung, *Dielectric Resonator Antennas*. Baldock, England: Research Studies Press, 2003.
- [129] C. Kumar and D. Guha, "Defected ground structure (DGS)-integrated rectangular microstrip patch for improved polarisation purity with wide impedance bandwidth," *Microwaves, Antennas & Propagation, IET*, vol. 8, pp. 589-596, 2014.
- [130] D. Guha, S. Biswas, T. Joseph, and M. T. Sebastian, "Defected ground structure to reduce mutual coupling between cylindrical dielectric resonator antennas," *Electronics Letters*, vol. 44, pp. 836-837, 2008.
- [131] A. H. Majeed, A. S. Abdullah, F. Elmegri, K. H. Sayidmarie, R. A. Abd-Alhameed, and J. M. Noras, "Aperture-Coupled Asymmetric Dielectric Resonators Antenna for Wideband Applications," *Antennas and Wireless Propagation Letters, IEEE*, vol. 13, pp. 927-930, 2014.
- [132] G. Yang, F. Zhenghe, and Z. Li, "Compact Asymmetrical T-Shaped Dielectric Resonator Antenna for Broadband Applications," *Antennas and Propagation, IEEE Transactions on*, vol. 60, pp. 1611-1615, 2012.
- [133] S. I. Yang, R. Chair, A. A. Kishk, K. F. Lee, and K.-M. Luk, "Study on Sequential Feeding Networks for Subarrays of Circularly Polarized Elliptical Dielectric Resonator Antenna," *Antennas and Propagation, IEEE Transactions on*, vol. 55, pp. 321-333, 2007.
- [134] D. Guha, B. Gupta, and Y. M. M. Antar, "Hybrid Monopole-DRAs Using Hemispherical/ Conical-Shaped Dielectric Ring Resonators: Improved

- Ultrawideband Designs," *Antennas and Propagation, IEEE Transactions on*, vol. 60, pp. 393-398, 2012.
- [135] K. S. Ryu and A. A. Kishk, "Ultra-wideband dielectric resonator antennas," in *Antenna Technology (iWAT), 2010 International Workshop on*, 2010, pp. 1-4.
- [136] A. H. Majeed, A. S. Abdullah, F. Elmegri, K. H. Sayidmarie, R. A. Abd-Alhameed, and J. M. Noras, "Aperture-Coupled Asymmetric Dielectric Resonators Antenna for Wideband Applications," *IEEE Antennas and Wireless Propagation Letters*, vol. 13, pp. 927-930, 2014.
- [137] A. Petosa, *Dielectric Resonator Antenna Handbook*. Artech House Publishers, 2007.
- [138] A. B. Kakade and M. S. Kumbhar, "Wideband circularly polarized conformal strip fed three layer hemispherical dielectric resonator antenna with parasitic patch," *Microwave and Optical Technology Letters*, vol. 56, pp. 72-77, 2014.
- [139] M. K. A. R. M. Khalily, A. A. Kishk, Sh. Danesh, , "Wideband P-Shaped Dielectric Resonator Antenna," *Radio engineering Journal*, vol. 22, No.1, pp. 281-285, 2013.
- [140] D. Guha, B. Gupta, C. Kumar, and Y. M. M. Antar, "Segmented Hemispherical DRA: New Geometry Characterized and Investigated in Multi-Element Composite Forms for Wideband Antenna Applications,"

- Antennas and Propagation, IEEE Transactions on*, vol. 60, pp. 1605-1610, 2012.
- [141] L. Yue, I. Shoaib, W. Shihua, C. Xiaodong, and Y. Zhinong, "A pattern reconfigurable DRA array for MIMO applications," in *Microwave Technology & Computational Electromagnetics (ICMTCE), 2011 IEEE International Conference on*, 2011, pp. 301-304.
- [142] P. Rezaei, M. Hakkak, and K. Forooraghi, "Dielectric resonator antenna for wireless LAN applications," in *Antennas and Propagation Society International Symposium 2006, IEEE*, 2006, pp. 1005-1008.
- [143] R. K. Mongia and P. Bhartia, "Dielectric resonator antennas—a review and general design relations for resonant frequency and bandwidth," *International Journal of Microwave and Millimeter-Wave Computer-Aided Engineering*, vol. 4, pp. 230-247, 1994.
- [144] M. H. a. K. F. P. Rezaei, "Design of Wideband Dielectric Resonator Antenna with a Two Segment Structure," *Progress in Electromagnetics Research, PIER* 66, pp. 111–124, 2006.
- [145] K. a. A. A. Kishk, "Dielectric Resonator Antenna- Possible Candidate for Adaptive Antenna Arrays," *Proceedings VITEL 2002, International Symposium on Telecommunications, Next Generation Networks and Beyond, Portoroz, Slovenia*, pp. May 13-14, 2002.

- [146] M. S. a. R. Yadla, "Microstrip-Fed Low Profile and Compact Dielectric Resonator Antennas," *Progress In Electromagnetics Research, PIER* 56, pp. 151-162, 2006.
- [147] H. G. Schantz, "A brief history of UWB antennas," *Aerospace and Electronic Systems Magazine, IEEE*, vol. 19, pp. 22-26, 2004.
- [148] W. Wiesbeck, G. Adamiuk, and C. Sturm, "Basic Properties and Design Principles of UWB Antennas," *Proceedings of the IEEE*, vol. 97, pp. 372-385, 2009.
- [149] D. Nyberg, P. S. Kildal, and J. Carlsson, "Effects of intrinsic radiation q on mismatch factor of three types of small antennas: single-resonance, gradual-transition and cascaded-resonance types," *Microwaves, Antennas & Propagation, IET*, vol. 4, pp. 83-90, 2010.
- [150] Y. Jian and A. Kishk, "A Novel Low-Profile Compact Directional Ultra-Wideband Antenna: The Self-Grounded Bow-Tie Antenna," *Antennas and Propagation, IEEE Transactions on*, vol. 60, pp. 1214-1220, 2012.
- [151] R. A. Abd-Alhameed, P. S. Excell, K. Khalil, R. Alias, and J. Mustafa, "SAR and radiation performance of balanced and unbalanced mobile antennas using a hybrid computational electromagnetics formulation," *Science, Measurement and Technology, IEE Proceedings -*, vol. 151, pp. 440-444, 2004.

- [152] P. Rezaei, M. Hakkak, and a. K. Forooraghi, "Design of wideband dielectric resonator antenna with a two segment structure," *Progress In Electromagnetics Research, PIER* 56, vol. PIER 66, pp. 111–124, 2006.
- [153] M. Khalily, M. K. A. Rahim, A. A. Kishk, and S. Danesh, "Wideband P-Shaped Dielectric Resonator Antenna," *Radioengineering*, vol. 22, pp. 281-285, April 2013.
- [154] A. H. Majeed, A. S. Abdullah, F. Elmegri, E. M. Ibrahim, K. H. Sayidmarie, and R. A. Abd-Alhameed, "Rectangular slot fed asymmetric Cylindrical Dielectric Resonators antenna for wideband applications," in *Antennas and Propagation Conference (LAPC), 2014 Loughborough*, 2014, pp. 244-248.
- [155] CST, "Computer simulation technology based on FDTD method," *CST Computer Simulation Technology AG*, 2014.
- [156] "CST Computer Simulation Technology AG, 2014.."
- [157] J. C. Johnstone, S. K. Podilchak, M. Clenet, and Y. M. M. Antar, "A compact cylindrical dielectric resonator antenna for MIMO applications," in *Antennas and Propagation Society International Symposium (APSURSI), 2014 IEEE*, 2014, pp. 1938-1939.
- [158] I. Messaoudene, T. A. Denidni, and A. Benghalia, "Two-port MIMO cylindrical dielectric resonator antenna for LTE systems," in *Antennas and Propagation Society International Symposium (APSURSI), 2014 IEEE*, 2014, pp. 1940-1941.

- [159] M. I. Sulaiman, S. K. Khamas, and H. Basarudin, "A singly-fed wideband circularly polarized cylindrical dielectric resonator antenna using conformal half-loop excitation," in *Engineering Technology and Technopreneuship (ICE2T), 2014 4th International Conference on*, 2014, pp. 209-212.
- [160] K. X. Wang and H. Wong, "A Circularly Polarized Antenna By using Rotated- Stair Dielectric Resonator," *Antennas and Wireless Propagation Letters, IEEE*, vol. PP, pp. 1-1, 2014.
- [161] S. Fakhte, H. Oraizi, R. Karimian, and R. Fakhte, "A New Wideband Circularly Polarized Stair-shaped Dielectric Resonator Antenna," *Antennas and Propagation, IEEE Transactions on*, vol. PP, pp. 1-1, 2015.
- [162] C.-C. Lin and J.-S. Sun, "Circularly-polarized Dielectric Resonator Antenna Fed by Off-centered Microstrip Line for 2.4-GHz ISM Band Applications," *Antennas and Wireless Propagation Letters, IEEE*, vol. PP, pp. 1-1, 2015.
- [163] S. Danesh, S. K. A. Rahim, M. Abedian, M. Khalily, and M. R. Hamid, "Frequency-Reconfigurable Rectangular Dielectric Resonator Antenna," *Antennas and Wireless Propagation Letters, IEEE*, vol. 12, pp. 1331-1334, 2013.
- [164] T. Apperley and M. Okoniewski, "A frequency reconfigurable dielectric resonator antenna using controllable air gaps," in *Antennas and*

- Propagation (EuCAP), 2014 8th European Conference on*, 2014, pp. 2923-2926.
- [165] S. Danesh, S. K. A. Abdul Rahim, M. Abedian Kasgari, and M. R. Hamid, "A compact Frequency Reconfigurable Dielectric Resonator Antenna for LTE/WWAN and WLAN applications," *Antennas and Wireless Propagation Letters, IEEE*, vol. PP, pp. 1-1, 2014.
 - [166] A. Voloshyn and Y. Prokopenko, "Frequency-tunable ring dielectric resonator antenna excited by waveguide," in *Electronics and Nanotechnology (ELNANO), 2014 IEEE 34th International Conference on*, 2014, pp. 58-61.
 - [167] M. J. Al-Hasan, T. A. Denidni, and A. R. Sebak, "Millimeter-wave compact EBG structure for mutual-coupling reduction in dielectric resonator antenna arrays," in *Antennas and Propagation Society International Symposium (APSURSI), 2013 IEEE*, 2013, pp. 95-96.
 - [168] M. J. Al-Hasan, T. A. Denidni, and A. R. Sebak, "Millimeter-Wave EBG-Based Aperture-Coupled Dielectric Resonator Antenna," *Antennas and Propagation, IEEE Transactions on*, vol. 61, pp. 4354-4357, 2013.
 - [169] R. M. Hashmi, B. A. Zeb, and K. P. Esselle, "Wideband High-Gain EBG Resonator Antennas With Small Footprints and All-Dielectric Superstructures," *Antennas and Propagation, IEEE Transactions on*, vol. 62, pp. 2970-2977, 2014.

- [170] B. Zeb, N. Nikolic, and k. Esselle, "A High-Gain Dual-Band EBG Resonator Antenna with Circular Polarization," *Antennas and Wireless Propagation Letters, IEEE*, vol. PP, pp. 1-1, 2014.

APPENDIX

Author's Publications List

Recent Publications

Journal Articles

1. A. H. Majeed, A. S. Abdullah, F. Elmegri, K. H. Sayidmarie, R. A. Abd-Alhameed, and J. M. Noras, "Aperture-Coupled Asymmetric Dielectric Resonators Antenna for Wideband Applications," *Antennas and Wireless Propagation Letters, IEEE*, vol. 13, pp. 927-930, 2014.
2. C. H. See, R. A. Abd-Alhameed, F. Elmegri, D. Zhou, J. M. Noras, N. J. McEwan, *et al.*, "Planar monopole antennas for new generation mobile and lower band ultra-

wide band applications," *Microwaves, Antennas & Propagation, IET*, vol. 6, pp. 1207-1214, 2012

3. F. Elmegri, 1- A. H. Majeed, A. S. Abdullah, R. A. Abd-Alhameed, J. M. Noras, K. H. Sayidmarie, "Dual Segment S-Shaped Aperture-Coupled Cylindrical Dielectric Resonator Antenna for X-Band Applications" *Microwaves, Antennas & Propagation, IET*, under review Jan 2015.
4. F. Elmegri, A. H. Majeed, A. S. Abdullah, R. A. Abd-Alhameed, J. M. Noras, K. H. Sayidmarie, "Balanced Dual-Segment Cylindrical Dielectric Resonator Antenna for Ultra-Wideband Applications" *Microwaves, Antennas & Propagation, IET*, under review Jan 2015.

International Conferences:

1. F Elmegri, C-E Zebiri, D Sayad, M Iashab, F Benabelaziz, R A Abd-Alhameed, J M Noras, N McEwan, Two cylindrical dielectric resonator antennas for extended-wideband applications, Festival of Radio Science 2014, School of Physics and Astronomy The University of Manchester on 16 December 2014, Paper Poster No. 7.

2. A Ali, A Atojok, E Ibrahim, R A Abd-Alhameed, P S Excell, F Elmegri, J M Noras, Design and optimisation of quadrifilar helical antenna for RFID applications using genetic algorithms, URSI, Festival of Radio Science 2014, School of Physics and Astronomy The University of Manchester on 16 December 2014, Session 3, Paper No. 5.
3. K.O.O. Anoh, Y.A.S. Dama, H.M. AlSabbagh, E. Ibrahim, 1R.A. Abd-Alhameed, 1F. Elmegri, 1T.T. Mapoka, Mohammad Ngala and S. M. R. Jones, An Evaluation of Spatial Modulation for MIMO Systems with QO-STBC, The 8th International Wireless Internet Conference - Symposium on Wireless and Vehicular Communication, November 13–14, 2014 Lisbon, Portugal, pp. 1-8.
4. Muhammad Adeka, Mohammad Ngala, Mohammad Bin-Melha, E. Ibrahim, Simon Shepherd, Issa Elfergani, Ash S Hussaini, Fauzi Elmegri and Raed Abd-Alhameed, Nigeria: Cyber Space Security vis a vis Computerisation, Miniaturisation and Location-Based Authentication, The 8th International Wireless Internet Conference - Symposium on Wireless and Vehicular Communication, November 13–14, 2014 Lisbon, Portugal, pp. 1-12.
5. C. Zebiri, F. Benabdelaziz, M. Lashab, R. A. Hameed, and F. Elmegri, "A novel grating monopole antenna: (With defected ground plane) for DVB-T

application," in Ultra-WideBand (ICUWB), 2014 IEEE International Conference on, 2014, pp. 162-165.

6. A.H. Majeed, A.S. Abdullah, F. Elmegri, E.M. Ibrahim, K.H. Sayidmarie, R.A. Abd-Alhameed, Rectangular Slot Fed Asymmetric Cylindrical Dielectric Resonators Antenna for Wideband Applications, 2014 Loughborough Antennas and Propagation Conference (LAPC), 10 - 11 November 2014, UK, pp. 244-248. ISBN: 978-1-4799-3662-5/14.
7. A Atojoko, N. A Jan, F. Elmgri, R. A. Abd-Alhameed, C. H. See, J. M. Noras, Energy efficient gully pot monitoring system using radio frequency identification (RFID), Loughborough Antennas & Propagation Conference (LAPC), 11-12 November 2013 in Burleigh Court International Conference Centre, Loughborough University, United Kingdom, pp. 333- 336. ISBN: 978-1-4799-0091-6/13
8. F. Elmegri, C. H. See, R. A. Abd-Alhameed, C. Zebiri and P. S. Excell, Dielectric Resonator Antenna Design For UWB Applications, Loughborough Antennas & Propagation Conference (LAPC), 11-12 November 2013 in Burleigh Court International Conference Centre, Loughborough University, United Kingdom, pp. 539-541. ISBN: 978-1-4799-0091-6/13.

9. H.A. Obeidat, R.A. Abd-Alhameed, E.A. Elkazmi, R. Asif, M. Usman, C.H. See, F. Elmegri, T.S. Ghazaany, Z. Sharon, J.M. Noras, and S.M.R. Jones, A Comprehensive Study for Indoor Localization Techniques using Received Signal Strength, Third International Workshop on Energy Efficient and Reconfigurable Transceivers (EERT): Towards a Green Wireless Internet, Proceedings of the fifth International Conference on Internet Technologies and Applications (ITA 13), Glyndŵr University, Wrexham, Wales, UK, Tuesday 10th – Friday 13th September 2013, pp. 405-414. ISBN 978-0-946881-81-9.
10. M.S. Bin-Melha, N.A. Jan, M. Usman, Fauzi Elmegri, C.H. See and R.A. Abd-Alhameed, P.S. Excell Investigation of Harmonic Rejection for Triangular Patch microstrip antenna, Third International Workshop on Energy Efficient and Reconfigurable Transceivers (EERT): Towards a Green Wireless Internet, Proceedings of the fifth International Conference on Internet Technologies and Applications (ITA 13), Glyndŵr University, Wrexham, Wales, UK, Tuesday 10th – Friday 13th September 2013, pp. 444-450. ISBN 978-0-946881-81-9.
11. R.A. Abd-Alhameed, K.O.O. Anoh, I. Ahmad, H.S.O. Migdadi, R. Asif, N.A. Jan, T.S. Ghazaany, S. Zhu, F. Elmegri, M. Bin-Melha, A. Atojoko, J.M. Noras, S.M.R. Jones, C.H. See, H. Alhassan and M.B. Child, A Review of Location Based Services: Current Developments, Trends and Issues, Third International Workshop on Energy Efficient and Reconfigurable Transceivers (EERT):

Towards a Green Wireless Internet, Proceedings of the fifth International Conference on Internet Technologies and Applications (ITA 13), Glyndŵr University, Wrexham, Wales, UK, Tuesday 10th – Friday 13th September 2013, pp. 451-464. ISBN 978-0-946881-81-9.

12. F. Elmegri, C.H. See, M. Bin-Melha, N.A. Jan, R.A. Abd-Alhameed, M.B. Child and P.S. Excell, Dielectric Resonator Antenna Design for Lower-UWB Wireless Applications, Third International Workshop on Energy Efficient and Reconfigurable Transceivers (EERT): Towards a Green Wireless Internet, Proceedings of the fifth International Conference on Internet Technologies and Applications (ITA 13), Glyndŵr University, Wrexham, Wales, UK, Tuesday 10th – Friday 13th September 2013, pp. 473-477. ISBN 978-0-946881-81-9.
13. Mohamed Lashab, C.H. See, Chems-Eddine Zebiri, Elmegri Fauzi, Fatiha Benabdelaziz, R.A. Abd-Alhameed, Naeem A. Jan, SRR Metamaterial Loaded on Horn Antennas for Broadband Application, Workshop on Challenges in Electromagnetic Simulation: supported by the Applied Computational Electromagnetics Society (ACES), Proceedings of the fifth International Conference on Internet Technologies and Applications (ITA 13), Glyndŵr University, Wrexham, Wales, UK, Tuesday 10th – Friday 13th September 2013, pp. 510-516. ISBN 978-0-946881-81-9

